

Design strategies of PHB/chitosan based electrospun nanofibrous scaffolds in promising biomaterial

A Thesis submitted in partial fulfilment of the requirements for the degree of

Doctor of Philosophy

By

Yansheng Zhou

Institute of Material Discovery, Department of Chemistry

University College London

Abstract

In recent years, the development of promising biomaterials that can stimulate tissue regeneration has become increasingly important, particularly in addressing Peripheral Nerve Injury (PNI). This condition, known for causing loss of nerve function, has garnered significant attention. Over the past two decades, research has progressively led to the discovery and advancement of novel, natural-based polymeric materials. These materials are used to construct scaffolds to tackle PNI challenges. The focus of this research is on the design of promising natural-based polymers, specifically Polyhydroxybutyrate (PHB) and chitosan (CS), for application in tissue implants. The study is divided into three distinct sections: an analysis of the stability of PHB/CS electrospun composites across various pH levels, surface modifications of PHB electrospun membrane to improve CS adhesion, and the study of forskolin release from polyethylene oxide (PEO) to PHB/CS co-electrospun fibre. This research presents an innovative approach and the potential application of PHB/CS natural-based polymeric scaffolds in tissue engineering.

In the chapter on PHB/CS electrospun membrane fabrication, a first-time examination compares electrospinning process parameters and solution properties. Key factors such as applied voltages, working distances, flow rates, solvent types, viscosity, and conductivity are explored. Results indicate that trifluoroacetic acid (TFA) and chloroform/dimethylformaldehyde (CF/DMF) effectively dissolve PHB. A crucial finding is that increasing PHB concentration to a 2:30 mass ratio initiates fibre electrospinning. SEM analysis shows uniform fibres are produced at PHB and CS ratios of 2:30 and 1:50, respectively. Optimal fabrication conditions are identified as voltages of 10 to 12 kV, flow rates between 1 to 1.25 ml/h, and working distances of 16 to 22 cm, enabling successful uniform fibre production. In the chapter examining the stability of PHB/CS under varying pH conditions, the materials demonstrated accelerated degradation in both acidic sodium lactate/HCl and alkaline NaOH solutions. Among three different mass ratios of CS (0, 1:100, and 1:50 m/m), the 1:50 m/m ratio exhibited the quickest degradation, followed by 1:100 and 0. In the chapter analyzing the adhesive properties of CS on PHB modified with potassium hydroxide (KOH) or hydrogen peroxide (H₂O₂) surface treatments, it was found that CS of varying concentrations successfully chemically bonded with PHB electrospun fibres. Notably, the adhesion in KOH-treated samples was 23% higher compared to H₂O₂-treated samples. In the chapter on the drug-release profile of PHB/CS, Forskolin-loaded PEO was electrospun with PHB/CS using different CF/DMF ratios in both single-jet and co-electrospinning techniques. The study revealed that a 10 w/v% PEO co-electrospun with an 8:2 CF/DMF volume ratio maintained a consistent release over 144 days with minimal pH change (pH=6.5 post-degradation). These findings suggest that

PHB/CS electrospun membranes hold significant potential as tissue implant materials. Future research will delve into more comprehensive in vitro biocompatibility assessments and in vivo studies.

Acknowledgments

I would like to express my deepest gratitude and appreciation to everyone who has contributed to the completion of this doctoral thesis. This research journey has been an enriching and transformative experience, and it would not have been possible without the support, encouragement, and assistance of numerous individuals.

Primarily, I am immensely grateful to my supervisors, Dr Fenglei Zhou, Professor Ying Li, and Dr Bing Li, for their unwavering guidance, invaluable expertise, and continuous encouragement throughout this entire process. Especially Dr Fenglei Zhou, his profound knowledge in the field and their commitment to excellence have been instrumental in shaping the direction of my research and refining my academic skills. I am indebted to their mentorship, patience, and the trust they placed in me, which empowered me to explore new avenues of knowledge and push the boundaries of my capabilities.

I extend my sincere appreciation to the members of my thesis committee, Fenglei Zhou, Ying Li, Bing Li, for their insightful feedback, constructive criticism, and thought-provoking discussions. Their expertise and scholarly inputs have significantly contributed to the rigor and quality of this thesis, and I am grateful for the time and effort they devoted to reviewing my work.

I would like to thank the faculty members and staff of the University College London, for providing a conducive academic environment and access to invaluable resources that have enriched my research endeavours. Their dedication to fostering an atmosphere of intellectual curiosity and scholarly pursuit has been instrumental in my growth as a researcher.

I am grateful to my colleagues and research collaborators who have shared their knowledge, ideas, and support throughout this journey. The vibrant academic community at the University College London has provided me with a platform for stimulating discussions, constructive feedback, and collaborations that have broadened my perspectives and enhanced the overall quality of my work.

I would like to express my heartfelt gratitude to my wife, Yidan Yin and my family for their unwavering love, encouragement, and understanding. Their constant support, belief in my abilities, and sacrifices have been the bedrock of my achievements. I am eternally grateful for their presence in my life.

Lastly, I would like to acknowledge the countless unnamed individuals who have played a role, however big or small, in the completion of this thesis. Your contributions, whether through conversations, resources, or assistance, have all contributed to the outcome of this research endeavour.

This thesis represents the culmination of years of dedication, perseverance, and collaboration. I am humbled and honoured to have had the opportunity to undertake this research, and I am grateful for the support and guidance that I have received along the way. This accomplishment would not have been possible without the collective efforts of all those mentioned and unmentioned.

Thank you all for your invaluable contributions.

List of Figures

Figure 2.1: Fabrication Process of PHB from Bacterial Metabolic Pathway [56].	28
Figure 2.2: Schematic diagram of Wet Spinning Process [95]	41
Figure 2.3: Schematic diagram of Dry-jet wet Spinning [98]	43
Figure 2.4: Schematic diagram of Dry spinning [96]	44
Figure 2.5: Schematic diagram of Melt spinning [102]	46
Figure 2.6: Schematic diagram of Flash spinning [105]	47
Figure 2.7: Schematic diagram of Gel spinning [107]	49
Figure 2.8: Schematic diagram of Centrifugal spinning techniques [20]	50
Figure 2.9: Schematic diagram of Emulsion techniques [91]	51
Figure 3.1: Electrospinning Equipment Setup for Nanofibres Fabrication, included electrospinning chamber, rotational speed, flow rate, syringe pump controller, high voltage supplier and spinneret with 18-gauge needle.	60
Figure 4.1: Conductivity and Mean viscosity of different concentration PHB and CS (a) 15 w/v% PHB in 0/1/2/3/4/5 w/v% CS (b) 12 w/v% PHB in 0/1/2/3/4/5 w/v% CS and (c) 10 w/v% PHB in 0/1/2/3/4/5 w/v% CS	69
Figure 4.2: Critical applied voltages VS CS concentration diagram of 15 w/v% PHB electrospun fibres at 20 cm working distance under 0,1,2,3,4 and 5 w/v% CS with different flow rates. (a) 0.25 ml/hr (b) 0.5 ml/hr (c) 0.75 ml/hr (d) 1 ml/hr (e) 1.25 ml/hr (f) 1.5 ml/hr	70
Figure 4.3: SEM of 15 w/v% PHB/1 w/v% CS electrospun fibres at applied voltages=12kV and flow rates=1 /hr with different working distance (a) 10 cm (b) 12 cm (c) 14cm (d) 16 cm (e) 18 cm (f) 20cm and (g) 22cm	71
Figure 4.4: SEM of 15 w/v% PHB/1 w/v% CS electrospun fibres at applied voltages=12kV, flow rates=1.5 ml/hr and working distance=20 cm with different concentration of CS (a) 1 w/v% CS (b) 2 w/v% CS (c) 3 w/v% CS (d) 4 w/v% CS (e) 5 w/v% CS	72
Figure 4.5: SEM of 15 w/v% PHB/1 w/v% CS electrospun fibres at applied voltages=12Kv and working distance=20 cm with different flow rates. (a) 0.25 ml/hr (b) 0.5 ml/hr (c) 0.75 ml/hr (d) 1 ml/hr (e) 1.25 ml/hr (f) 1.5 ml/hr	73
Figure 5.1: SEM images of PHB/CS electrospun scaffolds with different CS contents (a) 0 w/v%, (b) 1 w/v%, (c) 2 w/v% and (d) 3 w/v%.	76
Figure 5.2: FTIR spectra of PHB/CS electrospun scaffolds. (A) PHBCS0, (B) PHBCS1, (C) PHBCS2, (D) PHBCS3.	78
Figure 5.3: WCA measurements of PHB/CS electrospun scaffolds.	79

Figure 5.4: Thermal analysis of PHB/CS composite films (A) TGA and DTA graphs of PHB/CS composite films with different CS contents. (B) DSC graphs of PHB/CS composite films with different CS contents.	80
Figure 5.5 DSC analysis of of PHB/CS electrospun composite films. (a) Enthalpy fusion and (b) DSC curves of PHB/CS samples.	81
Figure 5.6: Remaining weight of PHB and PHB/CS electrospun mats between different pH levels in week 12. (**** (p < 0.0001), *** (p < 0.0005), ns (p > 0.1))	82
Figure 5.7: SEM graphs of remaining weight of PHB and PHB/CS electrospun mats in week 12.	83
Figure 6.1: SEM micrographs and fibre diameters of PHB/KOH-treated electrospun fibres with varying CS concentrations: (a) non-treated PHB fibres, (b) 0 w/v%, (c) 0.2 w/v%, (d) 0.5 w/v%, (e) 0.8 w/v% (f) 1 w/v%, (g) 1.5 w/v%, (h) 2 w/v%	89
Figure 6.2: SEM micrographs of PHB/H ₂ O ₂ -treated electrospun fibres with varying CS concentrations: (a) 0 w/v%, (b) 0.2 w/v%, (c) 0.5 w/v%, (d) 0.8 w/v% (e) 1 w/v%, (f) 1.5 w/v%, (g) 2 w/v%	90
Figure 6.3: FTIR spectra comparison between untreated and treated PHB samples. (a) H ₂ O ₂ -treated PHB-DA-GA-CS electrospun fibres with CS concentrations ranging from 0 to 2 w/v%. (b) KOH-treated PHB-DA-GA-CS electrospun fibres with CS concentrations ranging from 0 to 2 w/v%	93
Figure 6.4: TGA and DTA analysis of between untreated and treated PHB samples. (a) KOH -treated PHB electrospun nanofibres with 2, 1.5, 1, 0.8, 0.5 and 0.2 w/v% CS. (b) H ₂ O ₂ -treated PHB electrospun nanofibres with 2, 1.5, 1, 0.8, 0.5, and 0.2 w/v% CS (c) DTA for H ₂ O ₂ -treated PHB electrospun nanofibres with 2, 1.5, 1, 0.8, 0.5 and 0.2 w/v% CS. (d) KOH -treated PHB electrospun nanofibres with 2, 1.5, 1, 0.8, 0.5, and 0.2 w/v% CS	95
Figure 6.5: DSC analysis of PHB-KOH/ H ₂ O ₂ treated electrospun nanofibres with CS concentrations of 2, 1.5, 1, 0.8, 0.5, and 0.2 w/v%: (a) KOH-treated samples and (b) H ₂ O ₂ -treated samples.	98
Figure 6.6: The average water contact angles of the PHB-KOH/H ₂ O ₂ treated electrospun nanofibres with non-treated, 0, 0.5, 0.8, 1, 1.5, 2 w/v% CS.	101
Figure 6.7: BET analysis of macropore size, micropore size, specific surface area, and pore volume. of PHB-KOH/H ₂ O ₂ treated electrospun nanofibres with CS concentrations of 2, 1.5, 1, 0.8, 0.5, 0.2, and 0 w/v%, displaying. (a) KOH-treated and (b) H ₂ O ₂ -treated.	106
Figure 6.8: The UV-VIS of PHB electrospun fibres with (a) KOH and (b) H ₂ O ₂ treated electrospun nanofibres with 2, 1.5, 1, 0.8, 0.5, 0.2, and 0 w/v% CS.	107
Figure 6.9: Mechanical properties of PHB electrospun fibres with CS concentrations of 2, 1.5, 1, 0.8, 0.5, 0.2, and 0 w/v%: (a) Tensile	

properties of KOH-treated samples, (b) tensile properties of H ₂ O ₂ -treated samples, (c) toughness and Young's modulus for both KOH and H ₂ O ₂ treated samples, and (d) elongation and ultimate tensile strength (UTS) for both KOH and H ₂ O ₂ treated samples.....	108
Figure 7.1: SEM graphs PHB/CS electrospun fibres with different CF/DMF ratio. (a) 7:3 CF/DMF (b) 8:2 CF/DMF (c) 9:1 CF/DMF	114
Figure 7.2: SEM graphs PHB/CS electrospun fibres with different concentration of PEO and fabrication techniques. (a) PHB-2wt CS-5 w/v% PEO (8:2) Co-ESP (b) PHB-2wt CS-5 w/v% PEO (8:2) Single-ESP (c) PHB-2wt CS-10 w/v% PEO (8:2) Co-ESP (d) PHB-2wt CS-10 w/v% PEO (8:2) Single-ESP (e) PHB-2wt CS-5 w/v% PEO (9:1) Co-ESP (f) PHB-2wt CS-10 w/v% PEO (9:1) Single-ESP (g) PHB-2wt CS-10 w/v% PEO (9:1) Co-ESP (h) PHB-2wt CS-5 w/v% PEO (9:1) Single-ESP	114
Figure 7.3: Fibre diameter variation across 11 groups influenced by PEO concentration, fabrication techniques, PHB-CS solution ratios, and nitrogen treatments.....	116
Figure 7.4: Cumulative drug release of Forskolin in PHB-CS based electrospun membranes with various modification. (a) PHB-CS with different CF/DFM ratio, (b) PHB and PHB-CS electrospun membrane with different CS concentration, and fabricated in Single-ESP or Co-ESP.....	120
Figure 7.5: Percentage mass remain of PHB-CS based electrospun membranes with various modification. (a) PHB-CS with different CF/DFM ratio, (b) PHB and PHB-CS electrospun membrane with different CS concentration, and fabricated in Single-ESP or Co-ESP	124
Figure 7.6: pH analysis of PHB-CS based electrospun membranes with various modification in PBS solution.....	127

List of Tables

Table 1: Biomaterials and their applications in nerve tissue engineering..	31
Table 2: Comparison of Spinning Methods for Peripheral Nerve Injury: Advantages, Disadvantages, Fibre Sizes, and Applications with References	53
Table 3: Average fibre and bead diameter of PHB/CS nanofibrous membranes with different CS contents.	76
Table 4: Mean values of degradation temperature of PHB/CS composite films.	80
Table 5: DSC graphs of PHB/CS composite films with different CS contents.	81
Table 6: Average fibre diameter of PHB/CS nanofibrous membranes with different CS contents after 12 weeks of degradation in different pH values.	85
Table 7: Average Fibre Diameters and Standard Deviations for PHB Electrospun Fibres Subjected to KOH and H ₂ O ₂ Treatments with Varying CS Concentrations.	91
Table 8: TGA analysis for PHB-KOH treated electrospun nanofibres with 2, 1.5, 1, 0.8, 0.5, and 0.2 w/v% CS.	96
Table 9: TGA analysis for PHB- H ₂ O ₂ treated electrospun nanofibres with 2, 1.5, 1, 0.8, 0.5, and 0.2 w/v% CS.	97
Table 10: Enthalpy of fusion and crystallinity of the electrospun PHB-KOH/ H ₂ O ₂ treated electrospun nanofibres with 2, 1.5, 1, 0.8, 0.5, and 0.2 w/v% CS.	99
Table 11: Enthalpy of fusion and crystallinity of the electrospun PHB- H ₂ O ₂ treated electrospun nanofibres with 2, 1.5, 1, 0.8, 0.5, and 0.2 w/v% CS.	99
Table 12: Effect of CS Concentration on Macropore Size, Micropore Size, Specific Surface Area, and Pore Volume of PHB-K electrospun membranes	102
Table 13: Effect of CS Concentration on Specific Surface Area of PHB-H electrospun membranes	103
Table 14: Mechanical properties of PHB-KOH treated electrospun nanofibres with 2, 1.5, 1, 0.8, 0.5, 0.2, and 0 w/v% CS.	109
Table 15: Mechanical properties of PHB- H ₂ O ₂ treated electrospun nanofibres with 2, 1.5, 1, 0.8, 0.5, 0.2, and 0 w/v% CS.	110
Table 16: Fibre diameters of PHB/CS-based electrospun fibre.	116
Table 17: Comparative Release Kinetics Analysis of PHB-CS Electrospun Samples with Varying CF/DMF Ratios and Single-jet and co-electrospinning. (R ² represents the proportion of variance of regression line (ranges from 0 to 1)).	118

List of abbreviations

- ALS - Acidic lactate sodium
- AMD - age-related macular degeneration
- ATR- Attenuated total reflectance
- BET - Brunauer, Emmett and Teller method
- CF - Chloroform
- Co-ESP - Co-electrospinning
- CS - Chitosan
- CBR- Cibacron Brilliant Red 3B-A
- DA - Dopamine
- DFT - Density-functional theory
- DMF - Dimethylformamide
- DSC - Differential Scanning Calorimetry
- ECM - Extracellular matrix
- FGF - Fibroblast growth factor
- FTIR - Fourier Transform Infrared Spectroscopy
- GA - Glutaraldehyde
- GDNF - Glial cell line-derived neurotrophic factor
- HA - Hyaluronic acid
- HAMC - Hyaluronan/methyl cellulose

- HCl- Hydrochloric acid
- hESs-Human embryonic stem cells
- hMSC - Human Mesenchymal Stem Cells
- H₂O₂ - Hydrogen peroxide
- KOH - Potassium hydroxide
- LC-PHAs-long-chain length PHAs
- MC-PHAs-medium-chain length PHAs
- MMA- methyl methacrylate
- Mw-Molecular weight
- mRPCs-Mouse retinal progenitor cells
- NaOH- Sodium hydroxide
- NGF - Neuron growth factor
- PA6 - Polyamide 6
- PAN - Polyacrylonitrile
- PCL – Polycaprolactone
- PDA- Polydopamine
- PDLLA-Poly-D, L-lactic Acid
- PEO - Poly (ethylene oxide)
- PGA - Polyglycolic acid
- PHA - Polyhydroxyalkanoates
- PHB – Polyhydroxybutyrate

- PHEMA- Poly (2-hydroxyethyl methacrylate)
- PGS - Polyglycerol sebacate
- PLA - Polylactic acid
- PLLA - Poly (L-lactic acid)
- PNCs - Peripheral nerve conduits
- PNI - Peripheral nervous injury
- PS - Polystyrene
- PBS - Phosphate buffer solution
- SC-PHAs-short-chain length PHAs
- SD- Stargardt disease
- SEM - Scanning Electron Microscope
- Single-ESP-Single jet electrospinning
- TGA - Thermogravimetric analysis
- UHMWPE - Ultra-high molecular weight polyethylene
- UTS- ultimate tensile stress
- WCA - Water Contact Angle

Declaration page

I, Yansheng Zhou, confirm that the work presented in my thesis is my own. Where information has been derived from other sources, I confirm that this has been indicated in the thesis.

Impact Statement

This research bridges critical gaps in the field of peripheral nerve regeneration by investigating innovative nerve graft solutions. The exploration of biodegradable polymers, exemplified through the manuscript "A Comparison of CS Adhesion on KOH and H₂O₂ Pre-treated Electrospun Poly(3-hydroxybutyrate) Nanofibres," offers novel insights into enhancing adhesion properties for tissue engineering applications.

This study's importance is manifold. Initially, it provides a detailed methodology for creating and analysing biodegradable polymer-based materials for nerve grafts, establishing a foundation for future innovations in nerve repair methods. Additionally, the study enhances understanding in the field by examining the influence of KOH and H₂O₂ pre-treatments on the adherence of chitosan to these materials. This insight is crucial for refining material modification processes in the development of customised solutions for tissue engineering.

Drawing on interdisciplinary insights from materials science, biomedical engineering, and neurobiology, this study significantly enhances our comprehension of the complex interplay between biodegradable polymers and nerve tissue. The collective findings presented in Chapters 4 to 7 contribute substantially to the development of advanced nerve graft materials, characterised by their controlled release functionalities. This research marks a pivotal step in the field, underlining the potential for innovative and effective nerve regeneration strategies.

In conclusion, this study holds the potential to revolutionize peripheral nerve injury treatments by introducing advanced biomaterials with enhanced adhesion properties. Its findings offer a foundation for future research and development in the realm of nerve tissue engineering, ultimately impacting the quality of life for those affected by peripheral nerve injury.

List of Publications

Zhou, Y.; Li, Y.; Li, D.; Yin, Y.; Zhou, F. Electrospun PHB/CS Composite Fibrous Membrane and Its Degradation Behaviours in Different pH Conditions. *J. Funct. Biomater.* **2022**, *13*, 58. <https://doi.org/10.3390/jfb13020058>

Zhou, Y.; Li, D.; Li, X.; Li, Y.; Li, B.; Zhou, F. A Comparison of CS Adhesion to KOH and H₂O₂ Pre-Treated Electrospun Poly(3-Hydroxybutyrate) Nanofibres. *Fibres* **2023**, *11*, 91. <https://doi.org/10.3390/fib11110091>

Zhou, Y.; Li, D.; Li, X.; Li, Y.; Li, B.; Zhou, F. Electrospinning of PHB/CS nanofibres for tuneable drug delivery. Submitted

Contents

ABSTRACT	1
ACKNOWLEDGMENTS	3
LIST OF FIGURES	5
LIST OF TABLES	8
LIST OF ABBREVIATIONS	9
DECLARATION PAGE	12
IMPACT STATEMENT	13
LIST OF PUBLICATIONS	14
CONTENTS	15
1. CHAPTER 1: INTRODUCTION	19
2. CHAPTER 2: LITERATURE REVIEW	21
2.1 Neurodegenerative diseases.....	21
2.2 Material Selection and Electrospinning Techniques in Nerve Tissue Engineering.....	24
2.2.1 <i>Natural Polymers</i>	25
2.2.2 <i>Synthetic Polymers</i>	29
2.2.3 <i>Composite polymers</i>	30
2.3 Electrospinning process and parameters	33
2.4 Advantages of Electrospinning	34
2.4.1 <i>Precise Fibre Control</i>	34
2.4.2 <i>Material Versatility</i>	35
2.4.3 <i>High Surface-to-Volume Ratio</i>	35
2.4.4 <i>Interconnected Porosity</i>	35
2.4.5 <i>Scalability</i>	36
2.4.6 <i>Solvent Selection</i>	36
2.5 Applications of Electrospinning.....	37
2.5.1 <i>Biomedical Engineering</i>	37
2.5.2 <i>Filtration and Separation</i>	38
2.6 Other fabrication methods	39
2.6.1 <i>Wet spinning</i>	39
2.6.2 <i>Dry-jet wet spinning</i>	41
2.6.3 <i>Dry spinning</i>	43
2.6.4 <i>Melt spinning</i>	44
2.6.5 <i>Flash spinning</i>	46
2.6.6 <i>Gel spinning</i>	48
2.6.7 <i>Centrifugal spinning</i>	49
2.6.8 <i>Emulsion electrospinning</i>	50
2.7 Current challenges in electrospun fibres in tissue engineering	55

2.7.1	<i>Inadequate Guidance Cues</i>	55
2.7.2	<i>Mechanical Properties</i>	56
2.7.3	<i>Biocompatibility</i>	56
2.7.4	<i>Optimizing Topographical and Biochemical Cues</i>	57
2.8	Future perspective	58
3.	Chapter 3: Experimental details	60
3.1	Materials	60
3.2	Electrospinning Setup.....	60
3.3	Sample preparation	61
3.3.1	<i>Preparing PHB and CS solution with trifluoroacetic acid</i>	61
3.3.2	<i>Preparing PHB and CS solution with CF/DMF</i>	61
3.3.3	<i>Fabrication of PHB and PHB/CS electrospun fibres</i>	61
3.3.4	<i>Single-jet and Co-electrospinning Fabricating Methods of PHB/CS/PEO Electrospun fibres</i>	61
3.3.5	<i>Modifying the process parameters included concentration of working distance, flow rates and applied voltages</i>	62
3.3.6	<i>Degradation analysis in acidic (pH = 2), neutral (pH = 7) and alkaline solutions (pH = 12)</i>	62
3.3.7	<i>Surface functionalization of electrospun fibrous PHB membranes with DA and GA</i>	63
3.3.8	<i>Stability analysis of CS on KOH and H₂O₂ treated PHB-DA-GA-CS electrospun fibres</i>	63
3.3.9	<i>In Vitro Release, Remaining Mass, and pH Stability Analysis of Forskolin from PHB/CS-Based Electrospun Fibre Mats</i>	64
3.4	Characterization.....	64
3.4.1	<i>Scanning electron microscope (SEM)</i>	64
3.4.2	<i>Fourier transforme infra-red sepctrometer (FTIR)</i>	65
3.4.3	<i>Water contact angles (WCA)</i>	65
3.4.4	<i>Thermal gravimetric analysis (TGA)</i>	65
3.4.5	<i>Differentiate scanning calorimetry (DSC)</i>	65
3.4.6	<i>Porosity analysis by Brunauer–Emmett–Teller (BET)</i>	66
3.4.7	<i>Mechanical tests</i>	66
3.4.8	<i>Conductivity testing</i>	66
3.4.9	<i>Measurements of viscosity</i>	66
3.4.10	<i>Statistical analysis</i>	66
4.	Chapter 4: Optimization of PHB/CS Solution Properties for Electrospinning: Conductivity, Viscosity, and Process Parameters	67
4.1	Overview	67
4.2	Result and discussion.....	67
4.3	Summary	74
5.	Chapter 5: Electrospun PHB/CS Composite Fibrous Membrane and Its Degradation Behaviours in Different pH Conditions	75

5.1	Overview	75
5.2	Results and Discussion	75
5.2.1	<i>Morphology and Size of PHB and PHB/CS</i>	75
5.2.2	<i>FTIR analysis of PHB Electrospun Fibres before and after degradation</i>	76
5.2.3	<i>WCA Measurements of PHB/CS electrospun membranes</i>	78
5.2.4	<i>TGA and DSC Analysis</i>	79
5.2.5	<i>Degradation Analysis and SEM of PHB/CS after 12 Weeks Degradation in Acidic, PBS and Alkaline</i>	81
5.3	Summary	85
6.	Chapter 6: A Comparison of CS Adhesion on KOH and H₂O₂ Pre-treated Electrospun PHB Nanofibres	87
6.1	Overview	87
6.2	Results and discussion	87
6.2.1	<i>Morphology and size of Electrospun membranes with varying CS concentrations (0.2-2 w/v%) in PHB-KOH/H₂O₂</i>	87
6.2.2	<i>ATR-FTIR of PHB-CS Electrospun Fibres before and after KOH and H₂O₂ modification</i>	91
6.2.3	<i>TGA and DTA Analysis of PHB-CS Electrospun Fibres</i>	93
6.2.4	<i>DSC Analysis of PHB-CS Electrospun Fibres</i>	97
6.2.5	<i>Hydrophilicity analysis of PHB-CS Electrospun Fibres with contact angle measurements</i>	100
6.2.6	<i>Analysis of Specific Surface Area of PHB-CS Electrospun Fibres Using BET Method</i> 102	
6.2.7	<i>Stability Assessment of KOH/H₂O₂ PHB-DA-GA-CS Electrospun Samples: UV-Vis and CBR Analytical Techniques</i>	106
6.2.8	<i>Mechanical Properties of KOH- and H₂O₂-Treated PHB Electrospun Nanofibres with Varying CS Concentrations: Tensile Strength, Toughness, Young's Modulus, and Elongation at Break</i>	107
6.3	Summary	110
7.	Chapter 7: Electrospinning of PHB/CS nanofibres for tuneable Forskolin delivery	112
7.1	Overview	112
7.2	Results and Discussion	113
7.2.1	<i>SEM Analysis and Diameter Measurement of PHB/CS-based Electrospun Fibres</i> 113	
7.2.2	<i>In vitro drug release of Forskolin</i>	117
7.2.3	<i>Mass remaining analysis of PHB/CS-based electrospun fibres</i>	122
7.2.4	<i>pH analysis of PHB-CS based electrospun fibres</i>	126
7.3	Summary	127
8.	Chapter 8: Conclusion and Future works	128
8.1	Conclusion	128
8.2	Future Works	129

9. References..... 131

Chapter 1: Introduction

Peripheral nervous injury (PNI) refers to a group of neurodegenerative diseases with global healthcare costs surpassing \$3 billion annually [1]. The peripheral nerves system plays a critical role in controlling and coordinating bodily functions, and the effects of PNI can be debilitating, leading to conditions such as muscle weakness, deformity, and chronic pain [1]. Despite the significant advances in medical technology, current treatment methods, such as synthetic nerve grafts, have demonstrated limited efficacy, and often lead to severe secondary complications [2, 3].

This highlights the need for alternative solutions, and one potential avenue is the application of biodegradable polymers as nerve graft materials. For example, Polyhydroxybutyrate (PHB) [4-10] have shown promise in various medical applications, including drug delivery and organ tissue engineering, due to their unique properties of biodegradability and biocompatibility [11-13].) The use of single-component PHBs in nerve tissue engineering is constrained by their physical and chemical properties, which may not adequately match those of nerve tissues. Chitosan (CS), a natural polysaccharide derived from chitin, not only demonstrates excellent biocompatibility, and possesses inherent antibacterial properties but also has the ability to attract growth factors, thereby promoting cell growth and differentiation around the developing tissues. Furthermore, the creation of a network scaffold that possesses adequate mechanical properties and interconnectivity is crucial to support and promote the growth of nerve cells. Electrospinning is identified as the optimal technique for producing nano-sized fibres with high interconnectivity, making it the method of choice for this endeavour. This leads to the central research question of this thesis: How can we develop an optimized novel scaffold for peripheral nerve injury (PNI)? The hypothesis posited in this project is that a PHB/CS scaffold, fabricated through electrospinning, can serve as a suitable material for promoting nerve regeneration in cases of PNI. It aims to achieve the function of a nerve conduit through its nano-network structure and structural integrity, while also being capable of integration with other materials.

Consequently, the research objectives are designed to:

- 1) Prepare PHB and CS solutions using different solvents for electrospinning, optimizing process parameters such as flow rates, working distance, and applied voltages. This will involve investigating surface and structural properties including conductivity, viscosity, fibre dimensions, and uniformity.
- 2) Fabricate PHB/CS electrospun fibres under specific process parameters, analyzing their material properties, chemical structure, and thermal and mechanical stability to assess their suitability for nerve tissue engineering.

- 3) Enhance the surface properties of PHB/CS through advanced surface modifications, examining the impact on material properties, chemical structure, surface characteristics, thermal and chemical stability, and mechanical properties to optimize the scaffold for nerve cell growth and differentiation.

Chapter 2: Literature Review

2.1 Neurodegenerative diseases

Neurodegenerative diseases pose significant challenges for both patients and researchers due to their inherent difficulties in achieving full recovery and the high economic and psychological costs associated with treatments. Diseases affecting both the central nervous system (CNS), such as spinal cord injury (SCI) and glaucoma, and the peripheral nervous injury (PNI) can lead to widespread organ and neurological dysfunction, impairing muscular movements, causing respiratory issues, loss of independence, and increased psychological morbidities. In Canada, the annual costs associated with these conditions exceeded \$3 billion from 2001 to 2011. Moreover, 16 million people have suffered from blindness primarily due to glaucoma over the last decade, with predictions of a threefold increase by 2020.

The current challenges in repairing nervous system injuries, whether in the CNS or PNS, stem from limited regenerative capabilities following nerve damage or degeneration. As a result, 90% of neuron damage and neurodegenerative diseases result in devastating and permanent effects. The CNS presents more complex regenerative challenges compared to the PNS, due to its protective structure from glial cells and the secretion of anti-neural growth factors. In the PNS, mild or superficial nerve injuries rarely lead to gap formation between the proximal and distal ends, whereas severe damage can cause gaps ranging from 1mm to 20mm. Following nerve damage, Wallerian degeneration occurs, leading to scar tissue and neuroma accumulation, which can disrupt nerve regeneration and lead to functional impairment.

Despite over two centuries of development in treatment methods, including nerve grafts and nerve conduits in the PNS, fully operationalizing and understanding the mechanisms of neuronal regeneration and growth factor modulation remains challenging.

Selecting suitable cell types and growth factors, along with modified implanted biomaterials, could successfully induce neuron signaling pathways, becoming key requirements for re-establishing neural connections and reconstructing the cellular structure and its surrounding environment in both the CNS and PNS. Olfactory ensheathing cells (OECs), a type of glial cell, can support continuous axon regeneration and extension in both CNS and PNS injuries due to their myelinating abilities similar to Schwann cells, making them suitable for treating spinal cord injuries. OECs possess various molecular signals, including neurotrophic factors like NGF, BDNF, GDNF, and NT-4/5, extracellular matrix molecules such as N-CAM, and other growth factors.

Desirable material selections and designs can provide axonal guiding properties to facilitate neural regrowth and induce neuronal/glial migration. This includes selecting synthetic, natural, or combined materials, surface modifications, and designing bulk properties. Synthetic polymers, such as PCL, PLA, and PLGA, offer versatile properties that meet various tissue implant requirements. However, their foreign nature to the human body can provoke rejection, and their long degradation periods and toxic byproducts limit long-term implant applications. Surface modifications to improve cell attachment and encapsulate growth factors, along with controlling mechanical properties and degradation rates, are strategies believed to be future trends in bio-scaffold design.

Research on biomaterials for repairing both CNI and PNI has focused on autogenous nerves and artificial biomaterials, but few have been applied clinically. Although autogenous nerve repair strategies are considered the gold standard due to their compatibility and minimal side effects, they have drawbacks, including donor morbidity, sensation loss at the donor site, and complications such as tubular collapse and poor regeneration. Developing 3D living hybridized scaffolds for cell replacement and tissue engineering aims to promote regeneration after injury or disease, offering mechanical support and enhancing molecular interactions, including NGF secretion and modulation.

In the intricate domain of biomedical engineering, the judicious selection of biopolymers and materials is paramount, particularly when endeavouring to emulate the native extracellular matrix (ECM). The physicochemical properties, biocompatibility, biomechanical robustness, and enzymatic degradation kinetics of these selected polymers play a pivotal role in the success of tissue engineering interventions.

Electrospinning has emerged as a fundamental technique in the repertoire of advanced biomaterial fabrication. Through the application of a high-voltage electric field, electrospinning facilitates the extrusion of ultrafine fibres from a viscoelastic polymer solution or melt. Its capability to synthesize nanofibres with diameters similar to those of native ECM fibrillar components, combined with the precision in topographical alignment and hierarchical architecture, underscores its efficacy for biomimetic scaffolding across diverse biomedical applications [14-19].

In the realm of peripheral nerve regeneration, the design parameters of scaffolds take precedence. Peripheral nerve injuries, resulting from traumatic events or surgical resections, present with limited intrinsic regenerative capabilities. The consequent restoration of neuronal functionality mandates scaffolds that not only offer a conducive microenvironment for Schwann cell proliferation but also impart topographical cues for guided axonal sprouting and elongation [20-23]. Electrospinning, with its ability to generate aligned

nanofibres, is instrumental in crafting conduits that facilitate such directed neurite outgrowth. By calibrating parameters such as polymer solution rheology, electric field gradients, and collector design, one can fine-tune the morphological attributes of the electrospun scaffolds. This ensures enhanced cellular infiltration, bio-integration, and imparts both biomechanical resilience and axonotropic guidance for neurite extensions.

Furthermore, the surface chemistry of these electrospun nanofibres can be functionalized with bioactive moieties, neurotrophic factors, or specific ligands to enhance neuronal cell-matrix interactions, promoting neural cell adhesion, proliferation, differentiation, and even synaptogenesis. Electrospun conduits for peripheral nerve regeneration can be augmented further as stratified or composite structures, incorporating elements such as controlled-release microspheres delivering neurotrophic factors, or piezoelectric materials to modulate the cellular microenvironment.

2.2 Material Selection and Electrospinning Techniques in Nerve Tissue

Engineering

Selecting suitable materials is a pivotal aspect of electrospinning, directly influencing the characteristics and efficacy of the resulting scaffolds tailored for specific applications. The ideal scaffold for nerve regeneration should possess several key properties: biocompatibility to minimize inflammation, controlled biodegradability with non-toxic by-products, sufficient porosity to facilitate vascularization and cell migration, and a three-dimensional structure with mechanical properties that closely mimic the natural extracellular matrix. This process involves an array of options, encompassing natural and synthetic polymers, blends, and composites, each contributing uniquely to the scaffold's properties. The field of electrospinning commonly utilizes several categories of natural polymers, including collagen [24], gelatine [19, 25], chitosan (CS) [26-31], silk fibroin [32, 33], and hyaluronic acid (HA). These polymers are widely recognized for their applications in this area due to their biocompatibility, biodegradability, and ability to promote cell adhesion and growth. These polymers also closely mimic the structure and functions of ECM, which can be advantageous in applications such as tissue engineering. However, natural polymers exhibit batch-to-batch variability and limited mechanical strength.

Synthetic polymers, such as , Polylactic acid (PLA) [34-38], Poly (lactic-co-glycolic) acid (PLGA) [36, 39, 40], Polyethylene oxide (PEO) [16, 41-44], Polyglycerol sebacate (PGS) [45], Polycaprolactone (PCL) [19, 24, 30, 46, 47] and etc., are often used in electrospinning for their controllable degradation rates, tuneable mechanical properties, and processability. Synthetic polymers offer greater reproducibility and more predictable behaviour compared to natural polymers. However, they lack bioactivity and require surface modification to promote cell adhesion and proliferation.

Furthermore, blending polymers with both natural and synthetic polymers can help achieve a balance between the advantageous properties of both types of materials, including mechanical properties, controllable degradation rates, inducing growth and differentiation rates of cells and improved biocompatibility. [19, 41, 46]. Blending polymers to create electrospun scaffolds is a technique widely used in material science, especially for biomedical applications, where the customization of the properties of scaffold is crucial. The optimal blend ratio is determined based on the specific application and the desired characteristics of the scaffold. In tissue engineering, for instance, in nerve regeneration, the mechanical properties of the scaffold are of utmost importance. Scaffolds for this purpose require a delicate balance between strength and flexibility to support and guide the regeneration of delicate nerve tissues. The polymer blend ratio can be adjusted to achieve specific tensile strengths and elasticities that are conducive to nerve growth and protection. Controlled degradation rate

is another crucial factor. In nerve regeneration, the scaffold should degrade at a rate that corresponds with the regeneration and healing of nerve tissues, providing consistent support without hindering natural tissue growth. Scientists can modify the polymer blend to fine-tune this degradation rate, ensuring it aligns with the nerve healing process. Biocompatibility is essential, as the scaffold must not only support nerve cell adhesion and growth but also facilitate the intricate process of nerve differentiation and regeneration. Specific polymer blends can enhance these properties, making them ideal for scaffolds used in nerve repair and regeneration. Porosity and surface structure also play a significant role, influencing nerve cell migration and the distribution of nutrients and growth factors. A scaffold with optimal porosity can facilitate better cell infiltration and vascularization, essential for nerve tissue engineering.

Bioactive property is often essential for nerve regeneration, which requiring scaffolds potentially release neurotrophic factors or other substances that promote nerve growth and healing. Polymer blends can be engineered to include these bioactive substances, providing controlled release as required. Minimizing immunogenicity is also vital, as any immune response could potentially interfere with nerve regeneration. Scaffolds must be designed with non-immunogenic polymers to avoid inflammation or rejection when implanted.

Furthermore, composite materials which formed by incorporating inorganic materials, nanoparticles, or growth factors into the electrospinning process can create composite scaffolds with enhanced properties, such as enhanced mechanical strength, electrical conductivity, or biological activity. For instance, adding hydroxyapatite for bone tissue engineering or incorporating conductive materials like carbon nanotubes for nerve tissue engineering are notable examples.

In conclusion, the selection of materials for electrospinning is crucial in determining scaffold properties, including mechanical strength, biocompatibility, controlled degradation rate, porosity, surface topography, bioactivity, immunogenicity, and suitability for tissue engineering applications. A comprehensive evaluation of desired properties, alongside the advantages and limitations of various materials, is essential to optimize scaffold design and performance in tissue engineering and other biomedical applications.

2.2.1 Natural Polymers

Collagen, a primary constituent of the native ECM, collagen has been extensively electrospun to fabricate scaffolds for peripheral nerve repair. Its exceptional biocompatibility and bioactivity encourage Schwann cell adhesion, proliferation, and differentiation. The fibrous scaffolds derived from collagen closely emulate the native neural ECM, promoting axonal guidance and growth [24]. Collagen fibres can be electrospun into nano- to micro-scale fibres, creating a topographical environment that mimics the natural neural matrix. This

structural mimicry provides an ideal substrate for Schwann cell colonization and axonal regeneration [24, 30].

Collagen scaffolds promote cellular adhesion due to the presence of integrin-binding sites. This enhances Schwann cell proliferation, spreading, and phenotypic maintenance essential components for peripheral nerve regeneration [25, 48, 49]. Moreover, the fibrous collagen scaffold provides topographical cues, guiding the direction of neurite outgrowth. Due to its natural solubility, collagen easily blends with other polymers or incorporates neurotrophic factors. Additionally, cross-linking can be used to modulate the degradation kinetics and mechanical strength of collagen.

Gelatine, derived from collagen, possesses favourable gel-forming properties and is widely utilized in electrospinning. The biodegradability of gelatine-based scaffolds ensures a gradual replacement with the host tissue. When cross-linked, gelatine fibres exhibit enhanced mechanical properties can be enhanced, providing robust support to regenerating nerves [19, 25]. The thermo-reversible gelation properties of gelatine make it suitable for electrospinning, often producing smooth and uniform fibres. Blending it with synthetic polymers can further enhance the mechanical properties of the resulting scaffold. Much like collagen, gelatine scaffolds support cellular adhesion, proliferation, and differentiation. The presence of RGD (Arginine-Glycine-Aspartate) sequences in gelatine enhances integrin-mediated cell-matrix interactions [19, 25]. Gelatine can be chemically cross-linked to modulate its degradation rates. Incorporating bioactive molecules, like growth factors or anti-inflammatory agents can further optimize the regenerative environment.

CS, a natural polysaccharide derived from chitin, CS exhibits excellent biocompatibility and possesses innate antibacterial properties. Electrospun CS scaffolds can be tailored to feature aligned fibres, which provide directional guidance for axonal growth [29-31, 50]. Hydrophilicity of CS also makes it an attractive candidate for drug delivery within nerve conduits, allowing for the sustained release of neurotrophic factors. Due to its polycationic nature, CS can be smoothly electrospun, especially when blended with other polymers. Aligned CS fibres provide effective guidance channels for regenerating axons. The polycationic nature of CS enables strong interactions with negatively charged cell membranes, thereby promoting cellular adhesion [29-31, 50]. Furthermore, its hydrophilic nature ensures adequate nutrient diffusion, essential for cell survival and function. CS can be functionalized with peptides, growth factors, or other bioactive molecules, thanks to its reactive amino groups. Additionally, its hydrophilicity makes it conducive for encapsulating and releasing neurotrophic agents to aid nerve regeneration [51, 52].

Silk fibroin, extracted from silkworms, offers remarkable mechanical properties and biocompatibility. Electrospun silk fibroin scaffolds can be designed to exhibit controlled degradation rates, ensuring that the scaffold remains intact throughout the nerve regeneration process. Moreover, secondary structure of silk fibroin allows for functional modifications, such as the incorporation of bioactive peptides or growth factors. Silk fibroin can be electrospun into ultrafine fibres featuring smooth surface morphology. Its ability to form stable β -sheet structures enables the creation of fibres with impressive mechanical strength, essential for supporting regenerating nerve tissue [32, 33]. Notably, biocompatibility is a hallmark of silk fibroin, its interaction with neural cells facilitates cellular adhesion, proliferation, and differentiation. The mechanical strength of scaffold, combined with its bioactivity, creates an environment that not only supports but actively encourages nerve regeneration. Silk fibroin can undergo a variety of modifications. Enzymatic or physical treatments can adjust its degradation rate. Additionally, integrating bioactive molecules like neurotrophic factors or peptides into silk fibroin scaffolds to enhance their regenerative potential. Surface modifications can further improve cell adhesion and neurite extension [32, 33].

Alginate, derived from brown seaweed, is known for its excellent gel-forming properties. Although direct electrospinning of alginate can be challenging due to its high viscosity, blending alginate with other polymers, such as PVA, can be effectively electrospun to produce fibrous scaffolds suitable for nerve repair. **Electrospinning Properties:** Due to its high viscosity and ionic nature, direct electrospinning of alginate can be challenging. However, blending alginate with other polymers, like PVA or PEO, can facilitate its electrospinning [49, 53]. The resultant fibres maintain the biocompatibility and moisture retention capabilities of alginate, making them suitable for nerve tissue engineering. The hydrophilic nature of alginate favors cell encapsulation and nutrient diffusion. It provides a moist environment conducive for cell survival and proliferation. Moreover, its gentle gelation properties ensure minimal cell damage, making it suitable for co-electrospinning with cells or bioactive agents. Alginate can be modified to control its degradation rate and improve its mechanical properties. Cross-linking with divalent cations like calcium, can stabilize alginate scaffolds. Additionally, introducing functional groups enables the attachment peptides, growth factors, or other signalling molecules, amplifying its regenerative capabilities. alginate exhibits unique attributes that make them advantageous materials for crafting scaffolds aimed at peripheral nerve repair via electrospinning. Its biocompatibility, combined with their adaptability to various modifications, ensures an optimal environment for nerve regeneration [49, 53].

PHB, a member of the PHA family, is a biopolymer that has garnered attention in the field of tissue engineering. Extracted from various microorganisms, PHB and its derivatives are noted for their inherent biocompatibility with human tissues. These derivatives are classified based on the number of carbon atoms

in their chains, ranging from SC-PHAs containing 3-5 carbon atoms, MC-PHAs containing 6-14 carbon atoms, and LC-PHAs containing more than 15 carbon atoms. PHAs, including PHB, find diverse applications in biomedical fields such as tissue engineering, drug delivery, and the development of pharmaceutically active compounds.

The distinct properties of PHB, like high crystallinity and the ability to be fabricated into electrospun nanofibres with diameters typically ranging from 2-20 μm , make it a promising material for nerve tissue engineering. The alignment and physical guidance provided by PHB nanofibres support the growth of neurons and glial cells, effectively mimicking the ECM and facilitating cell adhesion [54]. Furthermore, due to its slow degradation rate under physiological conditions, PHB can provide a stable temporary support structure without leading to the accumulation of acidic byproducts at the implant site. Its excellent tensile strength and elasticity are crucial for enhancing the stability of PHB-containing composite scaffolds under high stress conditions [55].

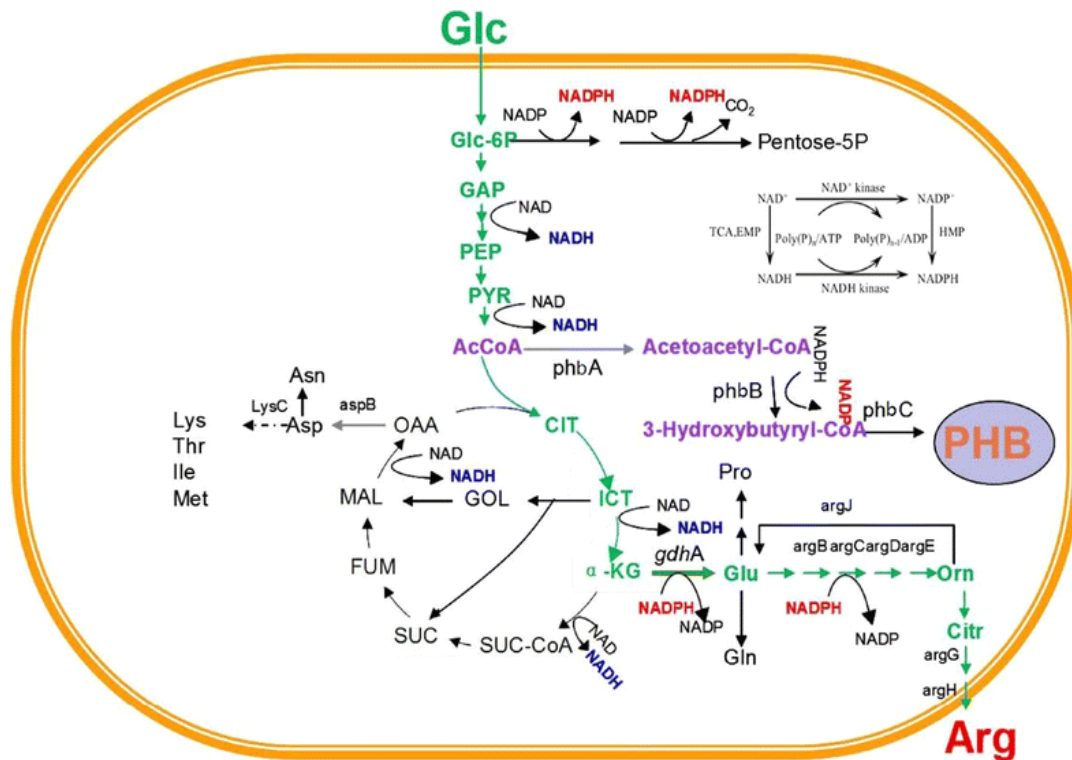


Figure 2.1: Fabrication Process of PHB from Bacterial Metabolic Pathway [56].

2.2.2 Synthetic Polymers

In the field of tissue engineering and regenerative medicine, synthetic polymers have garnered significant attention for their versatile properties and diverse potential applications. These polymers are particularly valued for their tuneable properties, biocompatibility, and their efficacy in supporting cell growth and facilitating tissue regeneration. Amongst the array of synthetic polymers being explored, certain candidates stand out due to their promising applications in the biomedical field. Notably, PLA[34-38], PLGA [36, 39, 40], PEO [16, 41-44], PGS [45], and PCL [19, 24, 30, 46, 47] have emerged as particularly promising materials. Each of these polymers brings distinct advantages and functionalities to the realm of biomedical applications, highlighting the expanding role of synthetic materials in advancing medical science (Table 1).

PLA is a thermoplastic polymer synthesized from lactic acid, known for its excellent mechanical strength, biocompatibility, and biodegradability. These properties render PLA an ideal candidate for drug delivery systems and tissue engineering applications [34-38]. Despite its advantages, relatively slow degradation rate of PLA and inherent hydrophobicity might restrict its use in some biomedical applications [34, 35]. Addressing these limitations, blending PLA with other polymers has shown potential in enhancing its properties, thereby broadening its applicability. Notably, PLA has been recognized for its efficacy in promoting nerve tissue regeneration, with promising applications in treatments for conditions such as glaucoma and aiding the regrowth of retinal ganglion cells [34].

PLGA is a copolymer of lactic acid and glycolic acid. It offers tuneable properties through the modification of the molar ratio. Exhibiting biocompatibility, biodegradability, and mechanical properties, it is suitable for tissue implantation, drug delivery, and neural tissue engineering [36, 39, 40]. Research has investigated the effectiveness of PLGA in promoting the growth and functional recovery of retinal ganglion cells and in preventing scar formation in glaucoma drainage devices[39, 40]. However, consideration should be given to the acidic degradation byproducts of PLGA and its potential to induce inflammatory reactions [36].

PEO is a synthetic polymer characterized by its biocompatibility, biodegradability, and processability. Electrospun PEO scaffolds have demonstrated potential in supporting axonal growth and enhancing nerve function recovery [44]. While PEO alone may lack optimal bioactivity for nerve regeneration, blending it with natural polymers has shown improvements in bioactivity and guided growth [41, 42]. Further research and optimization are required to enhance scaffold properties for nerve regeneration applications [44].

PGS is a biodegradable polymer synthesized from glycerol and sebacic acid. Due to its biocompatibility and tuneable mechanical properties, PGS is suitable

for tissue engineering and the replacement of various soft tissues, including cardiac muscle, nerves, blood vessels, cartilage, and the retina [45, 57, 58]. PGS has demonstrated promise in promoting cell attachment, proliferation, and ECM synthesis. Furthermore, PGS-based devices have been developed to closely mimic native physiological conditions.

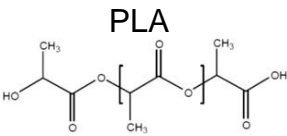
PCL is a semicrystalline polymer is a semicrystalline polymer, recognized for its biocompatibility and slow degradation kinetics. PCL has been widely utilized as a template in cell cultures, particularly demonstrating potential in enhancing cell differentiation in the field of retinal progenitor cells [24, 30, 47]. Blending PCL with other polymers, such as silk fibroin and gelatine, has been shown to improve properties and functionality, particularly in creating 3D scaffolds.

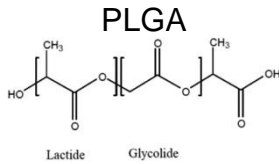
2.2.3 Composite polymers

Recent research has increasingly focused on multiphase polymers' system, particularly due to the anisotropic nature of various tissues, including nerves. While single polymers have shown promise in nerve fibre regeneration, issues such as mismatched mechanical properties or degradation rates compared to cellular growth and differentiation rates remain. For example, Radulescu et al. utilized PCL- Poly-D,L-lactic Acid (PDLLA) co-polymers created through ink-jet fabrication to produce cylindrical nerve conduits, which, when co-cultured with human embryonic kidney cells, supported neuron growth factor release and differentiation [59]. Similarly, Pant et al. discovered that PCL-PLA thin films with sodium hydroxide (NaOH) surface treatment enhanced nerve and glial cell adhesion [47]. However, merely mixing and fabricating polymer solutions often fails to adequately control nerve growth patterns. For instance, retinal ganglion cells, which are bipolar neurons, require tailored structures for effective connection to optical nerve heads. Milosevic et al.'s use of a PCL-PLGA-PCL tri-layer structure for controlled Rhodamine B release exemplifies innovation in postoperative therapy, yet practical applications in tissue engineering remain underexplored [60]. Building on this, composite materials have become prominent in electrospinning for nerve regeneration, combining the advantages of various materials for superior scaffold performance. These composites typically include both natural and synthetic polymers and bioactive molecules, enhancing biocompatibility, mechanical strength, and fostering cell attachment, proliferation, and axonal growth. While natural polymers like collagen, CS, gelatine, silk fibroin, and HA are known for biocompatibility and support cell adhesion and growth, they lack in mechanical strength and stability [41]. On the other hand, synthetic polymers such as PLGA, PCL, and PEO offer improved mechanical attributes and controllable degradation rates but might lack bioactivity for optimal nerve regeneration [61]. By merging natural and synthetic polymers, composite scaffolds achieve a balance of biocompatibility, mechanical properties, and degradation rates, suitable for nerve regeneration. For instance, PCL/collagen [62] or PLGA/gelatine [36] composites have shown promise in peripheral nerve regeneration and spinal cord injury repair. Additionally, the integration of bioactive molecules like growth factors or ECM components can further enhance scaffold performance, offering a versatile approach to scaffold design that caters to specific nerve regeneration needs

[63] [64]. This highlights the necessity for ongoing research to optimize composite scaffold properties and explore new material combinations for more complex nerve regeneration models.

Table 1: Biomaterials and their applications in nerve tissue engineering..

PLA			
Chemical structures	Treatment methods	Materials Processing and its Scaffold structure	Results
<p>Degradation time: 12-24 months for degradation Youngs modulus: 1.8-4.1GPa for modulus which depends on its crystallinity</p>			
 <p>PLA</p>	<p>RGCs only or combined with Netrin-1</p>	<p>1. Electrospinning with random alignment and radial alignment of fibre</p>	<ol style="list-style-type: none"> 1. Increased retinal ganglion cells (RGCs) survival while allowing the RGCs to retain their electrophysiological properties. 2. Help orient the axon growth of RGCs to align with axon bundles in the host retina. 3. Greater than 50% of RGCs direct their axons toward the scaffold centre with netrin-1 bonded.
PLGA			
<p>Mechanical stiffness: 1.4–2.8 GPa Degradation rate: 6-12 months for degradations</p>			



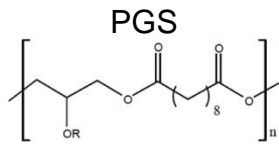
Human iPSCs
Human embryonic stem (hESs) cells

1. Electrospinning with the random alignment of fibres
2. Salt leaching PLGA scaffold structure.

1. Enhanced numbers of neural structures
2. Cultured with both Neuron growth factor (NGF) and NT-3 when compared with the control medium could enhance neural network set up and vascularization.
3. Provide a promising vehicle for a functional RGCs cell monolayer implantation in the subretinal space in patients

PGS

Mechanical stiffness: 0.282±0.025 MPa
Degradation rate: 1-2 months



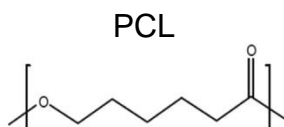
Mouse retinal progenitor cells biocompatibility

1. Electrospinning method
2. Good biocompatibility, elasticity, porosity, and a micro topology

1. Combining mRPCs with PGS scaffolds for subretinal transplantation is a practical strategy for advancing retinal tissue engineering as a restorative therapy.

PCL

Mechanical stiffness: 206-344 MPa
Biodegradation: >24 months



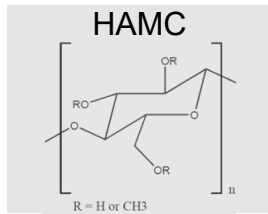
Mouse retinal progenitor cells (mRPCs) and Mouse retinal progenitor cells (mRPCs)

1. Electrospinning methods.
2. Random alignment scaffold

1. Increased mouse retinal progenitor cells (mRPC) integration rates and help cells localized around the plc.
2. RPCs proliferate and express mature retinal proteins which allow for the migration and differentiation of new cells into the normal and degenerated retina.

HAMC

Scaffold types: hydrogel
Mechanical stiffness: 1-100MPa
Degradation period:10-15 days



Deliver
neuroprotective
molecule,
erythropoietin (EPO)

Condensation
polymerization

1. Controllable
releasing rate of
growth factors or
drug.

2.3 Electrospinning process and parameters

Extensive research and developments on electrospinning techniques have been done during the last two decades. Electrospinning exhibits notable advantages owing to its versatility when compared to other nanofibre fabrication methods, such as self-assembly, phase separation, or solvent casting [65-67]. Particularly, in contrast to phase-separation techniques, electrospinning can generate nanofibres characterized by a high surface-to-volume ratio and a porous structure. These attributes lead to the formation of numerous inter- and intra-fibrous pores, greatly enhancing the ease of cell infiltration [68]. Electrospinning is composed of a controllable syringe with a viscous conductive polymer solution, a blunt metallic needle with a specific diameter, a high-voltage power supply, and a grounded conductive collector. Electrospinning is usually initiated by the voltage applied on the metallic needle, which allows electric charges to transfer into the polymer solution [69]. the internal charge inside the polymer solution will be whipped by the external voltage and drawn through the direction of the collector. The full motion will cause polymer chains to stretch and slide past each other and become fibres with micro to nano-sized[40]. Upon electrification, the electrostatic repulsion among the surface charges that feature the same sign deforms the droplet into a Taylor cone, from which a charged jet is ejected. When the critical applied voltage is reached, stretched polymer droplets form and draw out into ultrafine fibres and fabricate on the collector [70-72]. Achieving the desired uniform fibre dimensions and surface morphology requires the manipulation and variation of process parameters during electrospinning, especially when working with different solutions, applied voltages, working distance [70-72].

Electrospinning parameters can be adjusted, and their outcomes can be influenced by various factors. Ensuring a significant presence of smooth, bead-free areas with consistent fibre length is essential for customizing the biomaterial's biocompatibility to align with the precise demands of tissue implantation. It is worth highlighting that "smooth fibres" commonly refer to fibres characterized by their absence of beads or irregularities. Electrospinning

parameters are broadly classified into two types: solution parameters, which include molecular weight, viscosity, conductivity, and surface tension, and process parameters like applied voltage, working distance, and flow rate. Additionally, ambient conditions like humidity and temperature also play a significant role. These parameters are crucial as they influence the formation of smooth, bead-free fibres, essential for applications in tissue implantation. Mastery of these parameters is essential for fine-tuning electrospinning processes, particularly when targeting specific fibre characteristics. This precision is particularly critical in applications like tissue implantation, where the choice between smooth, non-cell adhesive surfaces, or rough, cell-adhesive surfaces, can significantly impact the success of the implantation procedure. Understanding and controlling these parameters thus lays the foundation for harnessing the advantages of electrospinning, as discussed in the following section.

2.4 Advantages of Electrospinning

Electrospinning, distinguished in the field of nanofibre fabrication, is particularly renowned for its capacity to precisely manipulate fibre size and morphology. Also, electrospinning showed a feature challenging to emulate using traditional fibre production methodologies. Its adaptability to a broad spectrum of materials, ranging from polymers to biological substances, is instrumental in the synthesis of fibres with specific functional attributes, tailored for an array of applications. One of the paramount benefits of electrospun fibres is their elevated surface-to-volume ratio, which significantly augments their efficacy in sectors such as drug delivery, filtration, and tissue engineering. In addition, the interconnection between each pore formed between fibres plays a crucial role in applications necessitating fluid transport and cellular interactions, exemplified in nerve regeneration and tissue scaffold development. The scalability of electrospinning is a salient feature, rendering it a viable option for industrial-scale production, pertinent across various industries. Furthermore, the role of solvent selection in the determination of fibre characteristics highlights the technique's adaptability, enabling the fine-tuning of fibres to meet specialized requirements in material science and biomedical engineering. Collectively, these attributes underscore the significance of electrospinning as a fundamental technique in the realm of advanced material fabrication, offering extensive prospects for innovation and diverse applications in multiple scientific disciplines.

2.4.1 Precise Fibre Control

A key advantage of electrospinning is its capacity for precise control over fibre size and morphology. By fine-tuning parameters such as applied voltages, flow rates, and collector configuration, the diameter of electrospun nanofibres can be accurately adjusted from a few nanometres to several micrometres. This degree of control over fibre dimensions is notably challenging to replicate with conventional processing techniques. Such precise control over fibre

characteristics allows for the customization of mechanical, chemical, and surface properties of the nanofibres, rendering them versatile for various applications. These include tissue engineering scaffolds, drug delivery systems, and filtration membranes.

2.4.2 Material Versatility

Electrospinning is compatible with a wide array of materials, including polymers, composites, ceramics, and biological substances [25, 73-79]. This versatility enables the fabrication of nanofibres with a wide range of functionalities and properties. Various polymers can be electrospun individually or in combination to create composite fibres boast enhanced mechanical strength or specific surface characteristics. The choice of materials in electrospinning can be strategically tailored to suit specific application needs. For instance, biocompatible polymers are ideal for developing tissue engineering scaffolds [80-82], whereas conductive polymers are apt for use in electronics and energy storage applications [83]. Besides, electrospinning can also be modified by different fabrication techniques, included co-electrospinning, co-axial electrospinning, emulsion electrospinning, near field electrospinning and etc. [83]

2.4.3 High Surface-to-Volume Ratio

The ultrafine structure of electrospun nanofibres results in an exceptionally high surface-to-volume ratio, a unique characteristic that offers numerous advantages across various applications. This large surface area facilitates efficient interactions with the surrounding environment, such as enhanced adsorption capabilities or increased catalytic activity. In drug delivery systems, this high surface area permits a greater drug loading capacity and facilitates controlled release kinetics [18, 84-87]. Moreover, the high surface-to-volume ratio augments the efficiency of filtration and separation processes by providing a larger capture area for particles or gases.

In tissue engineering, the high surface-to-volume ratio of these nanofibres is particularly advantageous. It promotes cell attachment, proliferation, and differentiation by offering an extensive surface area for cell adhesion and nutrient exchange. Moreover, this increased surface-to-volume ratio enhances the biomimetic properties of electrospun scaffolds, making them closely resemble the ECM, a crucial factor for successful tissue regeneration and integration of cells into the scaffold structure.

2.4.4 Interconnected Porosity

A notable characteristic of electrospun nanofibres is their interconnected porous structure. Research have observed that the cells were difficult migrate into the file membrane[11, 33, 44, 82]. Optimal interconnectivity between each pore can offer significant benefits in applications where fluid transport, cell infiltration, and nutrient diffusion are essential. In peripheral nerve regeneration,

for instance, scaffolds composed of electrospun nanofibres with interconnected pores have demonstrated efficacy in promoting axonal regeneration and guiding Schwann cell growth, essential for PNI repair [73, 76-78]. The porous structure of the scaffolds allows for nutrient and oxygen exchange, facilitating cell adhesion, proliferation, and tissue integration.

These scaffolds provide a biomimetic environment with their interconnected pores enabling cell migration and interaction, thus facilitating tissue regeneration and functional recovery [73, 88]. Additionally, the porosity of these scaffolds aids in the diffusion and controlled release of bioactive molecules like growth factors or drugs, enhancing the therapeutic efficacy of the systems [73, 88]. The interconnected pore structure of electrospun nanofibres can be tailored by adjusting electrospinning parameters such as polymer concentration, solvent choice, and collection setup. By optimizing these parameters, pore size, interconnectivity, and overall porosity can be controlled, allowing for the customization of scaffold properties to meet specific requirements in tissue engineering and regenerative medicine.

2.4.5 Scalability

Scalability is a critical advantage of electrospinning, rendering it highly suitable for industrial-scale production. The process can be readily adapted to larger setups and automated systems, facilitating the efficient and cost-effective fabrication of nanofibres in large quantities. This scalability proves particularly beneficial for applications requiring mass production, such as filtration membranes, tissue engineering scaffolds, and wound dressings. The ability to produce nanofibres in bulk not only ensures their availability for commercial use but also promotes their widespread implementation across various industries.

2.4.6 Solvent Selection

In the electrospinning process, the selection of solvents is critical and guided by two main criteria. Firstly, the solvent must be capable of completely dissolving the polymer intended for electrospinning. Secondly, the solvent should possess a moderate boiling point, which serves as an indicator of its volatility. Generally, solvents with higher volatility are preferred due to their rapid evaporation rates, which facilitate the swift removal of solvent from the nanofibres as they travel from the needle tip to the collector. However, solvents with excessively high volatility are typically avoided because their low boiling points and rapid evaporation rates can lead to premature drying at the needle tip, potentially clogging it and disrupting the electrospinning process. Conversely, solvents with low volatility are not favoured either, as their high boiling points can hinder complete drying during the nanofibre jet's flight, resulting in the deposition of solvent-laden nanofibres on the collector and consequently, the formation of beaded nanofibres. Various solvents, including CF, acetone, and DMF, have been utilized in PHB electrospinning. CF typically produces fibres with a narrow diameter distribution, whereas acetone and DMF

are known to result in fibres with a wider diameter distribution. Employing a solvent mixture, such as a CF and DMF blend, has been found effective in achieving fibres with a narrow diameter distribution. Moreover, the solvent choice also affects the fibres' crystallinity and mechanical properties. For instance, fibres spun using acetone exhibit higher crystallinity and improved mechanical properties compared to those produced with CF.

2.5 Applications of Electrospinning

Electrospinning, a technique integral to nanofibre fabrication, has found extensive applications across various scientific and industrial fields. Its ability to produce fibres with unique characteristics such as high surface area, porosity, and biomimetic features has made it indispensable in areas like biomedical engineering, filtration, and environmental protection. This section provides an overview of the key applications of electrospinning, demonstrating its versatility and the significant role it plays in advancing material science and technology.

2.5.1 Biomedical Engineering

Electrospun nanofibres have become a versatile and invaluable tool in biomedical engineering, with extensive applications in tissue engineering, drug delivery systems, wound dressings, and biosensors. Their distinct properties, including high surface area, porosity, and biomimetic characteristics, enhance cell adhesion, proliferation, and controlled release of therapeutic agents [7, 15, 21]

In tissue engineering, electrospun nanofibres serve as scaffolds that mimic the native ECM to support cell growth, migration, and tissue regeneration. The high surface area-to-volume ratio of the nanofibres facilitates effective nutrient exchange, oxygen diffusion, and waste removal, promoting favourable cellular responses [23, 35, 51, 89]. Additionally, the porous structure of electrospun nanofibre scaffolds allows for the infiltration and distribution of cells, enabling the formation of functional tissues. The alignment of nanofibres can also guide cell orientation and influence tissue organization [73]. These properties make electrospun nanofibre scaffolds highly desirable for the regeneration of various tissues, including skin, bone, cartilage, and nerve. In drug delivery, the large surface area and porosity of electrospun nanofibres enable a high drug-loading capacity and controlled release kinetics. This facilitates precise modulation of therapeutic agent delivery, optimizing therapeutic efficacy while minimizing side effects [18, 84-87]. By incorporating drugs or bioactive molecules into the electrospun fibres, controlled release profiles can be achieved, improving the therapeutic efficacy and minimizing side effects [46, 73, 75, 77, 83]. The ability to tailor the composition, morphology, and degradation properties of the nanofibres further enhances their potential as drug delivery systems [18, 84-87]. Electrospun nanofibres also play a vital role in wound healing. Their biomimetic properties, such as fibrous architecture and surface characteristics,

create an environment conducive to cell adhesion, migration, and proliferation, thus aiding in tissue regeneration [7]. Furthermore, the controlled release of growth factors or antimicrobial agents from the electrospun fibres can aid in wound healing processes [7]. In the field of biosensors, electrospun nanofibres offer unique advantages due to their high surface area and capacity to immobilize biomolecules, leading to improved sensitivity and selectivity in detecting target analytes [15]. The porous structure of the nanofibres also facilitates efficient analyte diffusion and interaction, enhancing the performance of the biosensing platform.

2.5.2 Filtration and Separation

The interconnected porous structure of electrospun nanofibres offers an efficient platform for filtration and separation processes, garnering significant attention in applications like air filtration, water purification, and protective clothing. In air filtration, nanofibres-based filters are highly effective at trapping airborne particulate matter, including pollutants, allergens, and microorganisms. The fine diameter and high surface area of these nanofibres enhance filtration efficiency through mechanisms like interception, diffusion, and impaction [90]. These filters offer improved air quality and find applications in industries, healthcare facilities, and home environments.

For water purification, electrospun nanofibre membranes, characterized by an optimal distribution of fine pores, structured arrangements, and high porosity, efficiently remove contaminants such as suspended solids, bacteria, and viruses from water, all while maintaining structural integrity without collapse. [19, 69, 93]. These membranes can also feature surface modifications or functional groups for improved selectivity and antimicrobial properties [19, 67, 91]. These membranes can be designed to have specific surface modifications or functional groups to enhance their selectivity and antimicrobial properties. Electrospun nanofibre-based membranes are utilized in portable water filtration devices, wastewater treatment systems, and desalination processes.

Electrospun nanofibres can offer enhanced barrier properties against hazardous particles, liquid droplets, and aerosols. The small pore size and complex network within the nanofibres provide effective protection, crucial in healthcare, cleanroom, and chemical handling environments [77, 92]. These protective garments find applications in healthcare settings, cleanrooms, and chemical handling environments.

The versatility of electrospinning allows for the customization of nanofibre membranes and filters by selecting suitable materials, fibre morphology, and pore size distribution. Current research is directed towards enhancing the filtration efficiency, durability, and scalability of these membranes to meet the increasing demand for advanced filtration and separation technologies.

2.6 Other fabrication methods

In the arena of advanced biomaterials for nerve regeneration, various fibre production techniques have garnered significant attention due to their ability to create specialized structures conducive to neural repair. Each method, with its unique mechanism and properties, contributes distinctly to the development of nerve conduits and scaffolds. These techniques include wet spinning, dry-jet wet spinning, dry spinning, melt spinning, flash spinning, gel spinning, centrifugal spinning, and emulsion electrospinning. They collectively offer a diverse array of fibre characteristics essential for nerve tissue engineering, such as controlled porosity, mechanical strength, biocompatibility, and tailored drug release profiles. This section provides a comprehensive overview of these fibre production methods, emphasizing their specific roles and contributions in fabricating scaffolds and conduits for nerve regeneration. It underscores the diverse potentials of these techniques in advancing nerve repair and regeneration, illustrating how each method's unique properties can be harnessed to develop effective solutions for neural tissue engineering.

2.6.1 Wet spinning

Wet spinning is a fibre production process in which a polymer solution is extruded through a spinneret into a coagulating bath of a non-solvent for the polymer (Figure 2.2). As the polymer solution enters the coagulating bath, the solvent is rapidly removed, causing the polymer to solidify and form a continuous fibre. The coagulating bath may be a liquid or a gas, depending on the specific polymer being used. In some cases, the bath may also contain additives that modify the properties of the resulting fibre, such as cross-linking agents or surfactants. Generally, three kinds of coagulation baths has been commonly used: acid, salt and solvent coagulation bath. For acid coagulation bath, the fibre is immersed in an acidic solution, such as sulfuric acid or HCl, to solidify the fibre. The advantages of this method include the ability to control the porosity and surface properties of the fibre, as well as the ease of the process. However, it may result in environmental concerns due to the hazardous nature of the acidic solution. In salt coagulation bath, the fibre is immersed in a solution of salt, such as sodium chloride or calcium chloride, to solidify the fibre. The advantages of this method include the ease of the process, the ability to produce uniform fibres, and the low cost. However, it may result in high salt concentrations in the wastewater, which can lead to environmental concerns. And for solvent coagulation bath the fibre is immersed in a solvent, such as acetone or methanol, to solidify the fibre. The advantages of this method include the ability to produce fibres with excellent mechanical properties and the ability to control the porosity and surface properties of the fibre. However, it may result in environmental concerns due to the toxicity of the solvents used.

Wet spinning is commonly used to produce synthetic fibres, such as rayon and acrylic, as well as some natural fibres such as lyocell (Tencel). The process can be used to produce fibres with a wide range of properties, including strength, flexibility, and moisture-wicking ability, by varying the polymer and coagulating bath compositions, as well as the spinning conditions. Wet-spun PHB fibres offers several advantages in the production of nerve conduits. Firstly, it allows for precise control over the diameter of the resulting fibres, which is important as the fibres need to be small enough to mimic the structure of natural nerve tissue and facilitate nerve regeneration. Additionally, wet-spun PHB fibres have shown high mechanical strength and stiffness, providing support and guidance for the regeneration of nerve cells[19, 93]. PHB is also a biocompatible and biodegradable polymer, which reduces the risk of complications or adverse reactions, when the nerve conduits are implanted. Wet spinning is a simple and cost-effective method for producing PHB fibres, making it a viable option for large-scale production of nerve conduits. Finally, PHB can be modified with various chemical and biological agents to enhance its bioactive and biocompatibility which could promote nerve growth, and wet spinning can be used to incorporate these agents into the fibres, allowing for customized nerve conduits with not only on promoting cell proliferation and differentiation, but also improve neurons infiltration through the scaffold structure, and provide guidance to axonal ingrowth between injured sites.

Bini *et al.* has reported the development of a nerve conduit made from PHB fibres produced by wet spinning, which were then characterized for their mechanical and biological properties [94]. Lezcano *et al.* had also describes the development of a PHB fibre mat produced by wet spinning, which was then used to create a scaffold for nerve tissue engineering [88]. The mechanical and biological properties of the fibre mats were characterized, and their ability to support nerve regeneration was evaluated. Furthermore, Li *et al.* has reports the development of a PHB/collagen fibre mat produced by wet spinning, which was then used to create a scaffold for nerve tissue engineering [11]. The fibre mats were characterized for their mechanical and biological properties, and their ability to support nerve regeneration was evaluated. Moreover, Kondyurin *et al.* described the development of a nerve conduit made from PHB fibres produced by wet spinning, which were then characterized for their mechanical and biological properties [93]. The PHB nerve conduits were evaluated for their ability to support peripheral nerve regeneration. In conclusion, these studies collectively indicate that PHB fibres, especially when produced through wet spinning, are promising materials for the development of nerve conduits and scaffolds. The focus on characterizing the mechanical and biological properties of these PHB-based materials underscores their suitability in supporting nerve regeneration. With their ability to be engineered for specific mechanical properties and biocompatibility, PHB fibres and composites are proving to be valuable in the creation of effective scaffolds for nerve tissue engineering.

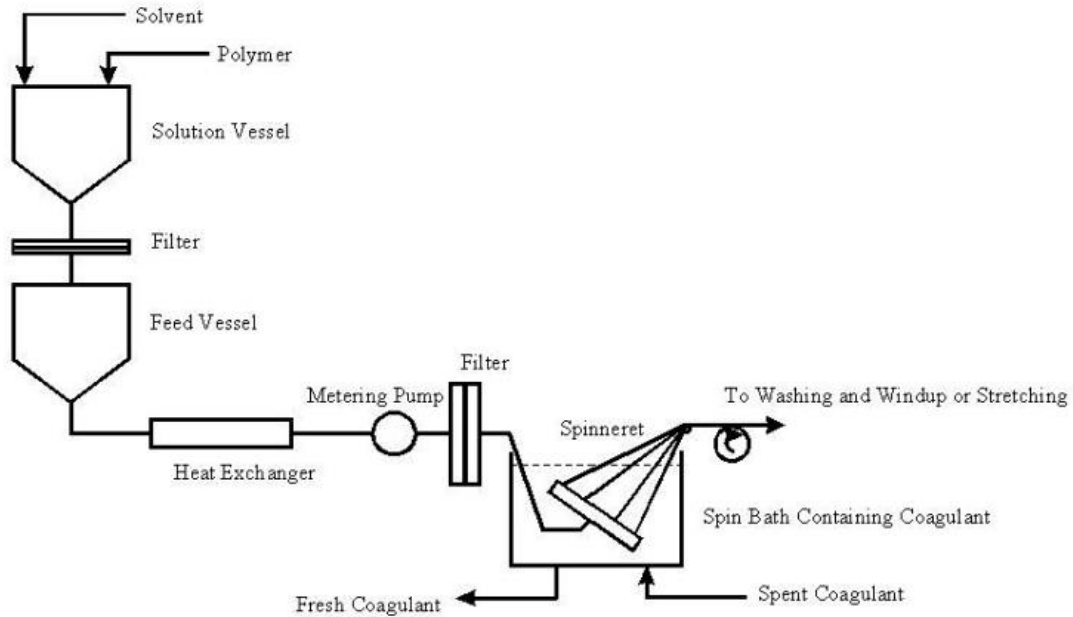


Figure 2.2: Schematic diagram of Wet Spinning Process [95]

2.6.2 Dry-jet wet spinning

Dry-jet wet spinning is a technique employed for creating continuous fibres or filaments from a polymer solution. This method is an adaptation of the traditional wet spinning process, where a polymer solution is extruded into a coagulation bath to form fibres. In dry-jet wet spinning, the polymer solution is extruded through a spinneret into a chamber, where a stream of warm air or gas is passed over the extruded filament (Figure 2.3). This warm air rapidly evaporates the solvent from the filament, forming a dry, solid filament. The dry filament is then passed through a coagulation bath to complete the solidification process and set the structure of the fibre. The coagulation bath used in dry-jet wet spinning is typically an aqueous solution, such as water, and may contain a coagulating agent or a cross-linking agent. The bath serves to further solidify the filament and remove any residual solvent. Dry-jet wet spinning offers a significant advantage over traditional wet spinning methods, primarily in its capability to fabricate fibres that consistently achieve dimensions in the nanometre range, enhancing the precision and applicability of the resulting materials in various scientific and industrial contexts. Specifically, this advanced technique can produce fibres with diameters <100 nanometres or even less, depending on the materials and specific process parameters used, as well as better control over the fibre diameter and the structure of the fibre. It also allows for higher production speeds and reduced solvent usage, making it more environmentally friendly. Dry-jet wet spinning is commonly used to produce synthetic fibres such as nylon, polyester, and polypropylene, as well as specialty fibres such as aramid and carbon fibres. It is also used to produce biopolymer fibres such as cellulose, chitin, and CS [96].

Dry-wet spinning is a promising method for producing PHB nerve conduits, which involves extruding a polymer solution through a spinneret into a coagulation bath, followed by washing and drying the resulting fibres. This method offers several advantages over other techniques for producing nerve conduits. Firstly, it allows to produce fibres with a wide range of diameters and porosities that can be tailored to meet specific requirements for nerve regeneration. The diameter and pore size of the fibres can be optimized to mimic the natural structure of nerve tissue and promote nerve growth. Secondly, dry-wet spinning is a simple and cost-effective method for producing PHB nerve conduits that can be easily scaled up for large-scale production. Additionally, PHB is a biocompatible and biodegradable polymer that is safe for use in the body and can be broken down over time, reducing the risk of complications or adverse reactions. Lastly, dry-wet spinning can be used to produce composite fibres by combining PHB with other materials, such as PLA or CS, to enhance their mechanical and biological properties and improve their effectiveness as nerve conduits. Overall, dry-wet spinning of PHB fibres shows great promise for the development of nerve conduits for tissue engineering applications, offering tuneable properties and a biocompatible and biodegradable material for nerve regeneration and repair.

Several recent studies have explored the use of dry jet wet spinning to develop composite fibres and fibre mats for nerve regeneration applications. Tian *et al.* developed composite fibres made from PHB and PLA using dry jet wet spinning and evaluated their mechanical and biological properties [93]. Bagheri *et al.* produced PHB/CS nanofibrous scaffolds via dry jet wet spinning and characterized their mechanical and biological properties, as well as their ability to support nerve tissue regeneration in vitro [37]. Wang *et al.* described the development of a nerve conduit made from PHB and PLA nanofibres produced by a modified dry/wet spinning method, which had a graded pore structure to mimic the natural environment of nerve tissue [73]. The nerve conduit was evaluated for its ability to support nerve regeneration in vitro and in vivo. Miao *et al.* developed composite fibre mats made from PHB and PLA using dry jet wet spinning and evaluated their mechanical and biological properties, as well as their potential for nerve regeneration in vitro [97]. These studies demonstrate the potential of dry jet wet spinning as a method for producing nerve regeneration materials with tuneable properties and structures.

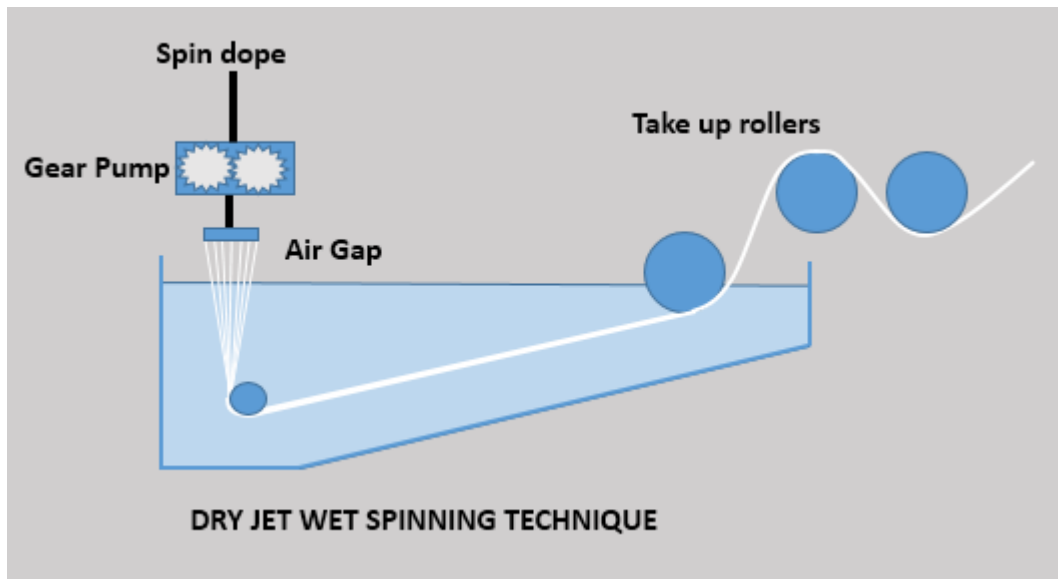


Figure 2.3: Schematic diagram of Dry-jet wet Spinning [98]

2.6.3 Dry spinning

Dry spinning is a fibre production process that involves the use of a solvent to dissolve a polymer and then extrude the solution through a spinneret into a warm air chamber (Figure 2.4). The warm air evaporates the solvent, leaving a solid polymer fibre. In dry spinning, the spinning solution is prepared by dissolving the polymer in a volatile organic solvent, such as acetone or DMF. The polymer is usually in the form of flakes or pellets, which are fed into a mixing vessel along with the solvent. The mixture is heated and agitated until the polymer is fully dissolved. The spinning solution is then extruded through a spinneret, which is typically made of metal or ceramic and has small holes or slits that determine the size and shape of the resulting fibre. The extruded fibres pass through a warm air chamber, where the solvent evaporates, leaving behind solid polymer fibres. After the fibres are formed, they may be stretched or drawn to orient the polymer molecules and improve the mechanical properties of the fibre. The fibres are then wound onto a spool or collected in a package for further processing. The advantages of dry spinning include the ability to produce fibres with elevated levels of molecular orientation and excellent mechanical properties. It also allows to produce fibres from polymers that are difficult to dissolve in water or other common solvents. However, it is a more expensive and complex process compared to wet spinning or melt spinning. Dry spinning is commonly used to produce synthetic fibres such as acrylic, polyamide, and polyurethane, as well as specialty fibres such as carbon fibre and aramid fibre. It is also used to produce diverse types of natural fibres, such as rayon and lyocell [19, 93, 96].

Several studies have explored the use of dry spinning to develop nerve conduits and fibres made from PHB for nerve regeneration applications. Zhang *et al.* developed electrospun PHB nerve conduits using dry spinning and evaluated

their mechanical properties and ability to support nerve regeneration in vitro [99]. Zhang *et al.* modified the surface of electrospun PHB nerve conduits using dry spinning to improve their biocompatibility and ability to promote nerve regeneration [100]. Kim *et al.* used dry spinning to produce PHB fibres for nerve regeneration applications and evaluated their mechanical and biological properties [76]. Wang *et al.* developed a PHB/PLLA blend nanofibres nerve conduit using dry spinning and evaluated its ability to support peripheral nerve regeneration in vivo [6]. These studies demonstrate the potential of dry spinning as a method for producing PHB nerve conduits with tuneable properties and structures that can promote nerve regeneration and repair, making it a promising approach for nerve tissue engineering.

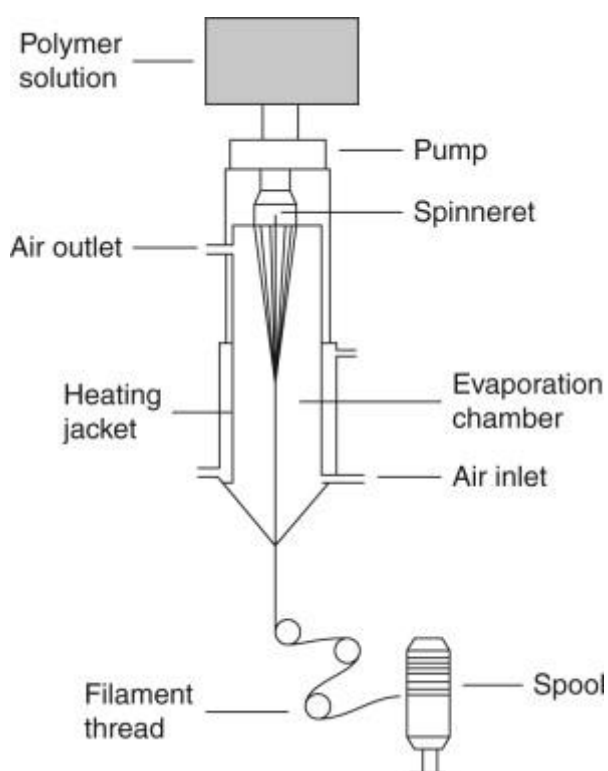


Figure 2.4: Schematic diagram of Dry spinning [96]

2.6.4 Melt spinning

Melt spinning is a fibre production process that involves melting a polymer and then extruding it through a spinneret to form continuous fibres (Figure 2.5). The process is commonly used to produce synthetic fibres such as polyester, nylon, and polypropylene. In melt spinning, the polymer is first melted using heat and mechanical agitation. The molten polymer is then forced through a spinneret, which is a metal plate or tube with multiple holes or slits that determine the size and shape of the fibres. The extruded fibres are then cooled and solidified as they pass through a cooling chamber. The solidified fibres are then drawn or

stretched to orient the polymer molecules and improve the mechanical properties of the fibre. This stretching process may be done by passing the fibres through a series of heated rollers, which apply tension and heat to the fibres. After the fibres are formed and oriented, they may be wound onto a spool or collected in a package for further processing. The resulting fibres are strong, durable, and have an elevated level of molecular orientation, which gives them excellent mechanical properties. The advantages of melt spinning include the ability to produce fibres with high tensile strength, excellent heat resistance, and good dimensional stability. It is also a simple and low-cost process compared to other fibre production methods.

Several studies have explored the use of melt spinning to develop nerve conduits and PHB fibres for nerve regeneration applications. Yu *et al.* developed a nerve conduit made from PHB fibres produced by melt spinning, which were characterized for their mechanical and biological properties [79]. The potential of the nerve conduit for peripheral nerve regeneration was evaluated in vitro and in vivo. Shi *et al.* produced composite fibres using dry spinning with PHB and PCL and evaluated their mechanical and biological properties, as well as their potential for nerve regeneration in vitro [46]. Krieg *et al.* also conducted a study where they developed microfibrils using melt spinning technique with PHB. The researchers evaluated the mechanical and biological properties of the microfibrils and investigated their potential for use in nerve tissue engineering in vitro [101]. The results of their study demonstrated that the PHB microfibrils have potential for use in nerve tissue engineering. These studies demonstrate the potential of melt spinning as a method for producing PHB nerve conduits and fibres with tailored properties and structures that can support nerve regeneration and repair.

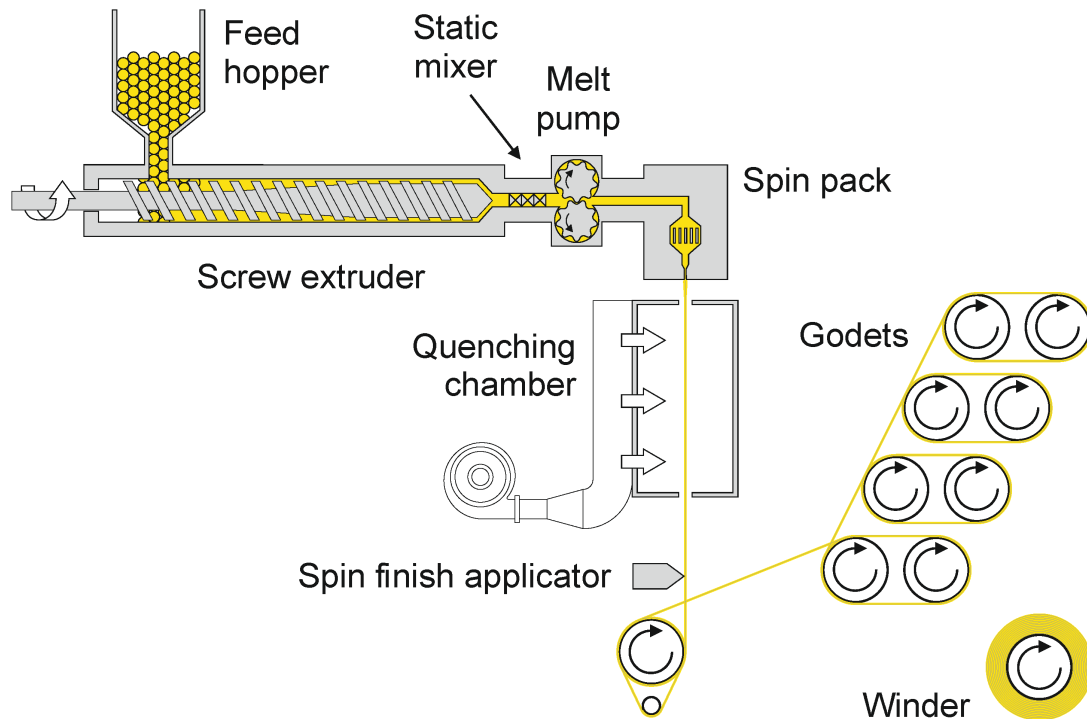


Figure 2.5: Schematic diagram of Melt spinning [102]

2.6.5 Flash spinning

Flash spinning is a process used to produce ultrafine fibres with diameters of microns or nanometres (Figure 2.6). It is a variation of the melt spinning process that involves rapid cooling of the extruded polymer to solidify it in the form of fine fibres. In flash spinning, the polymer is melted and extruded through a spinneret into a high-velocity stream of gas or air, typically at supersonic speeds. The high-speed gas rapidly cools and solidifies the extruded polymer, forming ultrafine fibres. The fibres produced by flash spinning are typically highly uniform in diameter and have a high degree of molecular orientation, giving them excellent mechanical properties. Several studies have mentioned that PAN, PS and PA6 which produced by flash spinning had an average diameter of 1.2-2.2 micrometres and a tensile strength of 0.2 to 1.9 GPa. These values are normally higher than any other spinning[13, 103, 104] They also have a high surface area-to-volume ratio, which makes them ideal for use in a wide range of applications, such as filtration media, medical textiles, and energy storage devices.

Flash spinning is commonly used to produce fibres from a variety of polymers, including nylon, polyethylene, and polypropylene. The process can be scaled up for commercial production and can be easily integrated with other processing steps, such as drawing or surface modification. However, the process can be more complex and expensive compared to other fibre production methods, and it involves the use of a high-pressure, rapid expansion process to create a web-like structure of interconnected fibres, and precise

control over the process conditions, which can be costly to set up and maintain. Flash spinning is an uncommon technique for producing fibres, and there is limited research available on its use in PHB nerve conduit applications. Compared to other spinning methods like wet spinning, dry spinning, and melt spinning, flash spinning has been less explored in the context of nerve conduit development. However, some studies have investigated the use of flash spinning for other biomedical applications, such as tissue engineering scaffolds and wound dressings. Bhardwaj *et al.* developed tissue engineering scaffolds made from polyurethane fibres produced by flash spinning and evaluated their mechanical and biological properties[18], as well as their potential for tissue regeneration in vitro and in vivo. Sun *et al.* developed a wound dressing made from CS and poly(ethylene oxide) fibres produced by flash spinning and evaluated its potential for wound healing in vitro and in vivo[7]. Desai *et al.* developed tissue engineering scaffolds made from poly(lactic acid) fibres produced by flash spinning and evaluated their mechanical and biological properties, as well as their potential for tissue regeneration in vitro and in vivo[90]. While there is limited work in using flash spun PHB for nerve conduit development, these studies suggest the potential of flash spinning as a method for producing fibres with tuneable properties and structures for various biomedical applications.

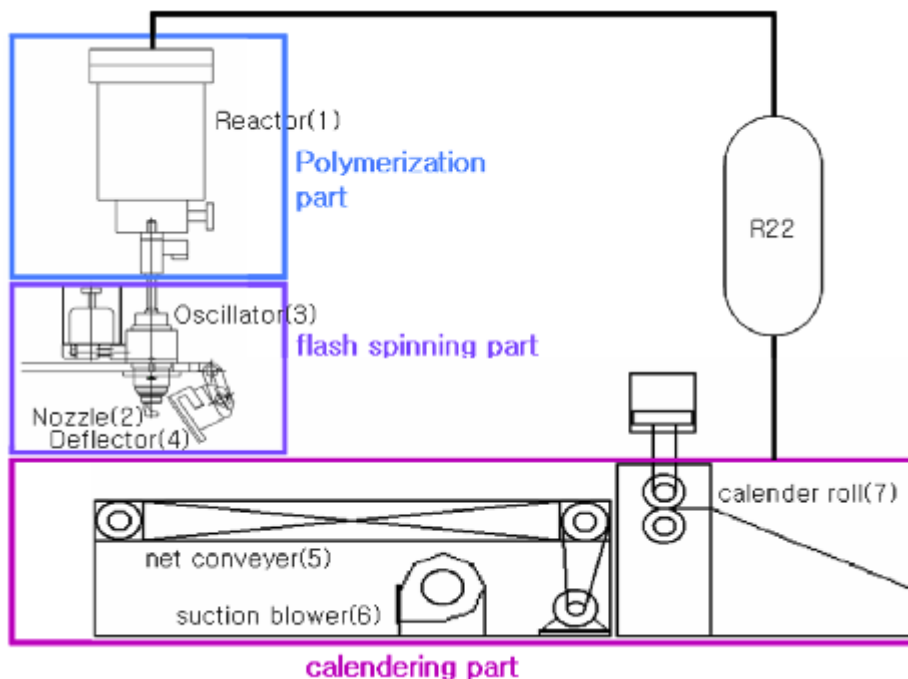


Figure 2.6: Schematic diagram of Flash spinning [105]

2.6.6 Gel spinning

Gel spinning, also known as solution spinning or dry-wet spinning, represents a sophisticated fibre fabrication technique that involves the utilization of a specialized spinning solution or gel. This process, intricately detailed in Figure 2.7, is pivotal in the production of high-strength fibres endowed with unique mechanical properties. Primarily employed in the synthesis of high-performance fibres, the method yields fibres with exceptional tensile strength, stiffness, and durability. Gel spinning can fabricate these fibres use in different applications, encompassing the use of advanced materials like aramids, ultra-high molecular weight polyethylene (UHMWPE), and a range of biopolymers. In gel spinning, a polymer is first dissolved in a suitable solvent to form a spinning solution or gel. The spinning solution or gel is then extruded through a spinneret into a coagulation bath, which causes the solvent to evaporate and the polymer to solidify into a fibre. The resulting fibres are typically highly oriented and have a high degree of crystallinity, which gives them excellent mechanical properties, such as high tensile strength and modulus, as well as resistance to abrasion, impact, and fatigue.

Gel spinning can be further classified into two types: dry spinning and wet spinning. In dry spinning, the spinning solution is extruded into a warm air chamber or oven to evaporate the solvent and solidify the fibre. Whilst in wet spinning, the spinning solution is extruded into a coagulation bath to solidify the fibre. Gel spinning is commonly used to produce fibres for a wide range of applications, including bulletproof vests, ropes, cables, and composites. However, the process can be complex and expensive, and may require specialized equipment and expertise.

For dry spinning of PHB nerve conduits, Yu *et al.* developed a nerve conduit made from PHB fibres produced by dry spinning. They found that PHB dry-spun fibrous membranes has increased 15% in both elongation and toughness compared to electrospun's, and its also showed 6% more human peripheral nerve cells proliferating within the membranes [77]. Kim *et al.* also used dry spinning to produce PHB fibres for nerve regeneration applications, and evaluated that PHB promotes more uniaxial nerve regeneration along the nerve conduits with 60 days, and remain its structure stability until 94[89]. Additionally, Wang *et al.* reported on the development of a PHB/PLLA blend nanofibre nerve conduit using dry-wet spinning, and evaluated its stability to support peripheral nerve regeneration in vivo [106].

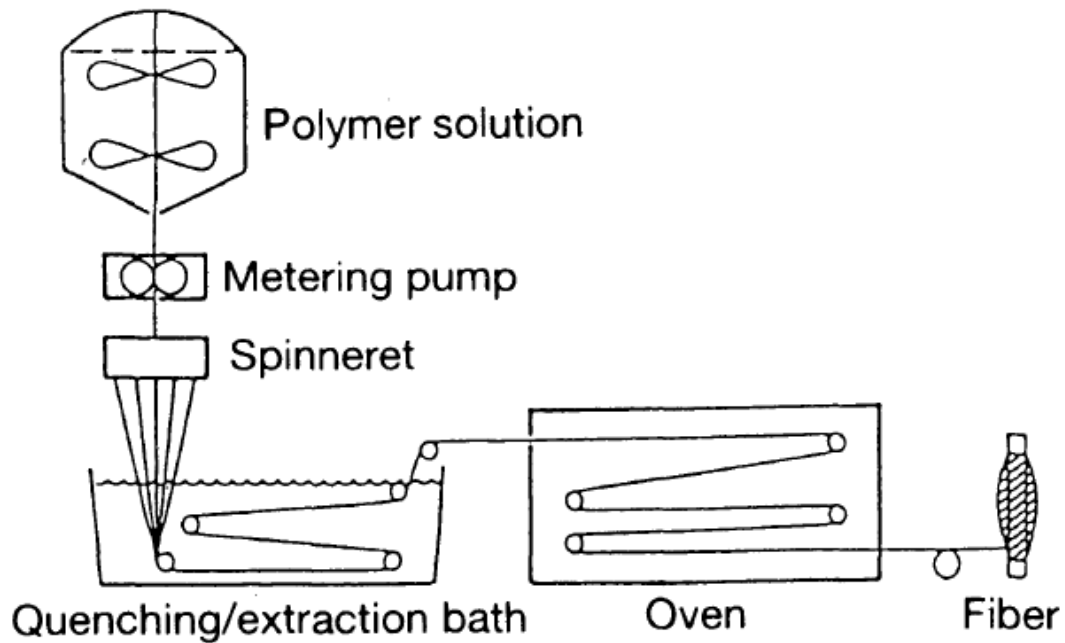
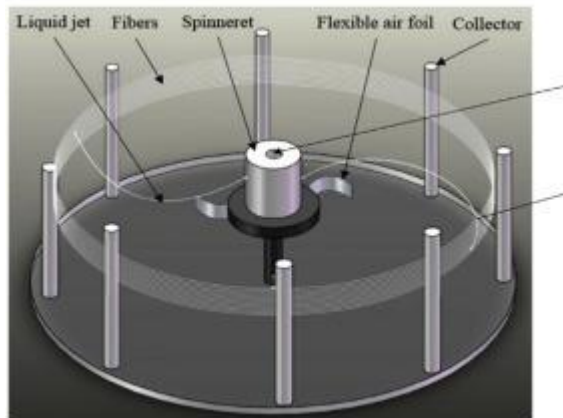


Figure 2.7: Schematic diagram of Gel spinning [107]

2.6.7 Centrifugal spinning

Centrifugal spinning is a fibre production process that involves the use of centrifugal force to extrude a polymer solution through a spinneret to form fibres (Figure 2.8). The process is commonly used to produce fibres from natural and synthetic polymers such as cellulose, proteins, and polyvinyl alcohol. In centrifugal spinning, the polymer solution is first prepared by dissolving the polymer in a suitable solvent. The solution is then placed in a spinning chamber, which is rapidly rotated around a central axis. The centrifugal force causes the solution to move outward towards the walls of the spinning chamber, where it is extruded through a spinneret to form fibres. The fibres produced through this process are typically highly uniform in diameter and exhibit a high degree of molecular orientation, which imparts excellent mechanical properties to them. The fibres may be further treated by drawing or stretching to improve their mechanical properties and enhance their performance.

Centrifugal spinning is commonly used to produce fibres for a wide range of applications, including medical textiles, filters, and packaging materials. It is a simple and low-cost process compared to other fibre production methods, and it can be easily scaled up for commercial production. Centrifugal spinning boasts several advantages, including the capacity to generate fibres that exhibit a high degree of uniformity and consistency in their mechanical properties. Additionally, this method allows for the production of fibres from a diverse array of polymers, further enhancing its applicability across various domains.



Centrifugal Spinning Device

Figure 2.8: Schematic diagram of Centrifugal spinning techniques [20]

Centrifugal spinning is a less common spinning technique compared to other methods such as wet spinning, dry spinning, and melt spinning, and there is limited research available on its use with PHB in nerve conduit applications. However, some studies have investigated the use of gel spinning for other biomedical applications, such as tendon and ligament repair. Li *et al.* developed fibres from a blend of polyethylene glycol terephthalate and polybutylene terephthalate using gel spinning and evaluated their mechanical and biological properties, as well as their potential for tendon and ligament regeneration *in vitro* and *in vivo*. Lu *et al.* reviewed the use of gel spinning to produce fibres from silk fibroin for various biomedical applications, including tissue engineering and drug delivery, and discussed the mechanical and biological properties of the resulting fibres. Dong *et al.* developed tissue engineering scaffolds made from silk fibroin fibres produced by gel spinning and evaluated their mechanical and biological properties, as well as their potential for tissue regeneration *in vitro* and *in vivo*. While there is limited research available on the use of gel spinning in PHB nerve conduit development, these studies suggest the potential of gel spinning as a method for producing fibres with tenable properties and structures for various biomedical applications. While there may not be much research specifically on gel spinning using PHB in nerve conduit applications, these studies provide some insight into the potential of gel spinning for biomedical applications.

2.6.8 Emulsion electrospinning

Emulsion electrospinning is a fibre production process that combines the techniques of electrospinning and emulsion polymerization to produce fibres with controlled morphology and properties (Figure 2.9). The process is commonly used to produce nanofibres from water-insoluble polymers and is useful in applications such as tissue engineering, drug delivery, and filtration.

In emulsion electrospinning, a polymer is first dispersed in a non-solvent medium to form an emulsion. The emulsion is then electrospun using a high-

voltage power supply to produce nanofibres. The high voltage electric field causes the polymer droplets to deform and elongate into nanofibres, which are collected on a grounded collector. The nanofibres produced high uniformity in diameter. Furthermore, emulsion electrospinning enables the fabrication of fibres with uniaxial orientation, significantly enhancing their mechanical properties. They may also have a porous structure, which makes them suitable for use in filtration and tissue engineering applications.

Emulsion electrospinning is commonly used to produce fibres from water-insoluble polymers such as PLGA and PS. The advantages of emulsion electrospinning include the ability to produce nanofibres with controlled morphology and properties, as well as the ability to produce fibres from water-insoluble polymers.

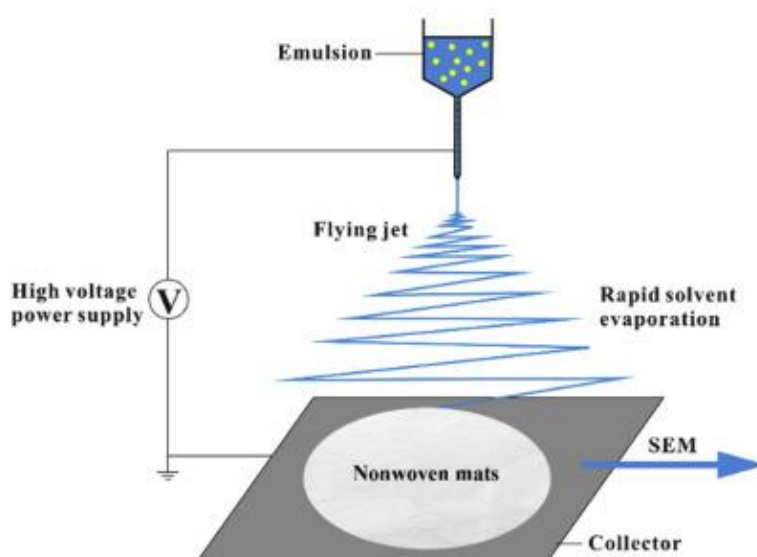


Figure 2.9: Schematic diagram of Emulsion techniques [91]

Emulsion spinning is a new spinning technique, and there is limited research available on its use with PHB in nerve conduit applications. However, some studies have investigated the use of emulsion spinning for other biomedical applications such as drug delivery and wound healing. Zhang *et al.* developed polymeric nanoparticles using emulsion spinning and evaluated their size, morphology, and drug release profile, as well as their potential for drug delivery in vitro [102]. Lomasney *et al.* produced hydrogels using emulsion spinning and evaluated their mechanical and biological properties, as well as their potential for wound healing in vitro and in vivo [102]. Liu *et al.* produced fibres made from a blend of PLA and gelatine using emulsion spinning and evaluated their mechanical and biological properties, as well as their potential for tissue engineering in vitro [91]. While there may not be much research specifically on

emulsion spinning using PHB in nerve conduit applications, these studies provide some insight into the potential of emulsion spinning for various biomedical applications. Further research is needed to determine the feasibility and effectiveness of using emulsion spinning for PHB nerve conduit.

Table 2: Comparison of Spinning Methods for Peripheral Nerve Injury: Advantages, Disadvantages, Fibre Sizes, and Applications with References

Spinning Method	Process	Pros	Cons	Fibre Sizes	Ref
Electrospinning	A process where a high voltage is applied to a polymer solution or melt to form a jet that is collected on a grounded target.	High surface area, high porosity, and small fibre diameter. Suitable for micro or nanomodification; Easy to fabricate in lab.	Hard to manufacture in large scale.	50 nm - 10 μ m	[6, 7, 16, 68, 108]
Wet Spinning	A process where a polymer solution is extruded into a coagulation bath to form fibres.	Suitable for large scale production, high mechanical strength.	Limited control over fibre diameter and requires solvents that may be harmful to cells.	1 - 50 μ m	[19, 93, 109]
Dry-Wet Spinning	A process where a polymer solution is extruded into a dry environment followed by coagulation in a wet bath.	High mechanical strength,	Limited to specific polymers and solvents and requires specialized equipment.	1 - 50 μ m	[96]

Dry Spinning	A process where a polymer solution is extruded into a dry environment followed by solvent evaporation to form fibres.	High mechanical strength,	Limited to specific polymers and solvents and may require toxic solvents.	1 - 50 μm	[96]
Melt Spinning	A process where a polymer melt is extruded into fibres.	Suitable for large scale production, and no solvent is required.	Limited to specific polymers, and large fibre diameter.	10 - 100 μm	[20, 28]
Flash Spinning	A process where a polymer solution is extruded into a high-speed air stream to form fibres.	Suitable for large scale production, and no solvent is required.	Limited control over fibre diameter and may result in low mechanical strength.	0.5 - 50 μm	[105]
Gel Spinning	A process where a polymer solution is gelled before being extruded into fibres.	High mechanical strength.	Limited to specific polymers and solvents and requires specialized equipment.	1 - 50 μm	[19, 73]
Centrifugal Spinning	Extruded into a rapidly spinning container to form fibres.	Suitable for large scale production.	Limited to specific polymers and solvents, and requires specialized equipment.	1 - 50 μm	[20]

2.7 Current challenges in electrospun fibres in tissue engineering

PNI present significant challenges in clinical practice, underscoring the need for effective nerve regeneration strategies. Currently, autologous grafts are traditionally considered the gold standard for treating neural defects due to their compatibility and effectiveness. However, they are limited by the availability of donor nerves from the patient, potential mismatches in nerve size between the donor and recipient sites, risk of neuroma formation, and incomplete functional recovery. Allogenic grafts, derived from cadavers, are not constrained by donor nerve availability but face challenges related to host-graft immune rejection. To address these issues, research has focused on the potential of acellular nerve grafts to bypass immune rejection. Nonetheless, the lack of viable cells in acellular grafts can impede nerve regeneration and extracellular matrix remodelling, leading to delays in recovery. Nerve scaffolds represent a promising approach in facilitating PNI repair. These scaffolds function as structural frameworks, guiding and supporting axonal growth, which is crucial for functional recovery. However, optimising the efficacy of nerve scaffolds in tissue engineering involves overcoming several challenges. This section highlights the importance of nerve scaffolds in PNI repair and provides an overview of the current challenges that need to be addressed for successful nerve regeneration.

2.7.1 Inadequate Guidance Cues

Current nerve scaffolds often lack effective guidance cues essential for guiding the direction of damaged nerve growth and facilitating nerve regeneration. Insufficient provision of aligned nanofibres, growth factors, or cell-adhesive molecules can impede axonal guidance, hindering functional recovery. Various growth factors such as NGF, GDNF, neurotrophin-3, and FGF have been incorporated into nerve scaffolds to manipulate cell signalling pathways and induce nerve regeneration. These factors contribute to axonal outgrowth, nerve survival, and renewal [35, 44, 76, 88, 89]. Growth factors play a role in manipulating the cell signal pathway that induces nerve regeneration, these include promoting axonal outgrowth, nerve survival, and renewal. Meanwhile, suppressing factors, such as myelin-associated inhibitors (MAIs) and the chondroitin sulfate proteoglycans (CSPGs), might also release during regeneration and delayed repair of nerve lesions, which happened in more significant nerve gaps.

Effective delivery of growth factors within scaffolds requires systems with controllable degradation rates that align with the release rate of these factors [84]. In addition to growth factors, providing adhesion sites within nerve scaffolds is critical. These sites are influenced by surface morphology, including roughness and surface area [23, 42, 43, 86]. Microspheres and other materials

such as fibronectin mats, collagen matrices, and BSA can enhance the internal structure of scaffold [99]. These elements can be added during the fabrication process to create gradients of growth factors along the length of the nerve tube, supporting sustained regeneration and preventing axonal trapping [110]. Understanding the dynamics and mechanisms of growth factor release from these scaffolds remains challenging. This includes the kinetics of incorporated growth factors and their behavior within the human body. Consequently, characterizing these aspects both in vivo and in vitro is essential yet complex.

2.7.2 Mechanical Properties

The mechanical properties of nerve scaffolds play a critical role in providing structural support and mimicking the native nerve tissue. Ideally, a scaffold should possess mechanical properties that align with the anatomical site of implantation. Practically, it must also be robust enough to withstand surgical handling during the implantation process. However, many current scaffolds exhibit inadequate mechanical strength, elasticity, or flexibility, leading to suboptimal nerve regeneration outcomes and potential scaffold failure. The design of mechanical properties of PHB in nerve applications should be carefully considered in future research. Mechanical strength is a critical factor in scaffold design, as many nerve injury sites experience channel collapse after long-term implantation in the human body. Factors like repetitive compressive forces, specialized cell interactions (such as with macrophages), and elements accelerating material degradation can contribute to scaffold collapse, especially at nerve injury sites. In exploring nerve conduit design, Belkas *et al.* investigated the use of PHEMA and its copolymerization with MMA, finding that the latter demonstrated a bimodal response, effectively preventing the collapse of implants at nerve injury sites [74]. Researchers have proposed various strategies to enhance the mechanical strength of implant materials, including crosslinking, blending different materials, and adjusting material compositions. However, there is a growing concern that excessive emphasis has been placed on mimicking the mechanical properties of bone and cartilage in scaffold development. This focus has led to materials with impressive mechanical strength but at the expense of high porosity. Furthermore, many materials showing promise in vitro have not succeeded in vivo due to inadequate vascularization capacity. It is evident that a delicate balance between mechanical properties and a porous structure that promotes cell infiltration and vascularization are also crucial.

2.7.3 Biocompatibility

Biocompatibility is paramount for promoting cell adhesion, proliferation, and tissue integration within nerve scaffolds, yet challenges arise with synthetic materials that may trigger inflammation or foreign body responses. PHB electrospun fibres have garnered attention in nerve tissue engineering due to their biocompatibility, biodegradability, and tuneable mechanical properties[77,

111, 112]. However, optimizing cell transplantation and migration on these fibres remains a significant challenge for effective nerve conduits. A major hurdle is the limited cellular adhesion and migration on PHB surfaces, impeding the effective colonization of cells like Schwann cells or neural stem cells on the scaffold [76, 113]. Surface modifications, such as blending with other polymers, coating with ECM proteins, or chemical treatments, are explored to enhance cell adhesion and migration [36, 46, 114]. Another challenge is aligning electrospun fibres to guide axonal growth linearly, necessitating specialized electrospinning setups and parameters [73, 76, 114]. Moreover, it is crucial to achieve an appropriate balance between the mechanical properties of the scaffold and the desired cell behaviour. A scaffold with suitable mechanical properties would provide adequate support for regenerating nerve tissue while ensuring proper cell migration and axonal extension [73, 76]. Current research outcomes have demonstrated promising results in overcoming these challenges. Combining PHB with other biopolymers, such as PCL or CS, has shown improved cell adhesion and migration on the scaffolds [76, 113]. Additionally, the use of aligned electrospun fibres has demonstrated improved axonal growth guidance [76, 113].

2.7.4 Optimizing Topographical and Biochemical Cues

Well defined nanostructured topographical cues such as grooves, ridges, pores, nodes can influence cell-substrate interaction by promoting cell adhesion, migration, proliferation and differentiation to new tissue [78, 115]. Currently, achieving optimal cues, such as aligned topographical features and controlled release of growth factors or signalling molecules, remains a challenge. These cues are essential for directing cell behaviour and promoting axonal regeneration. Surface modification plays a vital role in enhancing the interaction between cells or proteins and implanted materials for PNI applications. Although the structure of nanofibres can mimic the ECM, specific biological factors, such as NGF [76], cells, and proteins, require binding sites to improve treatment efficiency. In the case of PHB electrospun nanofibres, surface modification can further improve their biocompatibility and functionality for nerve regeneration. For PHB-based scaffolds, it is essential to provide adhesion sites and biological factors to enhance cell attachment [116]. One approach to achieve this is by modifying the surface of PHB nanofibres with bioactive molecules, such as laminin, fibronectin, or collagen, which can improve cell adhesion and promote neurite outgrowth [117].

Surface roughness is another factor that can affect cell attachment and proliferation on PHB scaffolds. It has been reported that the introduction of roughness on the surface of PHB nanofibres improves cell adhesion and growth [4]. This can be achieved by altering the electrospinning process parameters, such as solvent systems or humidity, to create rough surfaces on the electrospun PHB fibres [3]. Additionally, blending PHB with other polymers can also enhance its surface properties. For example, blending PHB with CS or

PLGA can improve hydrophilicity and surface roughness, leading to better cell adhesion and proliferation on the scaffolds [36, 39, 40]. PHB electrospun fibres have attracted considerable attention in the field of nerve tissue engineering due to their biocompatibility, biodegradability, and tuneable mechanical properties [3]. However, challenges persist in optimizing cell transplantation and migration on PHB electrospun fibres for effective nerve conduits. One major challenge is the limited cellular adhesion and migration on the PHB surface, which hinders the effective colonization of seeded cells, such as Schwann cells or neural stem cells, onto the scaffold [2]. Surface modifications, such as blending with other polymers, coating with ECM proteins, or chemical treatments, can enhance cell adhesion and migration [76, 113]. Another difficulty is the optimal alignment of electrospun fibres to guide axonal growth in a linear manner. The fabrication of aligned PHB fibres may require specialized electrospinning setups and parameters [36, 39, 40]. Moreover, it is crucial to achieve an appropriate balance between the mechanical properties of the scaffold and the desired cell behaviour. A scaffold with suitable mechanical properties would provide adequate support for regenerating nerve tissue while ensuring proper cell migration and axonal extension [5]. Current research outcomes have demonstrated promising results in overcoming these challenges. Combining PHB with other biopolymers, such as PCL or CS, has shown improved cell adhesion and migration on the scaffolds [30, 46, 47]. Additionally, the use of aligned electrospun fibres has demonstrated improved axonal growth guidance [76, 113].

2.8 Future perspective

The development of nerve scaffold designs and parameters has been the focus of extensive research and investigation. However, current scaffolds have yet to fully combine single or multiple material systems capable of promoting functional recovery after nerve injury. To achieve this, a highly integrated approach that closely mimics the permissive ECM environment is necessary. The ideal scaffold should possess physical, chemical, and biological properties that include biodegradability, surface morphology, electrical activity, topography, surface modifications, polymer properties, cell adhesivity, cell infiltration and transplantation, and biomolecular delivery.

While most scaffolds used in nerve repair only satisfy one or two requirements, more recent implant designs are focused on constructing stable, interactive environments to achieve more effective functional regeneration. Injectable hydrogels with fibre reinforcements have become popular due to their flexible structure in complex shapes. However, to optimize complex biomaterials, it is crucial to establish communication and collaboration between biomaterial designers, neurobiologists, and surgeons.

Consequently, the primary objective of my research in nerve regeneration focuses on the creation and design of synthetic ECM using natural-based polymers, specifically PHB and CS, by electrospinning. An ideal scaffold for nerve regeneration must exhibit key characteristics, including biocompatibility to reduce inflammation, controlled biodegradability yielding non-toxic by-products, ample porosity for promoting vascularization and cell migration, and a three-dimensional architecture endowed with mechanical properties that emulate those of the natural extracellular matrix.

Furthermore, Both in vitro three-dimensional models and in vivo animal models are essential for evaluating materials within a practical environment. . By doing so, researchers can gain a better understanding of the mechanisms of nerve tissue regeneration and efficacy of new scaffold designs. In conclusion, future research should prioritize the development of an integrated approach that combines multiple material systems to promote functional recovery after nerve injury.

Chapter 3: Experimental details

3.1 Materials

The materials used in this study included PHB ($M_w \approx 660,000$ g/mol) and GA solution (GA, 50 wt. % in H_2O), both supplied by Merck, London, UK. CS, (medium M_w) and a H_2O_2 (50 v/v% solution), along with KOH (>99%), Tris-HCl, CF (>99.8% grade), DMF (anhydrous, >99.8% grade), and Forskolin (>98% HPLC) were all obtained from Sigma-Aldrich in St. Louis, MO, USA. Additionally, DA-HCl was sourced from Merck, and (TFA) Reagent Plus®, 99% was also used, procured from Merck. Acetic acid (>99% grade) was another component, acquired from Merck.

3.2 Electrospinning Setup

Needle set up: As shown in Figure 3.1, the needle setup consisted of using 10 ml syringes from the Spinbox Limited (located in Barcelona, Spain) fitted with 0.76mm inner diameter capillary tubing from Sterilin (UK) and a steel needle (18 gauge, 2.06mm inner diameter, 2.67mm outer diameter) from Stainless Tube & Needle Co Ltd (located in Staffordshire, UK) for each test.

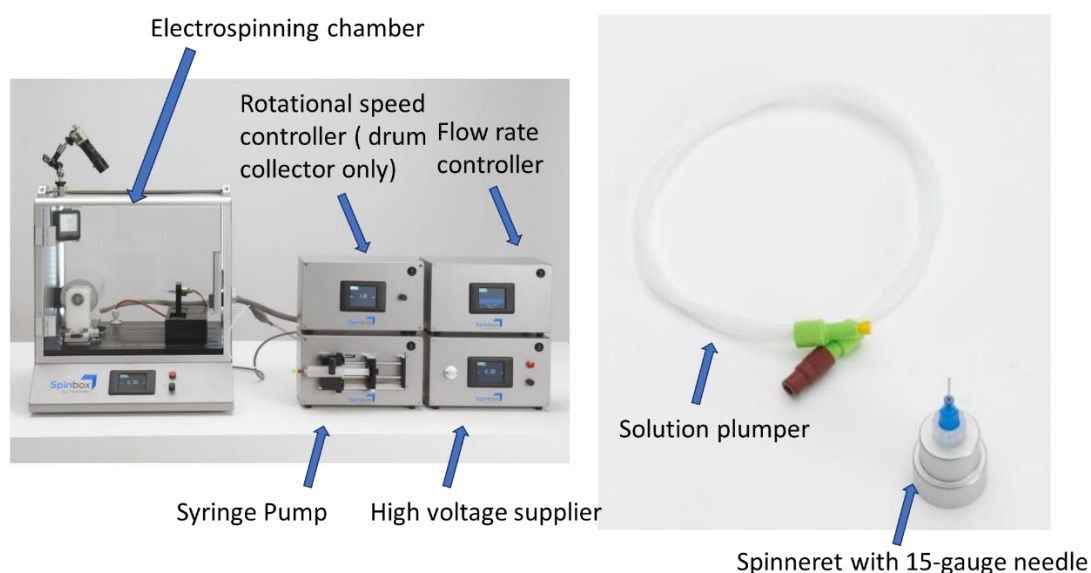


Figure 3.1: Electrospinning Equipment Setup for Nanofibres Fabrication, included electrospinning chamber, rotational speed, flow rate, syringe pump controller, high voltage supplier and spinneret with 18-gauge needle.

Syringe pump: The flow rates of the solution was controlled using a syringe pump (PHD 4400) from Harvard Apparatus (UK).

High voltage power supply: high precision voltage generator (FC 120W) from Spinbox Limited (Spain) with a voltage range of 0-30kV was utilized to connect the 18-gauge needle. The ground electrode was attached to a metal collector. Samples were collected on glass microscope slides and all experiments were conducted under ambient conditions (temperature of 21°C and humidity of 40-50%).

3.3 Sample preparation

3.3.1 Preparing PHB and CS solution with trifluoroacetic acid

Due to the large volume size of PHB pellets used in the polymer solution, mass to mass ratio (m/m%) will be used, whereas the others will be used as w/v%. the PHB solution was prepared by dissolving 1.5 g of PHB pellets and 0 to 0.5 g of CS separately in 10 ml of trifluoroacetic acid (TFA) and preparing 15 m/m% PHB with 0 to 5 w/v% CS in different compositions. During the dissolving, the PHB solution was first stirred for 4 h at room temperature at 400 rpm. Then, CS powder was gradually added into the PHB solutions and stirred at 100 rpm overnight until homogenous solutions formed.

3.3.2 Preparing PHB and CS solution with CF/DMF

In chapter 6-7, PHB solution was prepared by adding 1.5 g of PHB pellets into 10 ml CF/DMF (9:1 v/v) to form 15 m/m% PHB and stirring under reflux at 100°C for 3 hours until a homogenous solution formed. 2 w/v % of CS solution was prepared by adding 0.2g of CS powder into acetic acid/water mixing solution (1:9 v/v) and stirring at room temperature for 24 hours until homogenous. Furthermore, 0.2, 0.5, 0.8, 1, and 1.5 w/v% CS were prepared by serial dilution from 2 w/v% CS solution. All solutions were stored at room temperature and sealed with Parafilm until further use.

3.3.3 Fabrication of PHB and PHB/CS electrospun fibres

In all chapter, randomly PHB electrospun fibres were fabricated via single-jet electrospinning. 15 w/v % PHB solutions were placed in a 5 ml thermos syringe with an 18-gauge needle. Based on the operation diagrams of the PHB/CF/DMF solution system, the process parameters were set as below: flow rates at 2 ml/hr and electric field strength 0.5 kV/cm (applied voltages and working distance to ratio). The electrospun PHB membranes were collected by aluminium foil and washed with ethanol/de-ionised water after fabrication three times, this helped to remove extra CF and DMF present in samples.

3.3.4 Single-jet and Co-electrospinning Fabricating Methods of PHB/CS/PEO Electrospun fibres

In chapter 8, PHB/CS/PEO were fabricated in two different ways: single-jet electrospinning (Single-ESP): 10 and 5 w/v% of PEO was prepared by dissolve 1g and 0.5g PEO added into pure ethanol solution until homogenous and mixed with PHB-2 w/v% CS solution to reach final concentration at 10w/v% and 5w/v% respectively before electrospinning. Co-electrospinning (Co-ESP): For the co-electrospun fibres, adding 0.5 and 1 g of PEO powder into pure ethanol solution will form 5 w/v% and 10 w/v% PEO solution respectively, and these will electrospun parallel with the PHB solution with separate jet.

3.3.5 Modifying the process parameters included concentration of working distance, flow rates and applied voltages

The methodology involved modifying both PHB and PHB/CS solutions using TFA and CF/DMF solvents through electrospinning, which was influenced by various process parameters. Initially, three concentrations of PHB solution (10, 12, and 15 m/m%) were prepared, each mixed with five different concentrations of CS (0, 1, 2, 3, 4, and 5 w/v%) respectively. These solutions were then electrospun under a constant flow rate of 2 ml/hr and an electric field strength of 0.5 kV/cm. Following fabrication, viscosity and conductivity tests were conducted, with results to be discussed in a subsequent chapter.

Furthermore, to determine the optimal applied voltages, CS concentrations, and flow rates for achieving stable Taylor cone jet flow, a 15 m/m% PHB solution was selected and maintained at this concentration. It was mixed with CS at five different concentrations (0, 1, 2, 3, 4, and 5 w/v%), and electrospun under five varying flow rates (0.25 ml/hr, 0.5 ml/hr, 0.75 ml/hr, 1 ml/hr, 1.25 ml/hr, and 1.5 ml/hr). The experiment documented the initiation voltage (V_{start}), the voltage at which fibres began to straighten ($V_{straight}$), and the end voltage (V_{end}), all of which will be defined in a later chapter.

Additionally, the impact of flow rates, working distances, and applied voltages on the fibre diameter of PHB/CS electrospun membranes was investigated. A solution of 15 m/m% PHB with 1 w/v% CS was electrospun under three sets of conditions: 1) varying flow rates (0.5, 0.75, 1.0, 1.25, and 1.5 ml/hr) at an applied voltage of 12 kV and a working distance of 20 cm; 2) different working distances (10, 12, 14, 16, 18, 20, and 22 cm) at a constant flow rate of 1 ml/hr and an applied voltage of 12 kV; and 3) varying applied voltages (3, 6, 9, 12, 15, 18, and 21 kV) at a 20 cm working distance and a flow rate of 1 ml/hr. Following these experiments, fibre diameters were measured using the characterisation methods to be discussed later.

3.3.6 Degradation analysis in acidic (pH = 2), neutral (pH = 7) and alkaline solutions (pH = 12)

In chapter 4, the degradation properties of the electrospun PHB/CS nanofibre samples were analysed in three different solutions: (1) The acidic solution was prepared using acidic lactate sodium (ALS) and adjusting the pH to 2 by adding

HCl. (2) The neutral solution was prepared using PBS at pH 7.4. (3) The alkaline solution was prepared by adjusting the pH value of PBS to 10 by adding NaOH. For each tests, PHB/CS electrospun membranes were cut into 3 pieces, each was presented as a square ($1 \times 1 \text{ mm}^2$) shape with similar thickness, and pre-dried in a vacuum oven for 24 h before the experiments. The electrospun membranes were then submerged in 10 ml of the acidic, PBS and alkaline solutions in individual tubes with the screw caps tightened and maintained at 37 °C for 8 weeks. All solutions were changed every week. The scaffolds were removed at specified intervals for analysis, at which time they were rinsed thoroughly with de-ionized water, dried and placed in an oven at 35 °C for 24 h until a constant weight was obtained. The weight in each solutions was recorded and averaged from 3 samples, and the whole degradation analysis has been repeated for 3 times to minimize the effect of random errors.

3.3.7 Surface functionalization of electrospun fibrous PHB membranes with DA and GA

In chapter 6 and 7, we will treat PHB with dopamine (DA) with glutaraldehyde, to form chemical bonding with CS and improved the corrosion resistance, biosafety and adhesion strength. Firstly, 2 cm * 2 cm * 0.01 cm of PHB electrospun membranes were cut and immersed in 0.5M potassium hydroxide (KOH) or 50 v/v% hydrogen peroxide (H_2O_2) solutions separately for 1 hour, followed by washing with de-ionized water. Both KOH and H_2O_2 could create more hydroxyl groups, and form binding sites to DA on the surface of PHB electrospun fibres. Subsequently, the PHB fibre membranes were immersed in a 3 mg/ml dopamine (DA)/0.1 M Tris buffer solution at pH 8.5 and maintained at 60 °C for 24 hours. They were then stored in a fume cupboard and wrapped by aluminium foil to ensure they were kept in the dark. Following the completion of the anchoring reaction, the PHB membranes coated with DA (PHB-DA) were washed several times with deionized water. Furthermore, the membranes were submerged in a 3% GA aqueous solution for 6 hours and forming PHB-DA coated with GA (PHB-DA-GA) membranes. In this system, GA served as a coupling agent by providing reactive aldehyde groups for covalent interaction between DA and CS. By washing with deionized water, unbound GA was eliminated. After this, 2 ml of 0.2, 0.5, 0.8, 1, 1.5 and 2 w/v% CS was poured into the petri dish containing PHB-DA-GA membranes for surface coating and left for 24 hours at room temperature, and form PHB-DA-GA-CS membrane. The substrates were then cleaned with deionized water and vacuum-dried overnight at room temperature for further characterisation.

3.3.8 Stability analysis of CS on KOH and H_2O_2 treated PHB-DA-GA-CS electrospun fibres

In chapter 6, to analyse the binding efficiency of CS, Cibacron Brilliant Red 3B-A (CBR) was to measure the CS concentration leave in the solution. Firstly, each PHB/CS electrospun membrane was immersed in 10 ml PBS in solution

at room temperature for 14 days. On days 1, 3, 7, and 14 days, 1 ml of PBS solution was collected and ready for use. Secondly, 0.075 g of CBR powder (50% dye content) was dissolved in 0.5 L de-ionised water to form 0.075M dye solutions. PHB-CS solutions were added to glass tubes containing 0.1 ml buffer glycine/HCl and 1 ml dye. Thirdly, the final volume was diluted to 5 ml using de-ionised water. The tubes were sealed and kept at room temperature under continuous agitation. After 20 minutes, 1 ml from each tube was transferred to a tube determined measuring absorption relative to DW using the same spectrophotometer. The BR absorption spectrum exhibited a broad peak with a plateau between 506 and 550 nm in UV-vis. The actual amount of CS in 0.2, 0.5, 0.8, 1, 1.5 and 2 w/v% concentration was first determined in UV-vis at the wavelength at 530nm. These wavelength values correspond to the maximum wavelength for each concentration of CS. The results were reported as averages from at least five measurements.

3.3.9 In Vitro Release, Remaining Mass, and pH Stability Analysis of Forskolin from PHB/CS-Based Electrospun Fibre Mats

In chapter 7, prior to conducting the in vitro drug release tests, the fibrous membranes underwent a thorough drying process. The initial weights of these membranes were meticulously recorded using an analytical balance for precise measurements. Subsequently, the membranes were immersed in 10 ml of freshly prepared PBS with a carefully maintained pH of 7.4 ± 0.1 . The entire setup was maintained at a constant temperature of 37 °C. To ensure uniformity and thorough mixing within the solution, a constant-temperature shaker was employed, set to oscillate at a controlled rate of 100 rev/min. For scheduled sampling during the drug release experiment, 1.0 ml of the solution was meticulously withdrawn from the dissolution medium. Simultaneously, an equivalent volume of fresh PBS solution was promptly added to the medium to maintain a constant volume. The pH value of the updated solution was measured using a pH meter, ensuring precise monitoring of the pH conditions. The quantification of the released drug was performed using a UV-Vis spectrophotometer, which allowed for accurate determination based on absorbance measurements at specific wavelengths. This drug release experiment was rigorously repeated five times to ensure the reliability and consistency of the results. After each round of testing, the samples were placed in a vacuum oven for drying, following which their weights were once again measured using the analytical balance to assess any changes in mass.

3.4 Characterization

3.4.1 Scanning electron microscope (SEM)

Prior to scanning electron microscopy (SEM) analysis, distinct types of PHB nanofibres should be dried overnight in a fume hood. The samples were then examined using a Hitachi 8230 field emission SEM (Tokyo, Japan) after coating with a 6nm layer of gold using a sputter coater. The diameters of the

fibres were measured from the SEM images utilizing ImageJ software. In order to reach that, we will draw a 10 x 10 grid matrix and count fifty measurements on cross point that conducted for each sample. Besides, the percentage of beads pre were also counted in Chapter 5, by using the equation:

$$\% \text{ beads} = \text{surface area of beads} / \text{total surface area of fibres} * 100\%$$

3.4.2 Fourier transforme infra-red sepctrometer (FTIR)

FTIR spectroscopy was performed to investigate the functional groups present in the electrospun PHB/CS nanofibres. Before the test, PHB/CS electrospun fibres were rinsed with de-ionised water and dried in a vacuum dryer until all the water was removed. The FTIR spectra of the PHB/CS electrospun fibres were obtained from a 5 min scan ranging from 4000 cm^{-1} to 400 cm^{-1} wavenumbers with a 2.0 cm^{-1} resolution.

3.4.3 Water contact angles (WCA)

The wettability of the electrospun fibre mats was evaluated through the sensile drop WCA test using an OCA 15 plus contact angle measurement system (Data Physics, Germany) equipped with a CCD camera (precision $\pm 0.2^\circ$). All the measurements were performed by applying ultra-pure water at room temperature. The average values were evaluated based on five repetitions for each specimen, each specimen has 50 data points.

3.4.4 Thermal gravimetric analysis (TGA)

The electrospun PHB samples were subjected to TGA in a PerkinElmer 2000 instrument under a continuous nitrogen flow of 40 ml/min. Approximately 10 mg samples were prepared and then heated in a ceramic crucible from 50–400 $^\circ\text{C}$ at the heating rate of 10 $^\circ\text{C}/\text{min}$.

3.4.5 Differentiate scanning calorimetry (DSC)

DSC was performed by adding an approximately 2 mg sample to an aluminium crucible. The sample was heated from room temperature (25 $^\circ\text{C}$) to 550 $^\circ\text{C}$ at the heating rate of 10 $^\circ\text{C}/\text{min}$. Nitrogen was used with a gas flow rates of 20 ml/min. All samples were evaluated under the same conditions to obtain comparable TGA curves. The degree of crystallinity (χ_c) was calculated through the equation (1)

$$\chi = \left(\frac{\Delta H_f}{\Delta H_f^0} \right) \times \frac{100}{w} \quad (1)$$

where ΔH_f is the fusion enthalpy of composites, and ΔH_f^0 is the fusion enthalpy of 100% crystalline PHB. w is the mass fraction of PHB in the composite and ΔH_f^0 of PHB was calculated to be 146 J/g

3.4.6 Porosity analysis by Brunauer–Emmett–Teller (BET)

The specific surface area of the PHB and PHB-CS electrospun fibres was measured using BET equipment (NOVA Touch, Quantachrome Instruments, Boynton Beach, FL, USA). All the samples were dried under vacuum at room temperature for 24 hours and then weighed. The BET analysis was then conducted using nitrogen as the adsorbate gas at a bath temperature of 77.35 K. The bath thermal delay was set to 600 s with helium backfill mode. The adsorption isotherm (BET plot) was obtained for the calculation of the specific surface area of the monoliths. The half-pore width distribution was modelled by the DFT method.

3.4.7 Mechanical tests

The mechanical test was performed by Intron tensile tester, according to active standard test method D638 equipped with a 50N static load cell. During the test, the samples were all cut into 10 mm*10 mm square films with an average of 0.57 ± 0.02 mm thickness. Furthermore, the Young's modulus, toughness and ultimate tensile stress (UTS) tensile strength and elongation were calculated at break based on the measured thickness and width of each sample. A test speed of 10 mm/min was used. Each sample was tested at least five times.

3.4.8 Conductivity testing

The electrical conductivity of PHB and PHB/CS electrospun membranes with dimension of 1*1*cm was measured by a PalmSens4 potentiostat (PalmSens BV, Netherlands) at room temperature in air. The sample size was measured by a standard calliper. In the test, the current and output voltage of each sample was measured, and the electrical conductivity was calculated. This test was performed in triplicate

3.4.9 Measurements of viscosity

To ascertain the intrinsic viscosity, the PHB/CS solutions prepared as per sections 3.3.1 and 3.3.2 were evaluated at 25 ± 0.05 °C using a Ubbelohde C529 capillary viscometer, which has a capillary diameter of 0.63 mm, within a ThermoHaake DC30 temperature-controlled bath apparatus. To ensure accuracy and minimize variations, each concentration was measured three times.

3.4.10 Statistical analysis

Data analysis throughout this thesis was conducted using a one-way ANOVA test in Prism 8. This statistical method enabled the comprehensive examination of differences among various groups. A p-value of less than 0.05 was considered indicative of a statistically significant difference.

Chapter 4: Optimization of PHB/CS Solution Properties for

Electrospinning: Conductivity, Viscosity, and Process Parameters

4.1 Overview

This chapter focuses on modifying the solution properties of PHB/CS, including the conductivity, viscosity and two types of solvents: trifluoroacetic acid (TFA) and chloroform/dimethylformamide (CF/DMF). The conductivity of the solution depends on the concentration of each polymer, the solvent used, and the pH of the solution. Increasing the concentration of CS enhances conductivity, while PHB has low conductivity due to its polar and non-conjugated nature. The viscosity of the solution increases with the concentration of both PHB and CS, but excessive CS concentration leads to gel-like structures. The presence of CS in electrospun fibres provides unique properties like improved biocompatibility and antibacterial activity. However, the use of TFA as a solvent may have drawbacks, so alternative solvents and methods should be considered. Also, this chapter will further modify the process parameters of electrospinning process, such as applied voltages, flow rates and working distance, to create and control PHB/CS fibre diameter, morphology, and orientation.

4.2 Result and discussion

In this chapter, the fabrication process parameters of PHB/CS electrospun membranes, including the fibre diameter, were detailed and measured following the procedures outlined in Sections 3.4.1 and 3.4.5.

The minimum required viscosity and conductivity threshold for a solution to be suitable for electrospinning corresponds to a specific polymer concentration. This threshold varies according to the molecular weight of the polymer and the characteristics of the solvent used. Results have shown that the conductivity and viscosity of PHB/CS depend on several factors, such as the concentration of each polymer, the solvent used, and the pH of the solution. Figure 4.1 showed that when examining solutions with PHB concentrations of 15, 12, and 10 w/v%, an increase in CS concentration from 0 to 5 w/v% across the three different PHB concentration solutions led to a conductivity increase ranging from 28 to 33%. This indicates that enhancing the CS concentration positively affects the solution's conductivity. However, increasing the PHB concentration from 10 to 15 w/v%, while maintaining a constant CS concentration, did not result in significant differences in conductivity. PHB is not very conductive in both CF/DMF and TFA solvents because PHB is a highly polar and non-conjugated polymer, which means that it lacks the delocalized electrons that

are needed for electrical conductivity. Besides, PHB has a high degree of crystallinity, which makes it a good insulator and further limiting its electrical conductivity non-polar groups. CS has some conductivity due to its amino groups. Therefore, the conductivity of the PHB-CS solution will depend on the concentration of CS and the pH of the solution. Comparing CF/DMF and TFA at 15 w/v% PHB, the latter showed a 25% higher conductivity than CF. This suggests that the PHB/CS with TFA solution may have some conductivity due to the presence of ions from TFA and the amino groups in CS. Because the acidic solution will cause the CS protonated and will have a higher conductivity. In general, TFA is a polar solvent with a high dielectric constant, which means it can dissolve many ionic and polar substances, including salts and acids. CF is a nonpolar solvent with a low dielectric constant, while DMF is a polar solvent with a high dielectric constant. This mixture of solvents can be used to dissolve both polar and nonpolar substances, including PHB and CS. However, the exact conductivity of the PHB-CS solution in CF and DMF will depend on the concentration of the polymers and the solvents, as well as the temperature and pressure of the system.

The viscosity of the PHB-CS solution will also depend on the concentration of each polymer and the solvent used. In this experiment, we added a maximum 5 w/v% of CS in PHB solution because the solution has become too viscous to handle and formed a gel-like structure when concentration is over 5 w/v%. Figure 4.1 showed that increasing both PHB and CS concentration can increase its viscosity. CS tends to form a gel-like structure when dissolved in water. However, when concentration of CS reaches to 3, 4 and 5 w/v%, the viscosity has no significant increase. The viscosity of a PHB-CS solution can increase due to the formation of intermolecular interactions and the increase in the size of the polymer chains in the solution. It may be because the PHB carboxyl groups has reached its saturation connections with CS at 3 w/v%. Also, compared between using TFA and CF/DMF solvents, we found that there is no significant differences of the viscosity when CS concentration reaches to 5 w/v%, which showed that both solvents system showed a proper solubility to both PHB and CS. In conclusion, we selected PHB at 15 w/v% and CS at 0,1,2 w/v% to do further investigations. However, due to the limited number of concentration of PHB we used, we could also expect a higher or lower concentration of PHB will be more suitable conductivity and viscosity, and required future research on this.

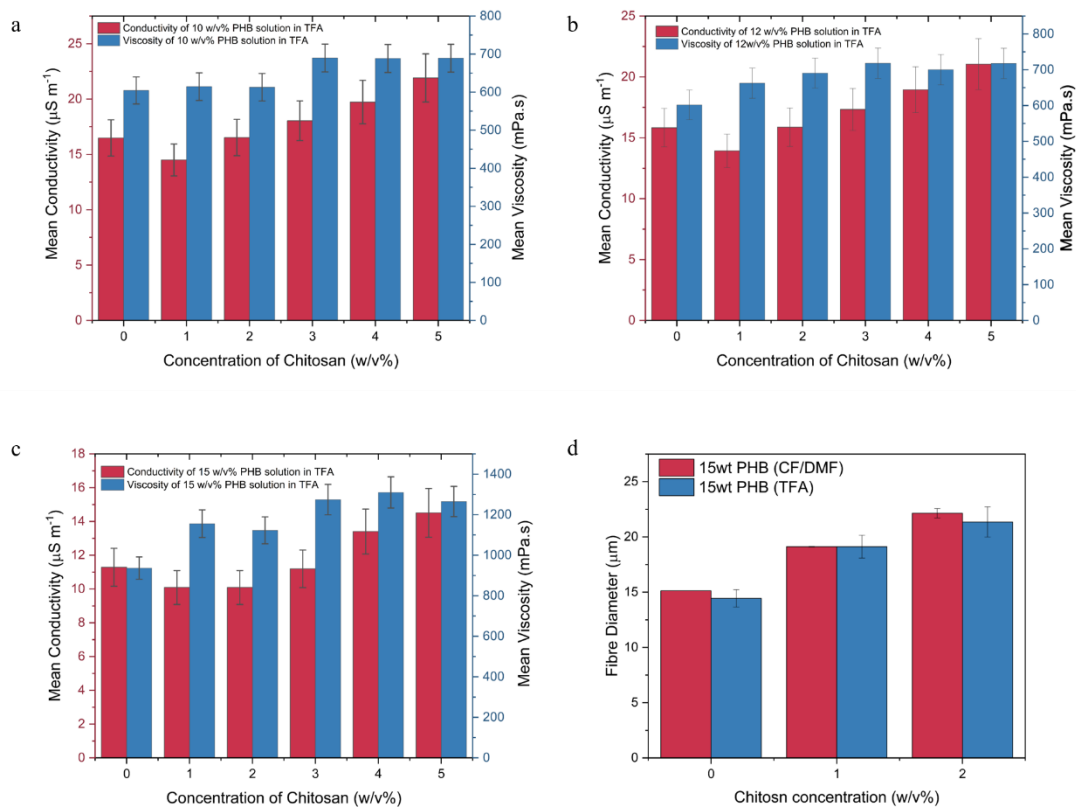


Figure 4.1: Conductivity and Mean viscosity of different concentration PHB and CS (a) 15 w/v% PHB in 0/1/2/3/4/5 w/v% CS (b) 12 w/v% PHB in 0/1/2/3/4/5 w/v% CS and (c) 10 w/v% PHB in 0/1/2/3/4/5 w/v% CS

The steady-state electrospinning process ensures a consistent voltage is applied to the spinneret or needle. This consistency is crucial for generating a stable Taylor cone, a pivotal element in the continuous extrusion of polymer solutions into fine jets, ultimately forming fibres. The importance of maintaining a stable Taylor cone cannot be overstated, as it plays a key role in ensuring the uniformity and consistency of the fibres. Therefore, Figure 4.2 presents the critical applied voltages of 15 w/v% PHB electrospun fibres under varying concentrations of CS (from 0 to 5 w/v%) and different flow rates (ranging from 0.25 ml/hr to 1.5 ml/hr). In this figure, we have defined three critical applied voltages: "Vstart" refers to the applied voltage at which the solution begins to emit from the spinneret and form a jet flow. "Vstraight" is the applied voltage at which a straight jet flow is achieved, characterized by a stable Taylor cone. "Vend" denotes the applied voltage at which the jet flow ceases, and no further solution is emitted. The results indicate that within a single CS concentration, all critical applied voltages increase with flow rates up to 1 ml/hr. Beyond this flow rate, Vstraight decreases until reaching 1.5 ml/hr. This phenomenon occurs because higher flow rates increase surface tension on the droplets at the spinneret, necessitating a greater electrostatic force from applied voltages to extrude the solution into a fibre, achieving force balance. Beyond 1 ml/hr, the

equilibrium between applied voltages and flow rates is disrupted, leading to unstable jet formation and a decrease in applied voltages. Additionally, at a constant flow rate, V_{straight} and V_{end} begin to converge when the CS concentration reaches 3 w/v%. Moreover, at higher flow rates, this convergence is less pronounced at 3 w/v%. This demonstrates that from 0 to 3 w/v% CS, the solutions facilitate proper Taylor cone formation and jet stability, as evidenced in the previous section. As the concentration approaches 3 w/v% CS, the observed convergence between V_{straight} and V_{end} indicates that the emitted jet becomes more susceptible to environmental conditions, such as humidity and temperature. Consequently, in subsequent sections, we have restricted our investigation to CS concentrations ranging at 0 to 2 w/v%.

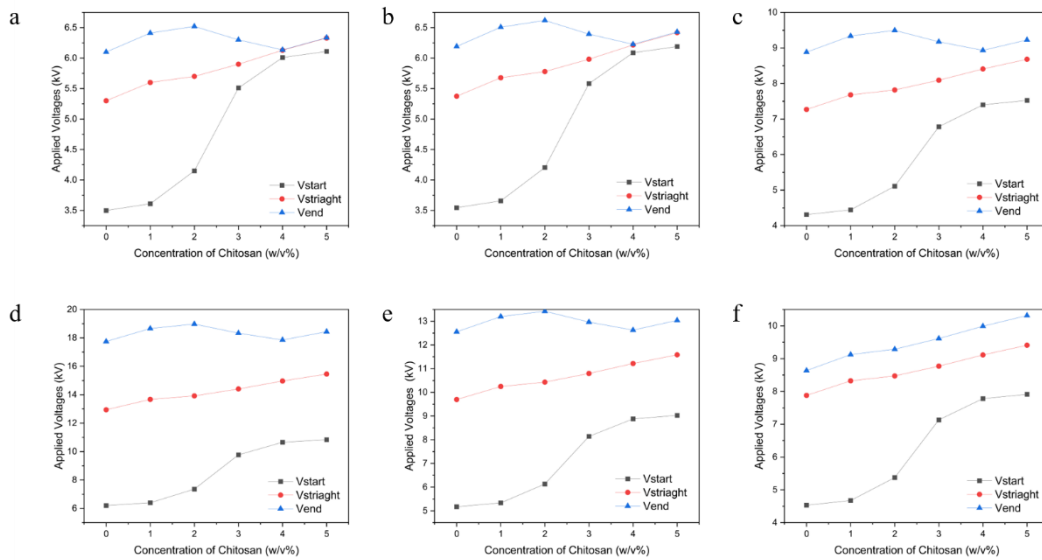


Figure 4.2: Critical applied voltages VS CS concentration diagram of 15 w/v% PHB electrospun fibres at 20 cm working distance under 0,1,2,3,4 and 5 w/v% CS with different flow rates. (a) 0.25 ml/hr (b) 0.5 ml/hr (c) 0.75 ml/hr (d) 1 ml/hr (e) 1.25 ml/hr (f) 1.5 ml/hr

Furthermore, Figure 4.3 focuses on the SEM images of 15 m/m% PHB with 1 w/v% CS electrospun fibres produced at a constant applied voltages of 12kV and flow rates of 1 l/hr, while varying the working distance from 10 cm to 22 cm. This range of working distances allows for a detailed examination of how the distance between the spinneret and the collector influences fibre morphology. The results showed that when working distance reaches between 10 and 16cm, the PHB/CS fibres formed with high non-uniformity, within beads formation. With the increase of working distance to 18 and 20 cm, uniform fibres has formed without beaded structure. And when working distance reach to 20 cm, non-uniform fibres started to form again. Also Figure 17 also indicated that The working distance in electrospinning significantly influences solvent evaporation, fibre stretching, and the deposition pattern on the collector. As the working

distance increases, fibres have more time for solvent evaporation and stretching prior to deposition, potentially resulting in fibres with reduced diameters and more uniform morphologies at longer distances. However, excessively long distances may lead to incomplete solvent evaporation or instability in the jet flow, thereby causing variations in fibre quality. Therefore, from 16 to 20 cm working distances will be suitable and applied in our PHB/CS electrospun membrane fabrication.

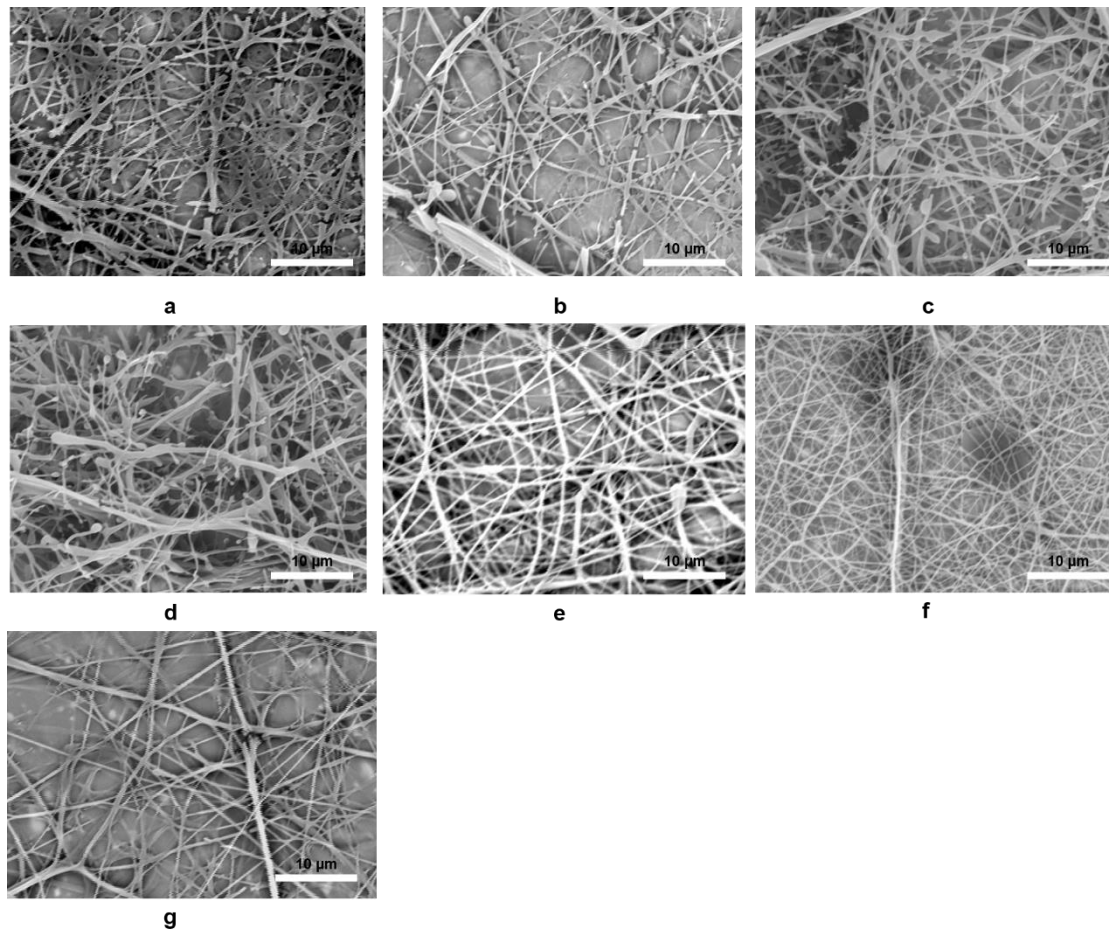


Figure 4.3: SEM of 15 w/v% PHB/1 w/v% CS electrospun fibres at applied voltages=12kV and flow rates=1 /hr with different working distance (a) 10 cm (b) 12 cm (c) 14cm (d) 16 cm (e) 18 cm (f) 20cm and (g) 22cm

Figure 15 explores the SEM images of 15 w/v% PHB/1 w/v% CS fibres at a constant applied voltages of 12kV, flow rates of 1 /hr, and working distance of 20 cm, while varying the concentration of CS from 1 w/v% to 5 w/v%. The results demonstrated that uniform and beadless PHB/CS fibre structures were achieved exclusively with CS concentrations of 0, 1, and 2 w/v%. Conversely, higher concentrations resulted in fibres exhibiting a more beaded structure. This outcome further corroborates our previous assumptions. As former discussed, the variation in CS concentration is expected to significantly influence fibre morphology due to changes in the viscosity and conductivity of solution. Higher

concentrations of CS will increase the viscosity, potentially leading to larger fibre diameters or bead formation. Conversely, lower concentrations could result in finer fibres. Additionally, the presence of CS, a natural polymer, in combination with PHB, a synthetic polymer, may lead to complex interactions affecting the stability and morphology of the electrospun fibres.

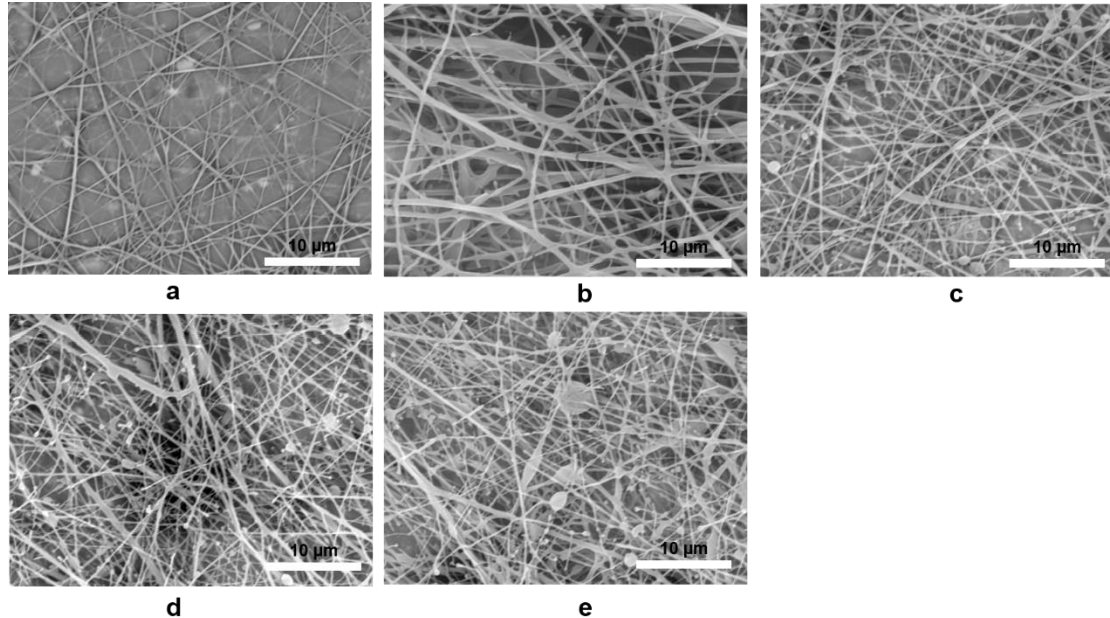


Figure 4.4: SEM of 15 w/v% PHB/1 w/v% CS electrospun fibres at applied voltages=12kV, flow rates=1.5 ml/hr and working distance=20 cm with different concentration of CS (a) 1 w/v% CS (b) 2 w/v% CS (c) 3 w/v% CS (d) 4 w/v% CS (e) 5 w/v% CS

Figure 4.5 presents the SEM images of 15 w/v% PHB/1 w/v% CS fibres electrospun at an applied voltages of 12 kV and working distance of 20 cm, with varying flow rates from 0.25 ml/hr to 1.5 ml/hr. The flow rates in electrospinning directly impacts the rate at which the polymer solution is fed to the spinneret, influencing the fibre formation process. A higher FR could lead to thicker fibres due to the increased volume of polymer solution being processed, whereas a lower FR might produce thinner and more uniform fibres. The results showed that a uniform PHB/CS fibres only formed at 0.5 and 1ml/hr flow rate. As previously discussed, the observed phenomenon is attributed to the high flow rates disrupting the equilibrium between the surface tension of the droplets and electrostatic attraction, resulting in greater variations in fibre diameter. Based on these findings, flow rates of 0.5 or 1 ml/hr are deemed suitable for our PHB/CS electrospun membrane fabrication.

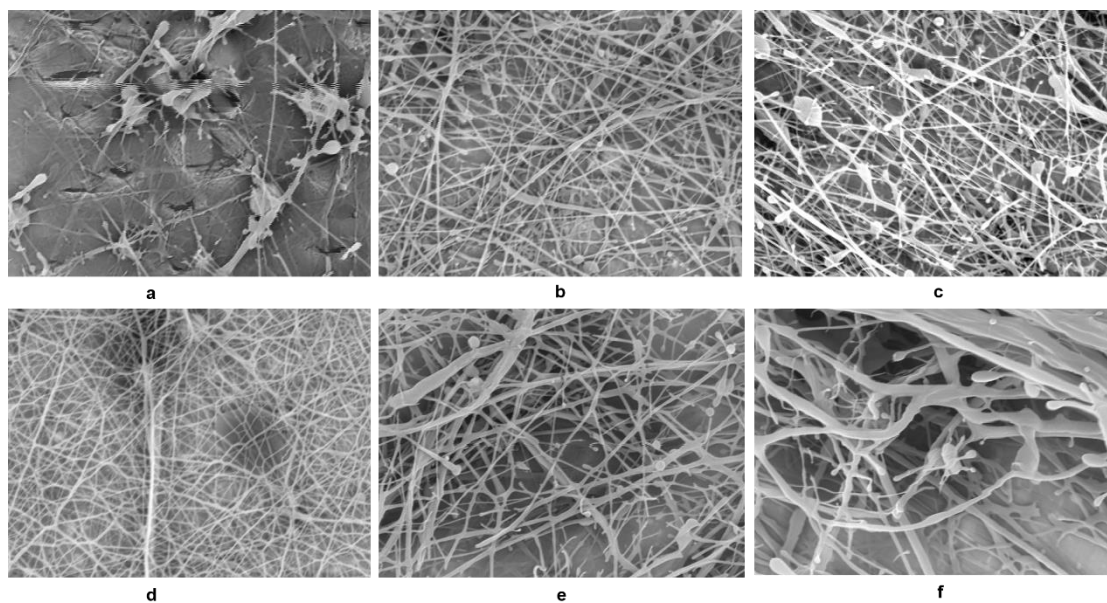


Figure 4.5: SEM of 15 w/v% PHB/1 w/v% CS electrospun fibres at applied voltages=12Kv and working distance=20 cm with different flow rates. (a) 0.25 ml/hr (b) 0.5 ml/hr (c) 0.75 ml/hr (d) 1 ml/hr (e) 1.25 ml/hr (f) 1.5 ml/hr

4.3 Summary

In summary, this chapter explores the impact of variation of PHB and CS concentration, flow rates, applied voltages and working distance on the morphology and structural properties of the fibres. The results demonstrated that both TFA and CF/DMF solvent systems could successfully dissolve PHB at concentrations of 10, 12, and 15 m/m%, achieving suitable conductivity and viscosity. Notably, TFA exhibited superior conductivity compared to CF/DMF. Additionally, increasing the CS concentration up to 3 w/v% resulted in a homogeneous solution. Comparative analysis of different process parameters—such as flow rate, working distance, and applied voltages—revealed that a 15 m/m% PHB solution with 0, 1, and 2 w/v% CS concentrations could be electrospun into uniform, continuous, and beadless fibre structures under specific conditions: a flow rate of 0.5 or 1 ml/hr, working distances of 16 or 20 cm, and applied voltages of 12 or 15 kV. However, given the limited range of PHB and CS concentrations tested, further research is warranted to explore a broader spectrum of conditions.

Chapter 5: Electrospun PHB/CS Composite Fibrous Membrane and Its

Degradation Behaviours in Different pH Conditions

5.1 Overview

PNI, a neurological disorder, impacts over nine million individuals by impairing their movement and sensory functions [3,4]. For decades, research has explored the creation of artificial nerve conduits from biodegradable polymers [51-53]. These conduits are designed to mimic the ECM and facilitate neuron regeneration at injury sites, showing promising results primarily in pre-clinical stages. However, constructing PNCs from biodegradable polymeric materials that either sustain their structure during nerve regeneration or completely degrade post-regeneration has been challenging. In this research, a novel material for PNCs was developed by electrospinning PHB/CS composite polymers. SEM analysis of the resulting PHB/CS nanofibres with 0, 1, and 2 w/v% CS displayed fewer and smaller beads compared to those with 3 w/v% CS. WCA measurements indicated enhanced wettability of the PHB/CS fibres with added CS. TGA and DSC analyses confirmed that PHB/CS polymers could blend in a single phase using a trifluoroacetic solvent across all compositions. Additionally, an increase in CS content resulted in reduced degradation temperature (from 286.9 to 229.9 °C) and crystallinity (from 81.0% to 52.1%). The study also found that the degradability of PHB/CS nanofibres varied with pH, ranking as acidic > alkaline > PBS. These findings suggest that PHB/CS electrospun fibres with different blend ratios could be effective in designing PNCs with controlled biodegradability.

5.2 Results and Discussion

5.2.1 Morphology and Size of PHB and PHB/CS

All scaffolds composed of PHB/CS were synthesized uniformly through the electrospinning technique, following the preparation procedure outlined in Section 3.4.1. The SEM images highlighted in Figure 5.1 illustrates the various fibre morphologies for each specific blend. In Figure 5.1a, the PHB/CS0 variant showed fibres with consistent connectivity and an average diameter of 331 ± 14 nm. As shown in Figure 5.1b and c, elevating the CS concentration to 2 w/v% led to an increase in fibre diameter, growing from 331 nm to 692 nm. Meanwhile, the figures also noticed that the fibre surface has a rise in the prevalence of irregular fibres and beads with increasing roughness. When the CS level was further increased to 3 w/v% (Figure 5.1d), there was a notable reduction in fibre diameter to 401 nm, and the fibres exhibited larger beaded structures. The analysis also indicated that with increasing CS concentration from 0 to 3 w/v%,

each sample showed a variation in beaded structure diameter, ranging from 314 nm to 1324 nm, as catalogued in Table 3.

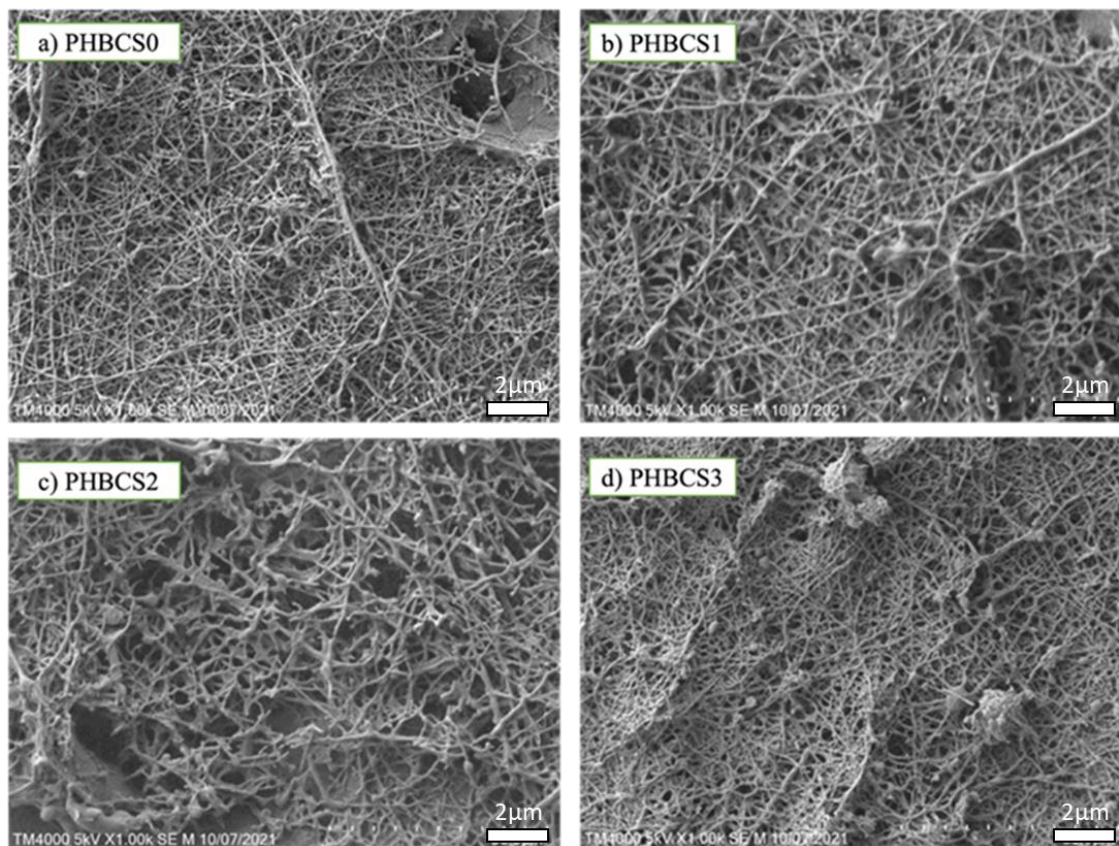


Figure 5.1: SEM images of PHB/CS electrospun scaffolds with different CS contents (a) 0 w/v%, (b) 1 w/v%, (c) 2 w/v% and (d) 3 w/v%.

Table 3: Average fibre and bead diameter of PHB/CS nanofibrous membranes with different CS contents.

Groups	Average Fibre Diameter (nm)	Percentage of Beads (%)
PHB/CS0	331 ± 14	13.7
PHB/CS1	428 ± 23	20.8
PHB/CS2	692 ± 101	14.3
PHB/CS3	401 ± 58	36.2

5.2.2 FTIR analysis of PHB Electrospun Fibres before and after degradation

Figure 5.2 displays the FTIR spectra for PHB, CS, and various PHB/CS mixtures by weight. In the PHB spectrum, the band characteristic falls within $1720\text{--}1722\text{ cm}^{-1}$, corresponding to the C=O group's stretched vibration. Peaks indicative of the crystalline phase of PHB appear at $816\text{--}826\text{ cm}^{-1}$, $1276\text{--}1278\text{ cm}^{-1}$, and $1720\text{--}1722\text{ cm}^{-1}$ in the FTIR spectrum. The amorphous phase of PHB is highlighted by peaks at 1130 cm^{-1} . Notably, the symmetrical wagging of the CH₃ group in PHB is identified at 1378 cm^{-1} . For CS, its defining peak at $3300\text{--}3550\text{ cm}^{-1}$ represents the stretching of OH and NH groups, with the amide I band appearing at 1540 cm^{-1} .

From the data in Figure 5.2A and D, it's observed that introducing CS to pure PHB causes the C=O peak at 1720 cm^{-1} to shift to a lower wavenumber. Additionally, the peaks at 973 cm^{-1} and 1293 cm^{-1} transition to higher wavenumbers. The C=O peak signals in all samples were significantly enhanced due to the polyester degradation in PHB. From the PHB appendix, the peak at 1227 cm^{-1} corresponds to the absorption of helical (α type) crystals, the 979 cm^{-1} peak to the crystalline phase at C-C stretching, and the 1180 cm^{-1} peak to the amorphous phase [3, 118]. Post acidic and alkaline degradation, an O-H stretching bond at 3550 cm^{-1} emerged in the alkaline solution after four weeks of degradation. Additionally, The study's findings showed that the peaks at 973 cm^{-1} and 1293 cm^{-1} shifted to higher wavenumbers due to the disturbance of the crystalline phase of PHB by CS, leading to an increase in the amorphous phase peaks [119]. This increase was predominantly influenced by the presence of intra-molecular hydrogen bonds. This occurrence is attributed to NaOH activating the hydroxide groups on the surfaces of PHB/CS fibres. Also, all samples exhibit a broader peak at 3550 cm^{-1} , and a pronounced C=O stretching signal peak emerges at 1750 cm^{-1} . This shift is attributable to the disturbance of the crystalline phase of PHB by the addition of CS, leading to an increase in the amorphous phase peaks. The rise in amorphous phases is predominantly governed by the presence of hydrogen bonds.

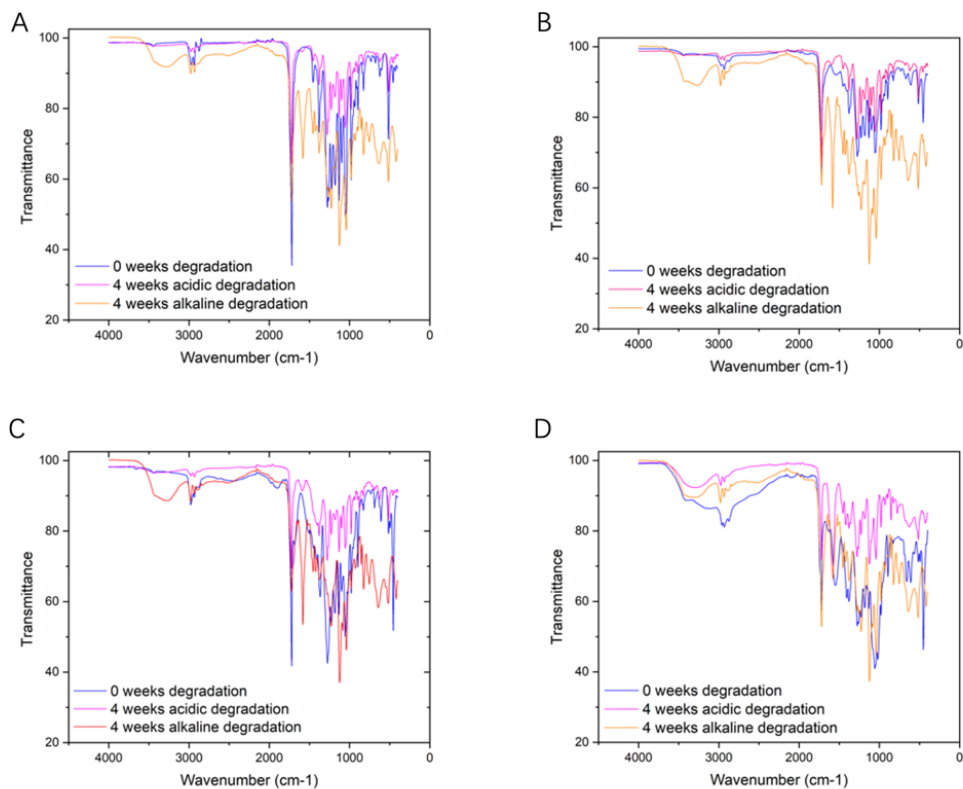


Figure 5.2: FTIR spectra of PHB/CS electrospun scaffolds. (A) PHBCS0, (B) PHBCS1, (C) PHBCS2, (D) PHBCS3.

5.2.3 WCA Measurements of PHB/CS electrospun membranes

To determine the hydrophilicity of PHB/CS nanofibrous mats with different CS levels, their WCA were measured, as illustrated in Figure 5.3. The PHB/CS0 variant demonstrated the averaged WCA at 89°. With an increase in CS content, there was a corresponding reduction in contact angles, dropping to 65. The addition of higher CS contents resulted in increased hydrophilicity. This is due to the rising number of terminal hydroxyl and amino groups in the CS chains, which readily interact with water molecules via hydrogen bonding.

	Time	
PHB/CS (w/w)	0 s	30 s

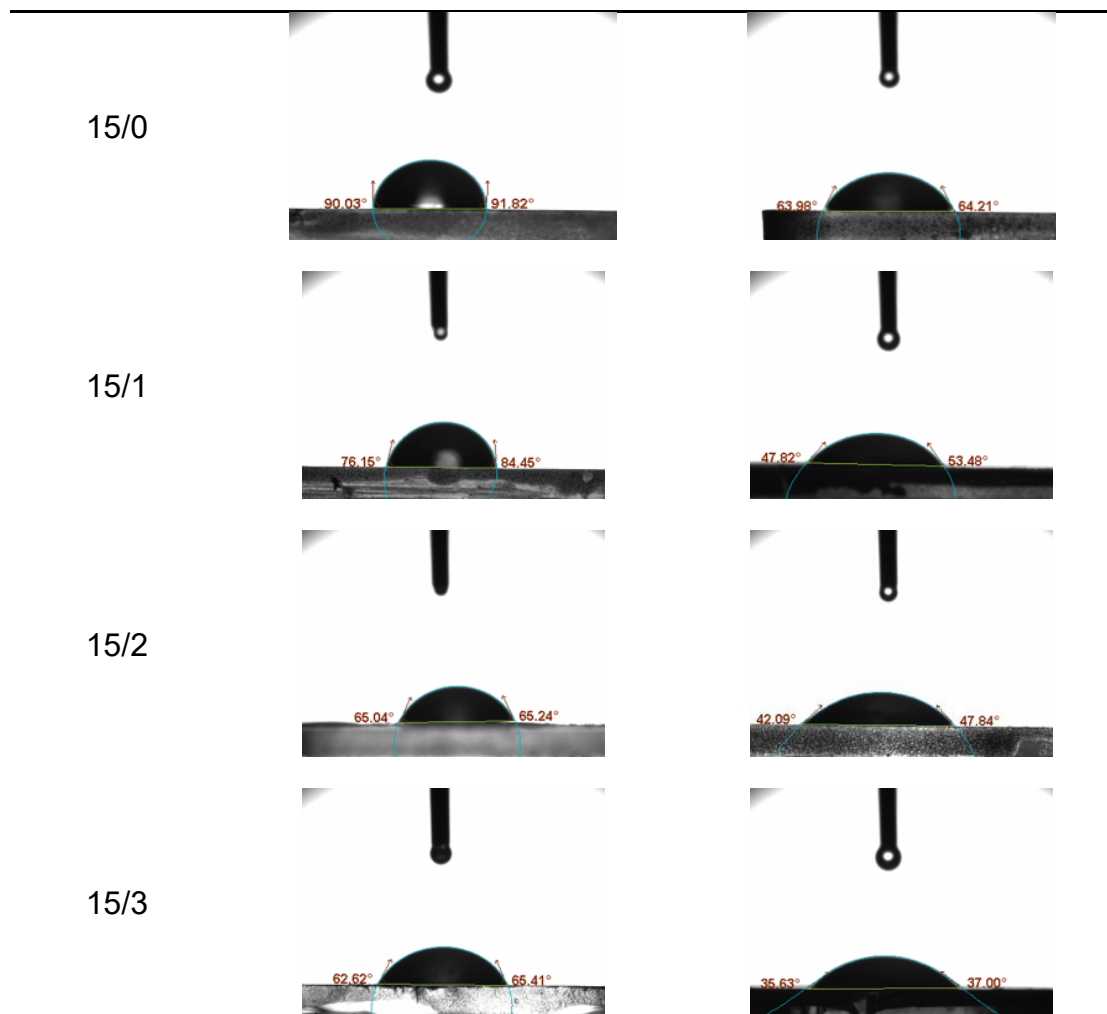


Figure 5.3: WCA measurements of PHB/CS electrospun scaffolds

5.2.4 TGA and DSC Analysis

The TGA curves of all PHB/CS fibrous mats were analysed alongside pure PHB and CS to evaluate variations in degradation temperature. Figure 5.4A and B present the TGA and DTA curves, with Table 4 summarizing the degradation temperatures for each group. The PHBCS0 and pure CS electrospun fibres showed degradation at 287°C and 288 °C, respectively. Additionally, PHBCS0 exhibited a second degradation point at 350 °C. Furthermore, the blended PHB/CS electrospun fibres displayed a shift to lower degradation temperatures of 277 °C, 231 °C, and 229 °C as the CS content increased from 1 to 3 w/v%. However, no second degradation temperature was observed with the addition of CS.

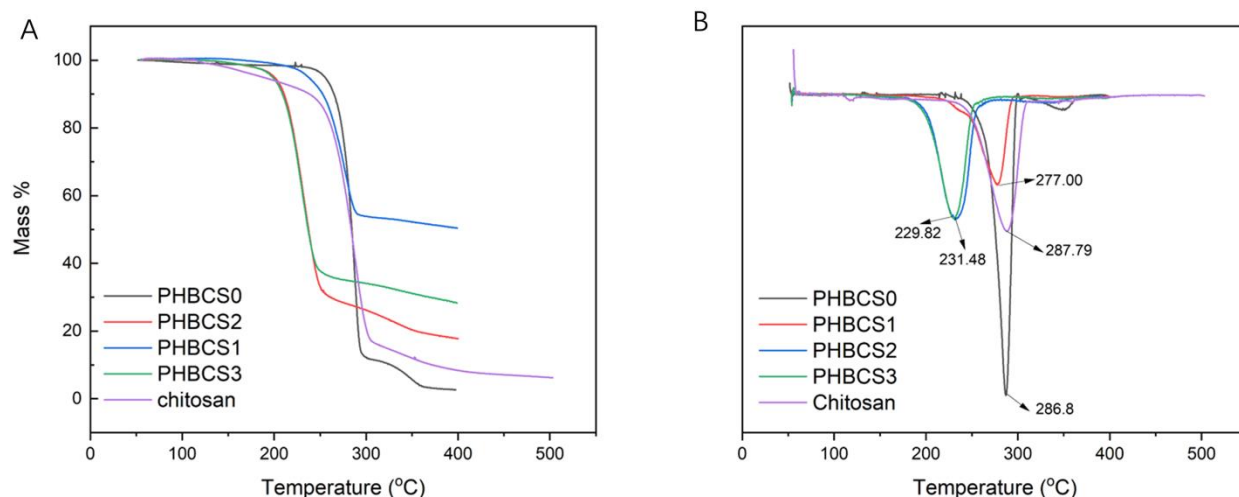


Figure 5.4: Thermal analysis of PHB/CS composite films (A) TGA and DTA graphs of PHB/CS composite films with different CS contents. (B) DSC graphs of PHB/CS composite films with different CS contents.

Table 4: Mean values of degradation temperature of PHB/CS composite films.

Groups	First Degradation Temperature (°C)	Second Degradation Temperature (°C)
PHBCS0	287	350
PHBCS1	277	/
PHBCS2	232	/
PHBCS3	230	/
CS	288	/

The DSC analysis, shown in Figure 5.5, revealed two endothermic peaks in all groups, representing the first and second crystallization temperatures. Table 5 details the melting points, enthalpy of fusion, and crystallinity for various groups. The melting point for PHBCS0 was noted at 268 °C, with a crystallinity of 81%, consistent with literature values [12, 28, 120, 121]. Table 4 also indicates a decrease in enthalpy of fusion from 125 to 76.1 J/g, and a reduction in crystallinity degree as the CS content increased from 0 to 3 w/v%. TGA analysis depicts a single degradation temperature in the TGA/DTA plots of all PHB/CS composites after blending, shifting to the right as CS content increased. This shift is indicative of proper miscibility between PHB and CS in different compositions, where the addition of CS disrupted the regularity of PHB and reduced its crystallinity [122, 123]. This is corroborated by the reduction in Hm observed in the DSC curves. The decreasing crystallinity from PHBCS0 to PHBCS3 can be attributed to the rigid CS molecules disrupting the lamellar thickness of PHB crystallites, thereby suppressing PHB crystallisation [124, 125].

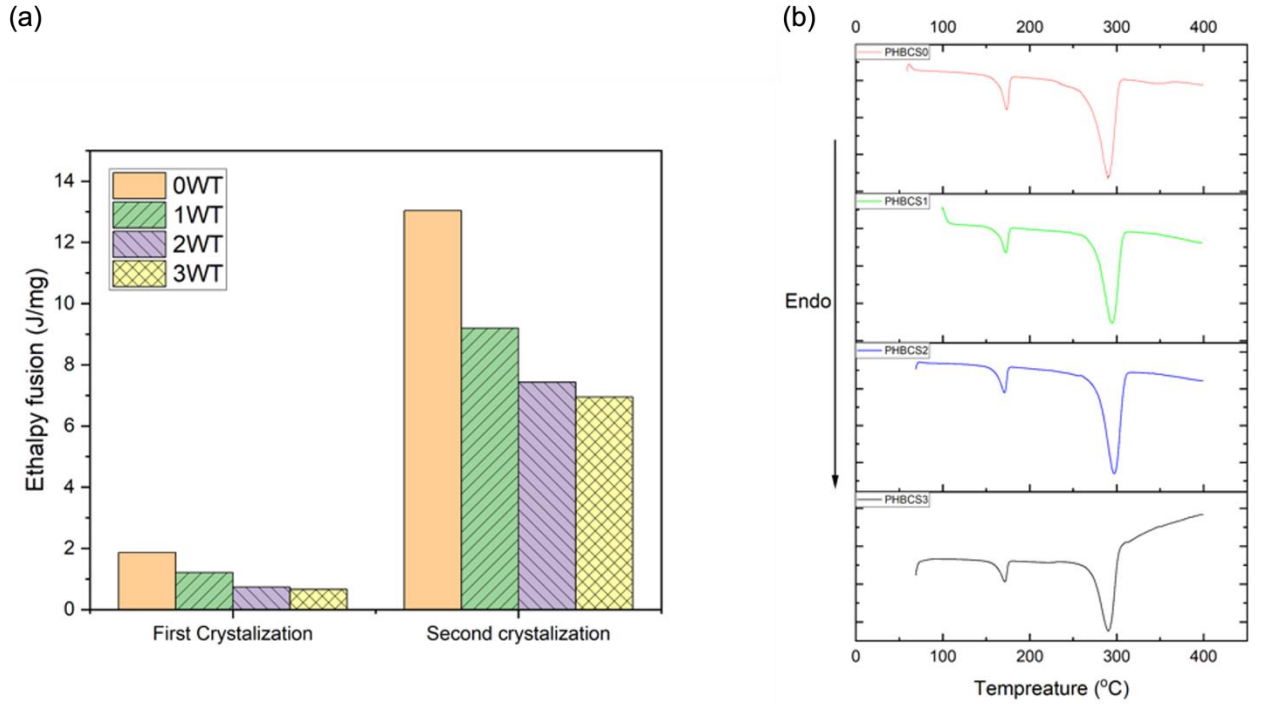


Figure 5.5 DSC analysis of of PHB/CS electrospun composite films. (a) Enthalpy fusion and (b) DSC curves of PHB/CS samples.

Table 5: DSC graphs of PHB/CS composite films with different CS contents.

Groups	T _m (°C)	H _m (J/g)	Crystallinity (%)
PHBCS0	268	125	81.0
PHBCS1	273	104	71.3
PHBCS2	276	81.6	55.9
PHBCS3	280	76.1	52.1

5.2.5 Degradation Analysis and SEM of PHB/CS after 12 Weeks Degradation in Acidic, PBS and Alkaline

In this section, all scaffolds composed of PHB/CS were tested under the degradation procedure outlined in Section 3.4.6 To simulate the conditions that PHB/CS electrospun membranes would encounter in physiological environments, we employed PBS solution to mimic the neutral body fluids, and a combination of PBS, ALS, and HCl to replicate the inflammatory conditions surrounding damaged nerves. Furthermore, to investigate the behaviour of these membranes under alkaline conditions, we utilized NaOH solutions as comparison groups to evaluate their performance. Figure 5.6 presents the in

in vitro degradation characterisation of the materials at various pH levels. In the PBS degradation study, the residual mass percentages at week 12 for each sample were as follows: PHBCS0 at $73.1 \pm 2.63\%$, PHBCS1 at $66.3 \pm 4.48\%$, PHBCS2 at $65.3 \pm 2.51\%$, and PHBCS3 at $43.8 \pm 5.61\%$. By the 12th week, PHBCS3 showed significantly greater degradation than PHBCS0, but there was no statistically significant difference between PHBCS1, PHBCS2, and PHBCS0. Under acidic conditions (pH = 2), the remaining mass percentages at week 12 were $42.6 \pm 4.85\%$ for PHBCS0, $31.3 \pm 8.85\%$ for PHBCS1, $4.15 \pm 7.18\%$ for PHBCS2, and 0% for PHBCS3. At this point, there was a significant difference in the remaining mass between PHBCS0 and both PHBCS3 ($P < 0.0001$) and PHBCS2 ($P < 0.0005$), while PHBCS1 did not show a significant difference ($P > 0.01$) when compared to PHBCS0. In alkaline conditions, the percentages of mass remaining at week 12 were $71.3 \pm 1.14\%$ for PHBCS0, $19.9 \pm 2.3\%$ for PHBCS1, $13.3 \pm 5.48\%$ for PHBCS2, and 0% for PHBCS3. Here, there were significant differences in the remaining mass of all samples when compared to PHBCS0 ($P < 0.0001$).

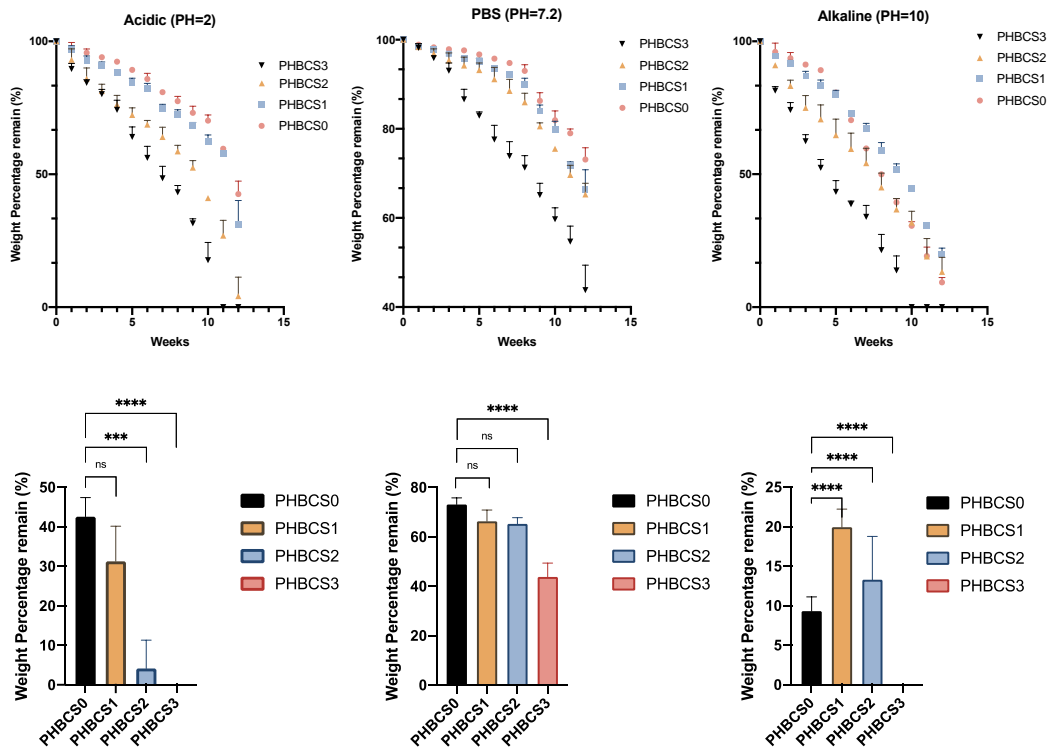


Figure 5.6: Remaining weight of PHB and PHB/CS electrospun mats between different pH levels in week 12. (**** ($p < 0.0001$), *** ($p < 0.0005$), ns ($p > 0.1$))

Figure 5.7 and Table 6 detail the SEM images and fibre diameters of PHB/CS electrospun nanofibres following a 12-week degradation period in PBS, acidic, and alkaline solutions. It was observed that in both acidic and alkaline conditions, the nano-fibrous structures diminished progressively as the CS content increased. Notably, under acidic conditions, the PHB/CS electrospun

scaffolds in all samples completely lost their nanofibrous structures. However, in alkaline and PBS conditions, the nanofibrous structure remained clearly visible in PHBCS0, PHBCS1, and PHBCS2 samples.

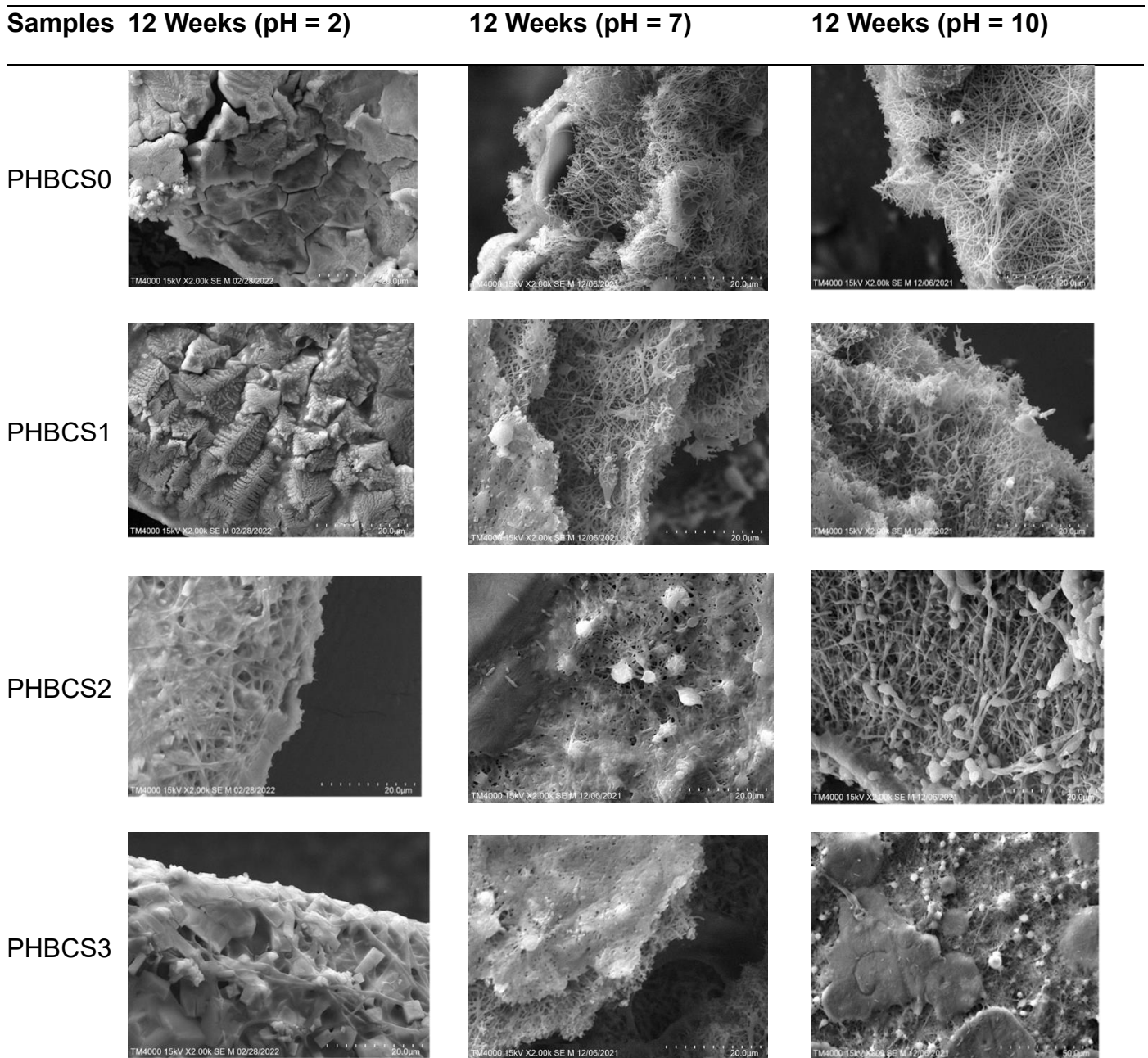


Figure 5.7: SEM graphs of remaining weight of PHB and PHB/CS electrospun mats in week 12.

Regarding in vitro degradation, PHB/CS showed varied behaviours with different CS contents under different pH levels. The presence of higher CS contents in the PHB/CS blends led to elevated degradation rates under different pH conditions. This phenomenon can be attributed to the increased loss of CS, which enhances the diffusion of water and, consequently, the interaction

between PHB and water molecules. Moreover, the observed decrease in crystallinity, coupled with an increase in hydrophilicity, facilitates accelerated hydrolysis within the PHB/CS scaffolds.

[124]. Compared to PBS solutions, PHB/CS degraded much faster in both sodium lactate/HCl and NaOH solutions. Notably, PHBCS3 completely disintegrated after 12 weeks of degradation in both acidic and alkaline solutions. This is attributed to the reduction in crystallinity and hydrophobic nature of PHBCS3, resulting in faster water penetration. In acidic conditions, samples with additional CS experienced a more rapid degradation rate than those without CS, due to the weak base nature of CS dissolving in acidic solutions. In the base solution, PHBCS0 broke down into small pieces after 12 weeks, while PHBCS1, PHBCS2, and PHBCS3 maintained structural integrity [125]. This is because pure PHB degrades into carboxylic acid and alcohol in the base solution, and hydroxyl anions can remove protons from the acid, producing negatively charged carboxylate ions.

Table 6: Average fibre diameter of PHB/CS nanofibrous membranes with different CS contents after 12 weeks of degradation in different pH values.

pH	Groups	Average Fibre Diameter (nm)
2	PHBCS0	/
	PHBCS1	/
	PHBCS2	321 ± 21.0
	PHBCS3	502 ± 103
7	PHBCS0	241 ± 13.0
	PHBCS1	401 ± 29.2
	PHBCS2	391 ± 34.4
	PHBCS3	388 ± 39.3
10	PHBCS0	298 ± 13.1
	PHBCS1	309 ± 89.3
	PHBCS2	545 ± 44.6
	PHBCS3	310 ± 98.7

5.3 Summary

This study explores the physical, chemical, and microstructural behaviours of PHB/CS electrospun fibres under acidic, neutral, and alkaline conditions with varying CS concentrations. Our findings reveal significant insights into the nano-surface morphology changes of PHB/CS. The electrospinning process successfully produced PHB/CS electrospun mats as a single phase for each composition tested. Notably, the addition of CS led to a decrease in both the hydrophobic nature and crystallinity of the PHB/CS electrospun fibres.

Further analysis focused on the degradability of PHB/CS under acidic, neutral, and alkaline conditions, revealing that the degradation rate of PHB/CS fibres increases with the addition of CS across all pH levels. The degradation rates among different pH conditions were observed in the order of acidic > alkaline > PBS, indicating that both acidic and alkaline environments significantly accelerate the degradation of PHB/CS, leading to complete dissolution at 12 weeks. Notably, acidic environments induce a more rapid degradation of the PHB/CS scaffold compared to alkaline and PBS solutions. However, either acidic or alkaline conditions in this chapter are not matched with the human

body's, which may cause misleading to degradation behaviour of PHB/CS after they planted with tissue. Therefore, Future research on *in vivo* or *in vitro* studies are necessary.

Chapter 6: A Comparison of CS Adhesion on KOH and H₂O₂ Pre-treated

Electrospun PHB Nanofibres

6.1 Overview

CS coatings are known to significantly enhance the biostability and biocompatibility of biomaterials while preserving their structural integrity. In this research, electrospun fibrous PHB membranes underwent pre-treatment with either KOH or H₂O₂, followed by modification with DA and GA to enhance their adhesion to CS. Techniques such as SEM, WCA, and FTIR were employed to confirm the successful creation of DA and GA-modified PHB fibres. It was found that PHB membranes pre-treated with KOH showed a higher binding efficiency with CS at lower concentrations compared to those pre-treated with H₂O₂. Thermal analysis revealed a notable reduction in both the degradation temperature and crystallinity for the KOH pre-treated membranes. Specifically, as the concentration of CS increased from 0 to 2 w/v%, the degradation temperature decreased from 309 °C to 266°C, and the crystallinity dropped from 100% to 25.6%. In contrast, H₂O₂ pre-treated membranes showed a modest decrease in degradation temperature from 309 °C to 285 °C and a substantial reduction in crystallinity from 100% to 43.0%. UV-Vis analysis using CBR demonstrated comparable binding efficiencies at low CS concentrations for both pre-treatment methods. However, at higher concentrations, the stability decreased for the KOH pre-treated membranes. Mechanical tests indicated a significant enhancement in the mechanical properties of KOH-treated membranes. With an increase in CS concentration from 0 to 2 w/v%, there was an increase in Young's modulus (2.0 to 14%), toughness (31 to 60%), and UTS (14 to 63%), in comparison to the H₂O₂ pre-treated membranes.

6.2 Results and discussion

6.2.1 Morphology and size of Electrospun membranes with varying CS concentrations (0.2-2 w/v%) in PHB-KOH/H₂O₂

Figure 6.1 and Figure 6.2 illustrate the morphologies and diameters of electrospun PHB fibres following various chemical post-treatments. Initially, the untreated PHB electrospun fibres had diameters averaging $5.22 \pm 0.05 \mu\text{m}$. However, post-treatment with KOH and H₂O₂, the fibre diameters were reduced to $1.90 \pm 0.42 \mu\text{m}$ and $2.78 \pm 0.12 \mu\text{m}$, respectively. This decrease is attributed to the hydrolysis effect of the KOH treatment and the hydroxyl functional groups formed onto the PHB surface by H₂O₂ treatment.

Additionally, Figure 23 shows the presence of small DA islets on the surfaces of both KOH and H₂O₂-treated fibres, a result of surface oxidation and altered roughness. A comparative analysis between KOH and NaOH reveals that KOH has slightly smaller molecular size allows for more rapid interaction with PHB, thereby improving hydrophilicity. The characteristic properties of KOH enable it to interact rapidly with PHB, thereby significantly enhancing its hydrophilicity. Additionally, the potent alkaline nature of KOH presents considerable advantages. Even at low concentrations, these properties facilitate more intense surface oxidation..

Figure 6.1 displays images and fibre diameter measurements of KOH and H₂O₂-treated PHB-DA-GA-CS with varying CS concentrations. As reported in Table 7, the mean fibre diameters of PHB-DA-GA-CS membranes showed a notable increase from 1.90 to 3.14 µm for CS concentrations ranging from 0.2 w/v% to 2 w/v% (and from 2.90 to 4.44µm respectively). At a 0.8 w/v% CS concentration, both KOH and H₂O₂ treated fibres exhibited a thin layer attached to the fibrous membrane surface. The KOH-treated fibres demonstrated a greater increase in fibre diameter compared to H₂O₂-treated fibres between 0.2 w/v% and 2 w/v% CS concentrations, which can be ascribed to the more effective oxidation from KOH pre-treatment, creating additional anchoring sites for DA and CS on the fibre surface.

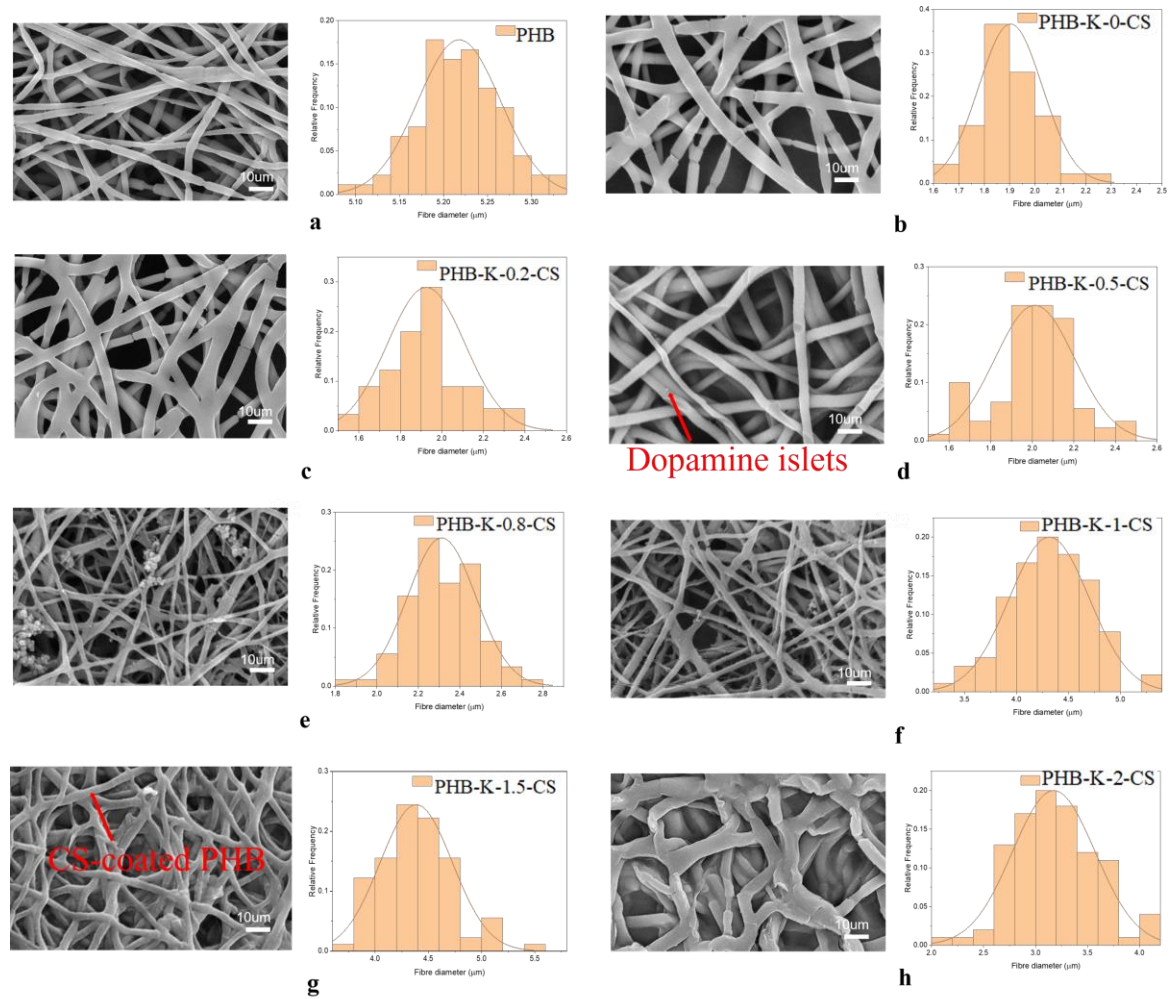


Figure 6.1: SEM micrographs and fibre diameters of PHB/KOH-treated electrospun fibres with varying CS concentrations: (a) non-treated PHB fibres, (b) 0 w/v%, (c) 0.2 w/v%, (d) 0.5 w/v%, (e) 0.8 w/v% (f) 1 w/v%, (g) 1.5 w/v%, (h) 2 w/v%

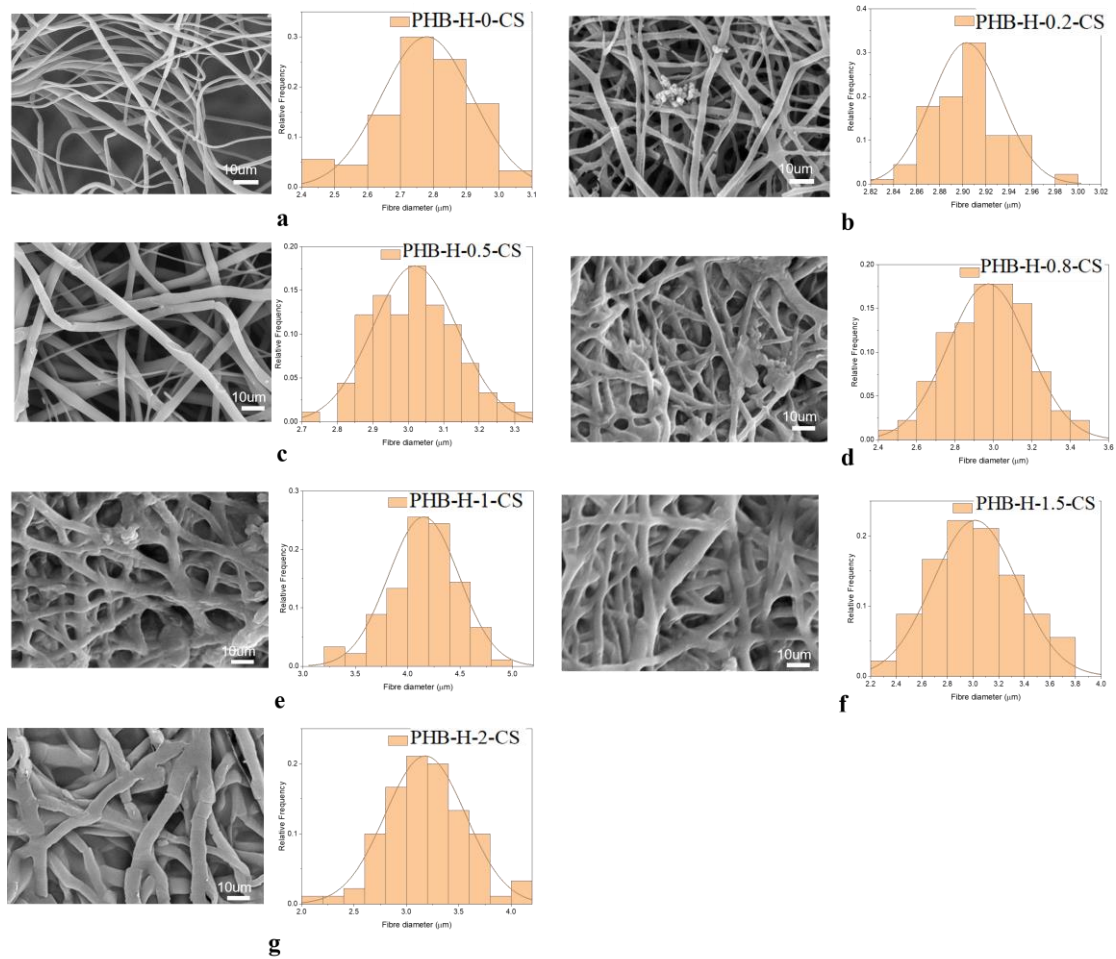


Figure 6.2: SEM micrographs of PHB/H₂O₂-treated electrospun fibres with varying CS concentrations: (a) 0 w/v%, (b) 0.2 w/v%, (c) 0.5 w/v%, (d) 0.8 w/v% (e) 1 w/v%, (f) 1.5 w/v%, (g) 2 w/v%

Figure 6.1, Figure 6.2 show that for CS concentrations ranging between 0.2 and 2 w/v%, fibres' diameter of PHB/CS has shown an increment from 2.78 to 4.41 µm and 1.90 to 3.14 for H₂O₂ and KOH treatments respectively, which proved that both KOH and H₂O₂ treatments lead to CS coatings on individual PHB fibres. Also, Figure 6.1d and g and Figure 6.2 When the CS concentration is increased between 0.8 and 2 w/v%, both H₂O₂ and KOH -treated fibres display more roughness fibre surface after CS coating compared to the lower CS concentration, where the majority of CS is observed between the fibre layers. When CS concentration reaches to 2 w/v%, neither KOH nor H₂O₂ treatments can show a clear fibrous structure as before, this could primarily due to the increased viscosity at this concentration.

Table 7: Average Fibre Diameters and Standard Deviations for PHB Electrospun Fibres Subjected to KOH and H₂O₂ Treatments with Varying CS Concentrations.

Groups	Fibre diameter (µm)	Standard deviation
PHB (Non-treated)	5.22	0.05
PHB-H-0-CS	2.78	0.14
PHB-H-0.2-CS	2.90	0.03
PHB-H-0.5-CS	3.01	0.11
PHB-H-0.8-CS	3.00	0.20
PHB-H-1-CS	4.10	0.33
PHB-H-1.5-CS	4.32	0.37
PHB-H-2-CS	4.41	0.34
PHB-K-0-CS	1.90	0.12
PHB-K-0.2-CS	1.93	0.18
PHB-K-0.5-CS	1.98	0.19
PHB-K-0.8-CS	2.31	0.18
PHB-K-1-CS	2.78	0.31
PHB-K-1.5-CS	2.98	0.35
PHB-K-2-CS	3.14	0.42

6.2.2 ATR–FTIR of PHB-CS Electrospun Fibres before and after KOH and H₂O₂ modification

Figure 6.3 presents the ATR-FTIR spectra of untreated and chemically treated electrospun PHB fibres. In its original state, PHB exhibits characteristic peaks for C=O stretching at around 1725 cm⁻¹ and ν(C-H) stretching between 2950 and 2820 cm⁻¹. After undergoing KOH or H₂O₂ treatment, PHB retains these peaks and additionally develops a bandwidth related to -OH groups in the 3600–3200 cm⁻¹ range, indicating successful enhancement of hydrophilicity.

Post-DA coating, the spectrum shows a broad peak between 3630-3120 cm⁻¹, which signifies the presence of hydroxyl and catechol groups. Peaks at 520 cm⁻¹ and 2945 cm⁻¹ are attributed to the stretching of aromatic C=C bonds in indole

and N-H amines, characteristic of DA, as validated by previous studies [8, 31, 81]. These findings confirm the successful bonding of PHB fibres with PDA. These peaks are also visible in the PHB-DA-GA and PHB-DA-GA-CS spectra, with a noted decrease in signals due to the lower number of hydroxyl groups, further indicating PDA grafting on PHB fibres.

In Figure 6.3, the FTIR spectra of KOH/ H₂O₂-treated PHB electrospun fibres after different CS concentrations show that KOH treatment leads to a greater amplification of signals at peaks 3415 cm⁻¹ (-OH groups) and 1557 cm⁻¹ (-NH₃ groups) compared to H₂O₂. This suggests that KOH induces hydrolysis degradation of PHB, breaking ester bonds and resulting in more -OH groups on the PHB surface, whereas H₂O₂ primarily performs a simple oxidation reaction. The higher efficiency of KOH pre-treatment in binding to active sites of chemicals or proteins is thus highlighted.

With increasing CS concentrations in KOH-treated PHB fibres, the signals in the fingerprint region at 816–826 cm⁻¹ and 1276–1278 cm⁻¹ diminish, indicating a decrease in PHB crystallinity. However, H₂O₂-treated PHB shows no significant differences in this region, suggesting minimal changes in crystallinity after CS addition. Moreover, N-H amine peaks at 3372 cm⁻¹ and 1623 cm⁻¹ are observed at different CS concentrations [126-128]. These results indicate that both KOH and H₂O-treated PHB/CS electrospun fibres successfully bind to PHB fibres at both high and low CS concentrations.

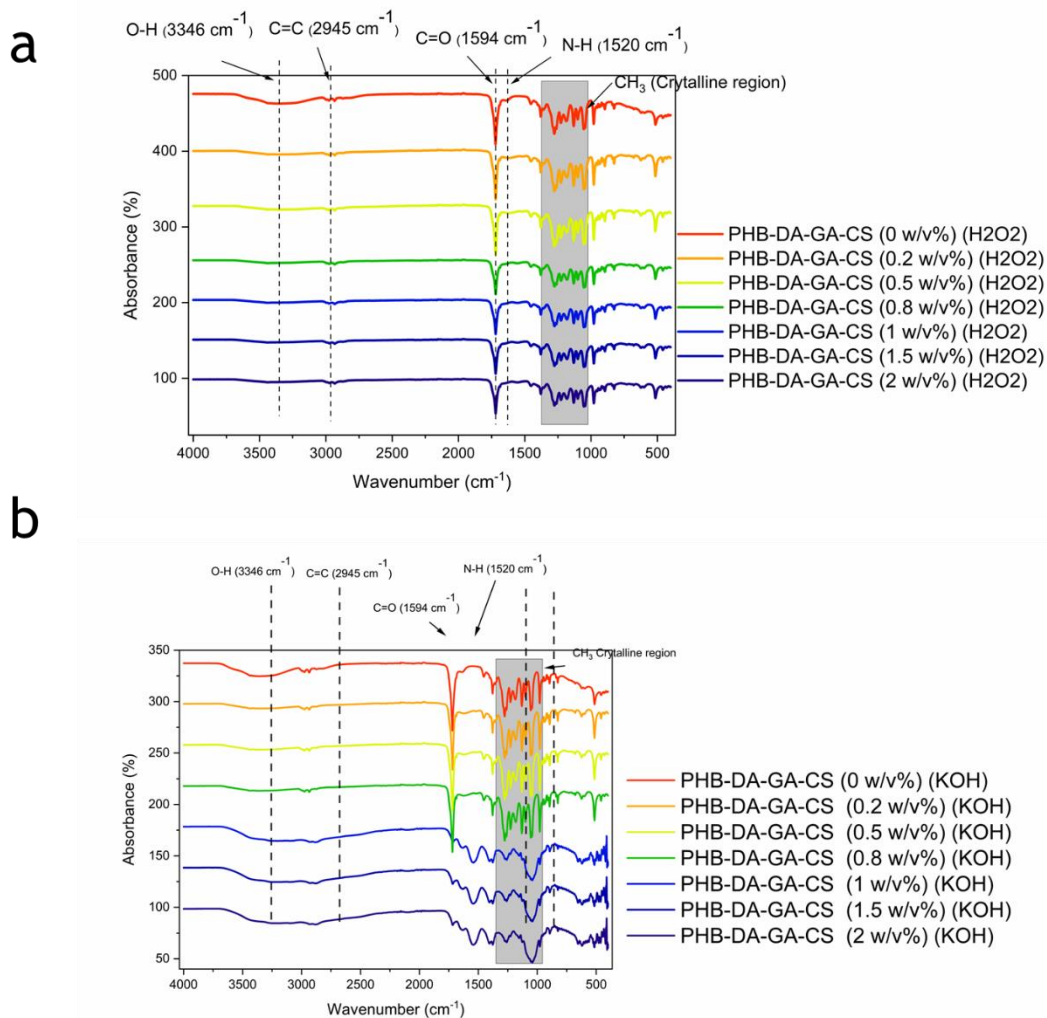


Figure 6.3: FTIR spectra comparison between untreated and treated PHB samples. (a) H₂O₂-treated PHB-DA-GA-CS electrospun fibres with CS concentrations ranging from 0 to 2 w/v%. (b) KOH-treated PHB-DA-GA-CS electrospun fibres with CS concentrations ranging from 0 to 2 w/v%.

6.2.3 TGA and DTA Analysis of PHB-CS Electrospun Fibres

The study meticulously examined the impact of H₂O₂/KOH surface modifications and varying CS concentrations on the structural properties of PHB electrospun fibres using thermal analysis. During thermal analysis, it was observed that the instruments encountered challenges, primarily attributed to the low weight of the polymer membrane samples. This issue could result in sample displacement and, consequently, the reporting of potentially negative weight percentages. Despite these challenges, the data obtained was consistently replicated and deemed reasonably reliable. Employing techniques such as TGA and DTA, the study analysed the changes induced by surface modifications and CS concentrations. The results, depicted in Figure 6.4, show that all samples exhibited two distinct peaks at high temperatures on their

heating curves. According to Table 8 and Table 9, The first melting temperature (T1) correlates with the amorphous regions of PHB or the existing CS contents, thereby illuminating their thermal properties. The second melting temperature (T2) marks the onset of degradation for the crystalline phase of PHB [31].

The thermograms (Figure 6.4a to d) reveal comparable profiles across all curves, showcasing significant changes compared to untreated PHB. Previous research supports these findings, with T1 and T2 temperatures ranging between 250-300 °C and 340-390 °C, respectively [31, 111]. This consistency validates the reliability of studies. Upon applying H₂O₂/KOH pre-treatments to PHB along with DA, there was a marked decrease in both T1 and T2 temperatures of the electrospun PHB fibres. Specifically, T1 temperatures reduced to 233.3 °C and 221.4 °C, while T2 temperatures dropped to 348.2 °C and 344.6 °C, as detailed in Table 3. KOH had a more pronounced effect on the thermal stability of the electrospun PHB nanofibres compared to H₂O₂, attributed to strong alkaline nature of KOH, which reduces crystallinity of PHB and damages its lamellar structure through hydrolysis into carboxylic acid and alcohol [31, 111, 129]. Moreover, KOH has more potent surface oxidation compared to H₂O₂ resulted in a stronger enhancement in DA coating deposition, providing greater protection to PHB fibres against thermal breakdown. This was evidenced by the initial stage breakdown (150 °C - 250 °C) of KOH-DA coating (red curve), which showed better thermal stability than the H₂O₂-DA coating. Additionally, the lower weight loss of KOH-DA-treated PHB fibre in the 300-400 °C range indicated an increase in thermal stability post-PDA breakdown. This reduction in weight loss is attributed to the increased affinity between the hydroxyl (-OH) groups introduced onto the PHB fibre surface through KOH treatment and the amine and catechol moieties of DA, leading to higher surface adherence and stability.

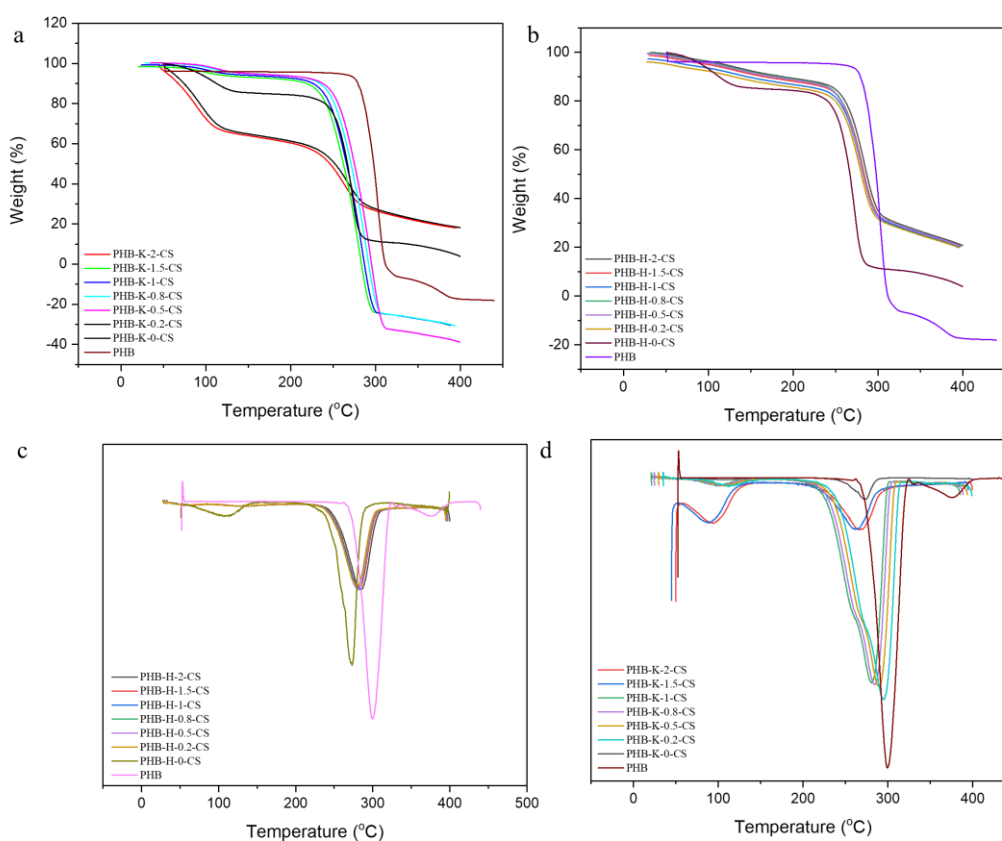


Figure 6.4: TGA and DTA analysis of between untreated and treated PHB samples. (a) KOH -treated PHB electrospun nanofibres with 2, 1.5, 1, 0.8, 0.5 and 0.2 w/v% CS. (b) H₂O₂ -treated PHB electrospun nanofibres with 2, 1.5, 1, 0.8, 0.5, and 0.2 w/v% CS (c) DTA for H₂O₂ -treated PHB electrospun nanofibres with 2, 1.5, 1, 0.8, 0.5 and 0.2 w/v% CS. (d) KOH -treated PHB electrospun nanofibres with 2, 1.5, 1, 0.8, 0.5, and 0.2 w/v% CS

Upon incorporating different concentrations of CS, the study observed variations in the T1 temperature values for both KOH and H₂O₂-treated PHB, as detailed in Table 8 and Table 9. The results indicated that the T1 temperatures for KOH-treated PHB remained within the range of 92.9 °C to 102.4 °C, whereas H₂O₂-treated PHB showed a broader range, spanning from 110 °C to 128.7 °C, across CS concentrations from 0 to 2 w/v%. For the T2 temperature, which reflects the thermal stability of the crystalline phase, KOH-treated PHB maintained a range of 280 °C – 290 °C for CS concentrations between 0 and 1 w/v% and experienced a decrease to 268.5 °C at a 2 w/v% CS concentration. In contrast, H₂O₂-treated PHB displayed less variation in the T2 temperature, ranging from 274.6 °C to 284.4 °C across different CS concentrations. The T1 temperature is typically associated with the evaporation of water and acetic acid and is highly dependent on the CS content bound to PHB fibres. The findings suggested that KOH-treated PHB fibres could bind

more CS compared to H₂O₂-treated PHB fibres. However, the T₂ degradation temperature indicated that the crystallinity phase of KOH-treated PHB was lower than that of H₂O₂-treated PHB. This could be attributed to the fact that the addition of CS potentially decreases the thermal stability of PHB as its concentration increases, a phenomenon also supported by the study of Rajan, which found that increasing concentrations of CS reduce the thermal stability of composites [130].

Table 8: TGA analysis for PHB-KOH treated electrospun nanofibres with 2, 1.5, 1, 0.8, 0.5, and 0.2 w/v% CS.

Temperature	First melting temperature (T₁)	Second melting temperature (T₂)	P value (compared to PHB-KOH-DA-GA-0 w/v% CS)
PHB-K-0-CS	113 ± 4.14	280 ± 13.2	/
PHB-K-0.2-CS	98.7 ± 5.43	290 ± 12.2	0.712
PHB-K-0.5-CS	93.7 ± 7.32	289 ± 6.62	0.691
PHB-K-0.8-CS	100 ± 6.12	285 ± 8.34	0.681
PHB-K-1-CS	102 ± 4.12	281 ± 7.12	<0.05
PHB-K-1.5-CS	88.8 ± 6.13	263 ± 5.12	<0.05
PHB-K-2-CS	92.9 ± 8.12	269 ± 5.32	<0.05

Table 9: TGA analysis for PHB- H₂O₂ treated electrospun nanofibres with 2, 1.5, 1, 0.8, 0.5, and 0.2 w/v% CS.

Temperature	First melting temperature (T ₁)	Second melting temperature (T ₂)	P value (compared to PHB- H ₂ O ₂ -DA-GA-0 w/v% CS)
PHB	309 ± 3.41	368 ± 5.12	<0.05
PHB-H-0-CS	110 ± 8.12	275 ± 11.1	/
PHB-H-0.2-CS	128 ± 5.123	282 ± 9.77	0.555
PHB-H-0.5-CS	128 ± 4.53	282 ± 6.99	0.781
PHB-H-0.8-CS	128 ± 6.21	282 ± 4.51	0.841
PHB-H-1-CS	128 ± 5.12	281 ± 6.34	0.813
PHB-H-1.5-CS	128 ± 3.53	282 ± 5.32	<0.05
PHB-H-2-CS	129 ± 5.12	284 ± 6.54	<0.05

6.2.4 DSC Analysis of PHB-CS Electrospun Fibres

Table 10 and Table 11 presents the enthalpies of fusion (H_f) associated with the amorphous phase (H₁) and the crystalline phase (H₂), as well as the crystallinity percentages calculated from DSC scans by using equation (1) [131]. Figure 28 illustrates that one of the key factors contributing to the lowered melting temperature in polymer blends with a crystallizable component is the miscibility of the constituents in the amorphous phase. Specifically, for both KOH and H₂O₂ treated PHB-GA-DA-CS electrospun fibres, the enthalpy of fusion (H₂) associated with the crystallinity phase showed a significant decrease. For KOH-treated fibres, this value dropped from 95.3 J/g to 32.8 J/g, and for H₂O₂-treated fibres, it decreased from 117.9 J/g to 58.7 J/g when the CS content increased from 0 to 2 w/v%. In contrast, the amorphous phase (H₁) exhibited only slight variations, ranging between 3.9 and 7.2 J/g. This reduction in crystallinity can be attributed to the presence of rigid CS molecules surrounding the PHB molecules, making the PHB less flexible and leading to less crystallization compared to neat PHB. This effect is likely due to a decrease in the lamellar thickness of PHB and a reduction in the percentage of its crystalline phase structure [28]. The presence of CS in the blend fibres suppresses the crystallinity of PHB through chemical interactions (such as hydrogen bonding) between the two polymers, which act as a bridge and enhance their miscibility [10, 120, 132]. Furthermore, the crystallinity of KOH and H₂O₂ treated PHB-GA-DA-CS electrospun fibres showed a reduction of approximately 45% and 40%, respectively. This decrease in crystallinity can be linked to the de-esterification of PHB caused by both KOH and H₂O₂, which directly impacts the crystalline

structure. Additionally, the introduction of CS has been reported to further reduce crystallinity [31]. The hydrolysis of PHB due to KOH treatment also contributes to this effect by reducing the lamellar thickness of the PHB.

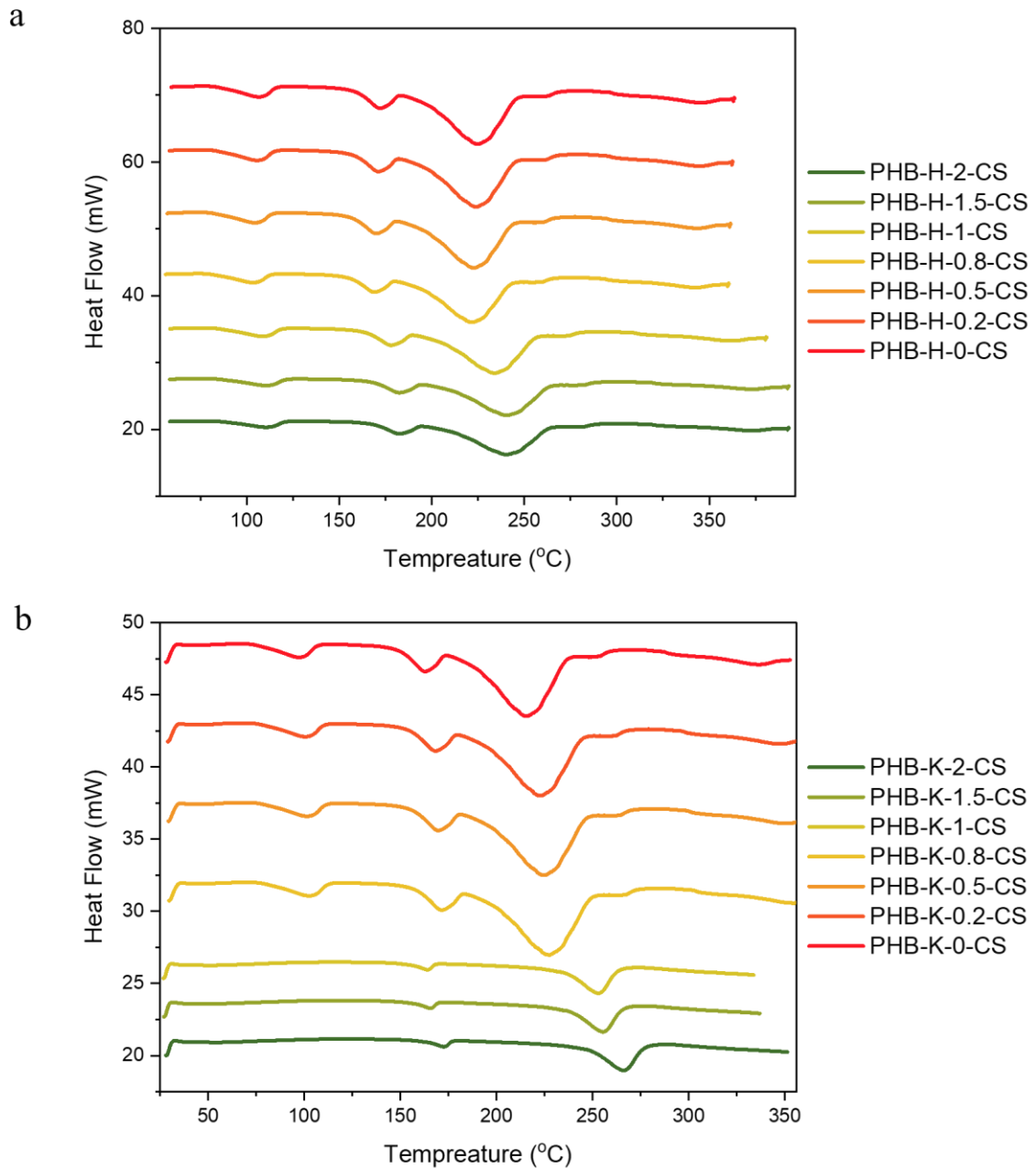


Figure 6.5: DSC analysis of PHB-KOH/ H₂O₂ treated electrospun nanofibres with CS concentrations of 2, 1.5, 1, 0.8, 0.5, and 0.2 w/v%: (a) KOH-treated samples and (b) H₂O₂-treated samples.

Table 10: Enthalpy of fusion and crystallinity of the electrospun PHB-KOH/ H₂O₂ treated electrospun nanofibres with 2, 1.5, 1, 0.8, 0.5, and 0.2 w/v% CS.

	Enthalpy of fusion		Crystallinity
	ΔH_{fusion} (J/g)		%
	H ₁	H ₂	
PHB-K-0-CS	4.87	95.31	70.40
PHB-K-0.2-CS	3.83	42.60	31.81
PHB-K-0.5-CS	4.03	41.52	31.12
PHB-K-0.8-CS	4.32	38.24	29.14
PHB-K-1-CS	4.34	37.01	28.31
PHB-K-1.5-CS	4.51	35.13	27.12
PHB-K-2-CS	4.52	32.81	25.62

Table 11: Enthalpy of fusion and crystallinity of the electrospun PHB- H₂O₂ treated electrospun nanofibres with 2, 1.5, 1, 0.8, 0.5, and 0.2 w/v% CS.

Groups	Enthalpy of fusion		Crystallinity
	ΔH_{fusion} (J/g)		%
	H ₁	H ₂	
PHB-H-0-CS	6.80	117.92	85.21
PHB-H-0.2-CS	5.91	72.31	53.62
PHB-H-0.5-CS	6.27	71.23	53.13
PHB-H-0.8-CS	7.02	70.82	53.32
PHB-H-1-CS	7.16	65.21	49.63
PHB-H-1.5-CS	7.19	62.82	47.91
PHB-H-2-CS	7.39	58.73	45.34

6.2.5 Hydrophilicity analysis of PHB-CS Electrospun Fibres with contact angle measurements

Figure 6.6 showed the hydrophilic characteristics of ten different PHB membrane groups at various stages of functionalization, highlighting significant differences in their WCA. The untreated PHB electrospun membrane exhibited a notably high WCA of $95^{\circ} \pm 7.2^{\circ}$, indicating its inherent hydrophobic nature. In contrast, treatments with KOH and H_2O_2 , which promote the formation of surface hydroxyl groups, substantially reduced the WCAs to 0° and $10^{\circ} \pm 2.2^{\circ}$, respectively. Following the deposition of DA on the PHB membranes, the WCAs of both KOH- and H_2O_2 -treated PHB increased significantly to $35^{\circ} \pm 5.3^{\circ}$. This indicates that while the initial hydrophobic properties of electrospun PHB fibres were altered by post-treatment, the application of a DA coating further transformed the PHB fibre membranes towards increased hydrophilicity [61, 111]. The study also examined the reduction in fibre diameter of PHB after treatment with KOH and H_2O_2 , as presented in Table 7. It was found that the increase in surface roughness contributed to the enhanced surface hydrophilicity [15,17,21]. Despite these modifications, the DA-coated membranes maintained improved hydrophilicity compared to the untreated PHB membrane even after undergoing various treatments. The addition of GA and CS further increased the hydrophilic nature of the membranes, as indicated by a slight decrease in WCA values to approximately 32° . This trend aligns with findings from previous studies [26, 129]. The incorporation of CS into the PHB membranes reduced the WCA to $20^{\circ} \pm 4.1^{\circ}$ for KOH-treated PHB and to $35^{\circ} \pm 3.1^{\circ}$ for H_2O_2 -treated PHB, across various CS concentrations (0.2% to 2% w/v). Interestingly, PHB-DA-GA-CS membranes treated with KOH consistently exhibited a WCA of $22^{\circ} \pm 3.2^{\circ}$, regardless of the increasing CS content, whereas those treated with H_2O_2 showed slightly higher WCA values. This disparity can be attributed to the different processes and effectiveness of surface oxidation by KOH and H_2O_2 . KOH facilitates a stable hydrolysis reaction on PHB, breaking ester linkages and creating carboxyl and hydroxyl groups [3, 10, 51, 114, 120]. Conversely, H_2O_2 generates unstable active oxygen species on the PHB surface over time, resulting in less consistent outcomes [3, 114].

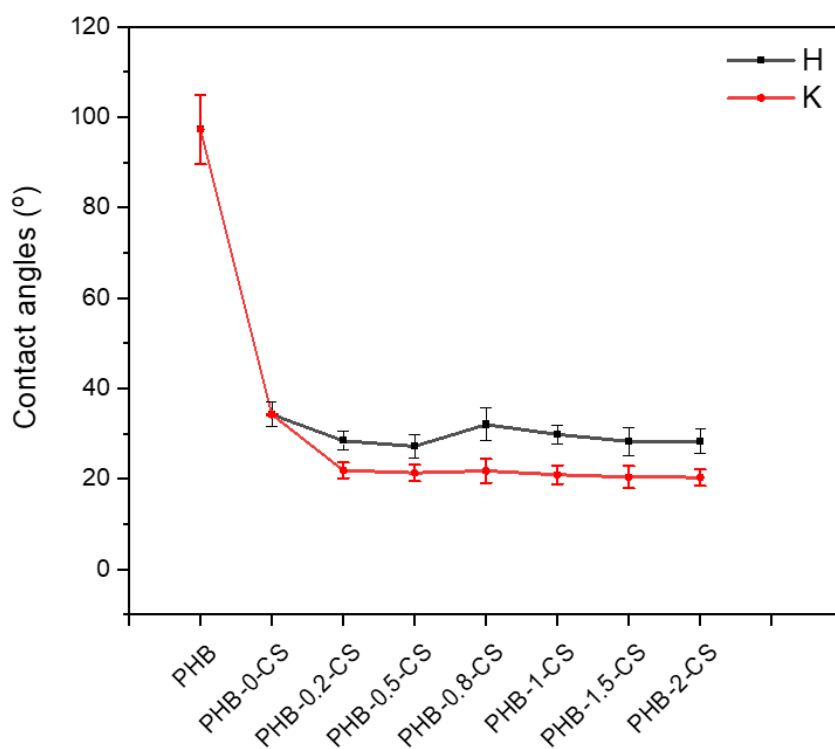


Figure 6.6: The average water contact angles of the PHB-KOH/H₂O₂ treated electrospun nanofibres with non-treated, 0, 0.5, 0.8, 1, 1.5, 2 w/v% CS.

6.2.6 Analysis of Specific Surface Area of PHB-CS Electrospun Fibres Using BET Method

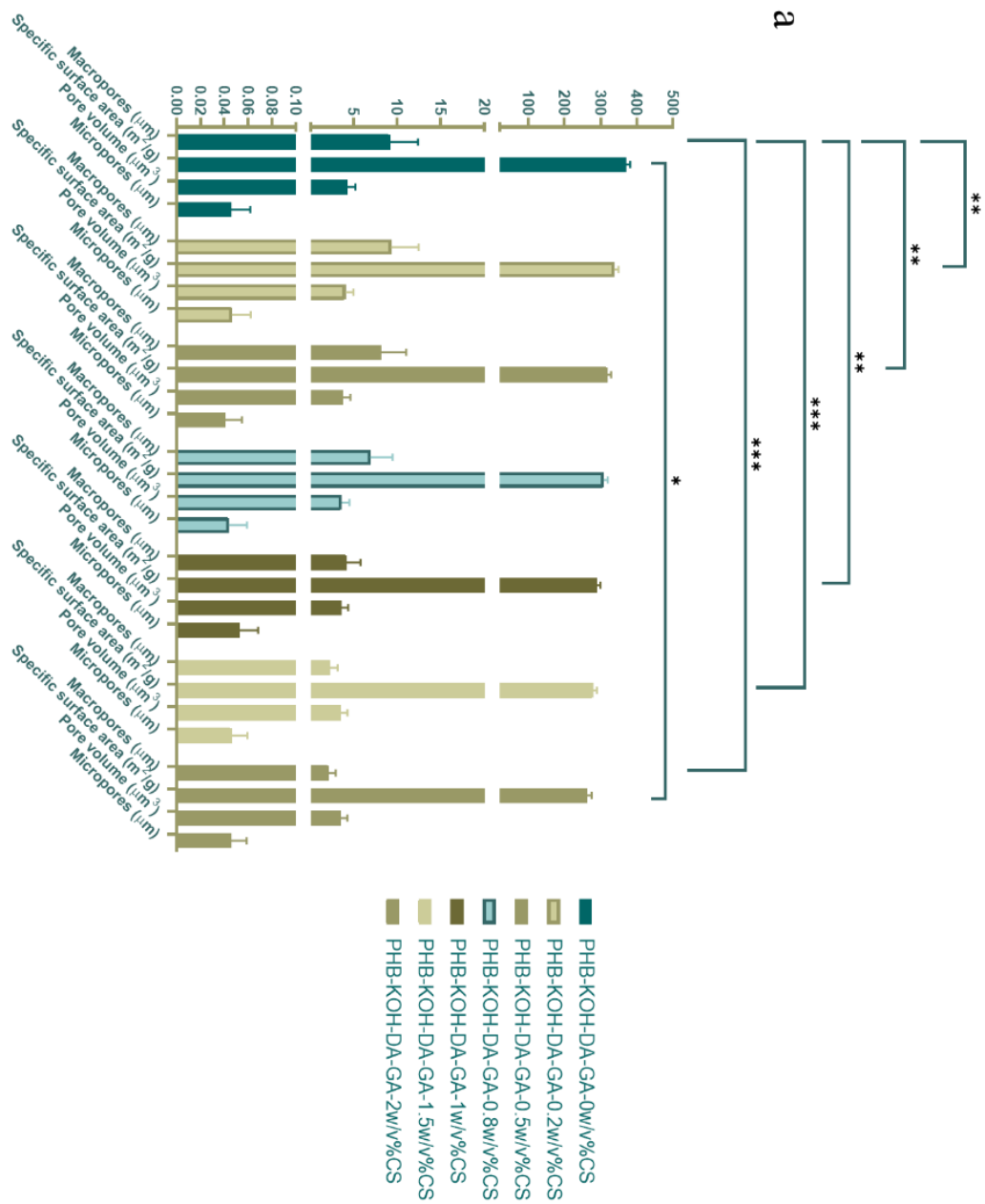
Figure 31, Table 12 and Table 13 presented the results of the specific surface area between KOH/ H₂O₂-treated PHB electrospun nanofibres. Seven fibrous samples were examined for their specific surface area various with CS concentration. the specific surface area of KOH-treated PHB electrospun fibres decreased from $338 \pm 12.3 \text{ m}^2/\text{g}$ to $264 \pm 12. \text{ m}^2/\text{g}$, whereas H₂O₂-treated PHB dropped from $338 \pm 12.3 \text{ m}^2/\text{g}$ to $260 \pm 11. \text{ m}^2/\text{g}$. The decrement in specific surface area with increasing CS concentration in the PHB matrix can be attributed to a combination of factors, including CS particle size and distribution, viscosity and processing conditions, influence on crystallinity, and crosslinking or physical entanglements [31, 52, 90]. As CS concentration increases, particle agglomeration may lead to a more compact structure with fewer voids [30, 54] [14, 38]. Additionally, the potential role of CS as a nucleating agent might promote the formation of denser crystalline regions with reduced surface area compared to amorphous regions [31]. Furthermore, both physical entanglements induced by CS and chemical crosslink formed between PHB can create a more compact and dense structure, ultimately decreasing the specific surface area and pore volume in the composite material [29, 31, 116].

Table 12: Effect of CS Concentration on Macropore Size, Micropore Size, Specific Surface Area, and Pore Volume of PHB-K electrospun membranes

Groups	Specific surface area(m ² /g)
PHB-K-0-CS	371 ± 11.3
PHB-K-0.2-CS	338 ± 12.3
PHB-K-0.5-CS	319 ± 10.2
PHB-K-0.8-CS	309 ± 11.2
PHB-K-1-CS	291 ± 8.92
PHB-K-1.5-CS	280 ± 10.2
PHB-K-2-CS	264 ± 12.1
PHB (Non-treated)	276 ± 10.2

Table 13: Effect of CS Concentration on Specific Surface Area of PHB-H electrospun membranes

Groups	Specific surface area(m ² /g)
PHB-H-0-CS	371 ± 11.3
PHB-H-0.2-CS	338 ± 12.3
PHB-H-0.5-CS	319 ± 10.2
PHB-H-0.8-CS	309 ± 11.2
PHB-H-1-CS	291 ± 8.92
PHB-H-1.5-CS	280 ± 10.2
PHB-H-2-CS	260 ± 11.1



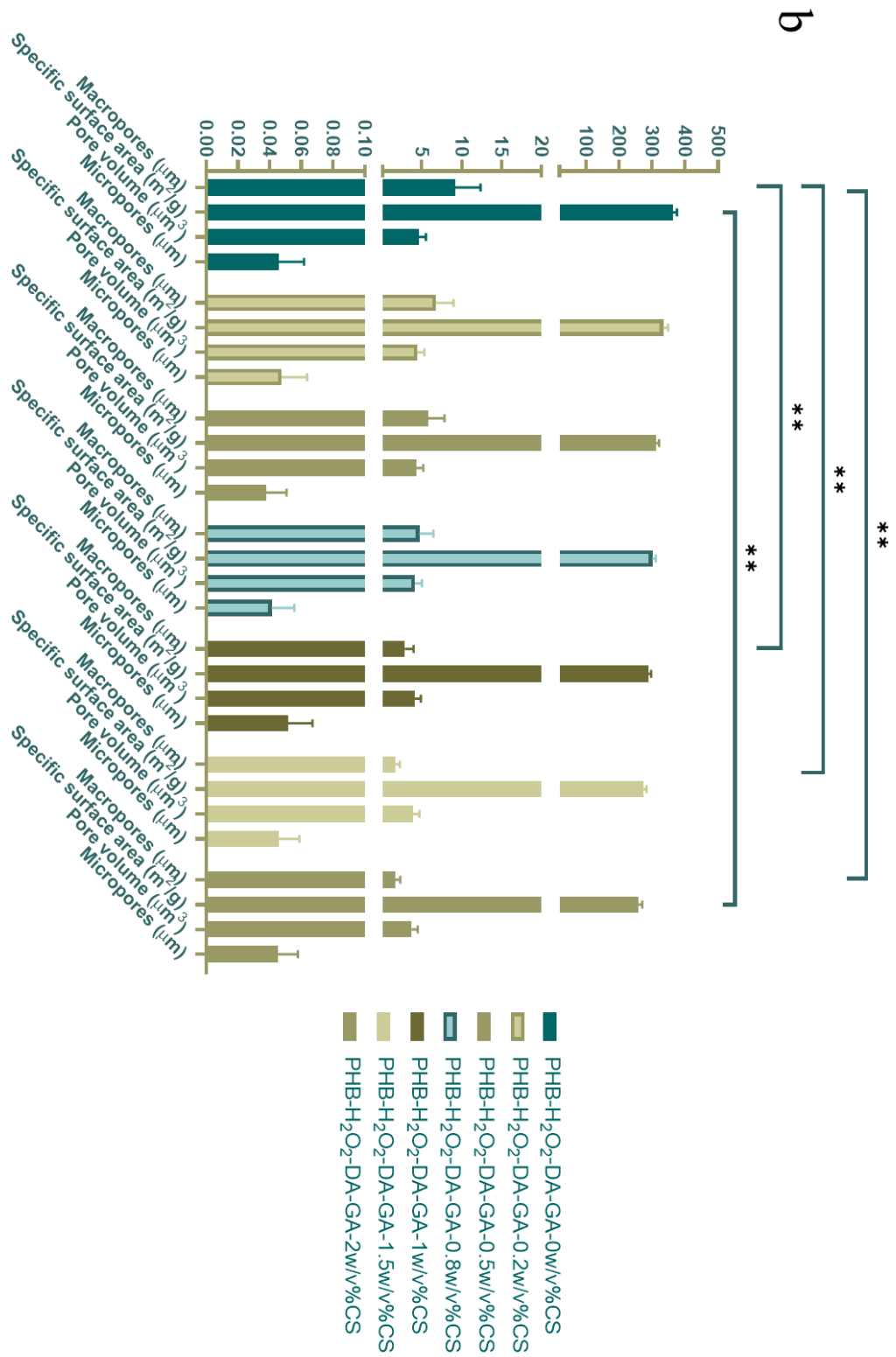


Figure 6.7: BET analysis of macropore size, micropore size, specific surface area, and pore volume. of PHB-KOH/H₂O₂ treated electrospun nanofibres with CS concentrations of 2, 1.5, 1, 0.8, 0.5, 0.2, and 0 w/v%, displaying. (a)KOH-treated and (b) H₂O₂-treated.

6.2.7 Stability Assessment of KOH/H₂O₂ PHB-DA-GA-CS Electrospun Samples: UV-Vis and CBR Analytical Techniques

Figure 6.8 presents the UV-Vis analysis of the stability of KOH/ H₂O₂-treated PHB-DA-GA-CS electrospun samples using CBR analytical techniques. The analysis focused on the release of CS, as indicated by the peak intensity between 506 and 550nm, as established in Figure 9. The study found that the release percentages of CS from the KOH-treated PHB-DA-GA-CS electrospun fibres varied with the concentration of CS. Specifically, the release percentages were 57.7% (0 w/v% CS), 64.0% (0.2 w/v%), 84.0% (0.5 w/v%), 61.9% (0.8 w/v%), 84.3% (1 w/v%), 89.4% (1.5 w/v%), and 103.2% (2 w/v%). In comparison, the H₂O₂-treated PHB-DA-GA-CS electrospun fibres exhibited lower release percentages at corresponding CS concentrations: 45.2% (0 w/v%), 53.8% (0.2 w/v%), 65.7% (0.5 w/v%), 48.4% (0.8 w/v%), 66.5% (1 w/v%), 69.9% (1.5 w/v%), and 80.7% (2 w/v%). The maximum release of CS from the KOH-treated samples was observed to be 23% higher than that from the H₂O₂-treated samples. This difference is attributed to the hydrolysis effect of KOH on PHB, which leads to the de-esterification of its chemical structure. Additionally, the acidic by-products of PHB cause the CBR to turn red. The initial slope of the cumulative release profile of CS across different concentrations indicates the rate at which CS was released from the samples [111, 118, 129]. Overall, the KOH-treated PHB-DA-GA-CS electrospun membranes demonstrated a faster release rate compared to the H₂O₂-treated ones, corroborating findings from other research studies [22, 25, 33]. This faster release rate in KOH-treated samples can be linked to the altered chemical structure of PHB due to the hydrolysis effects of KOH [111, 127, 129].

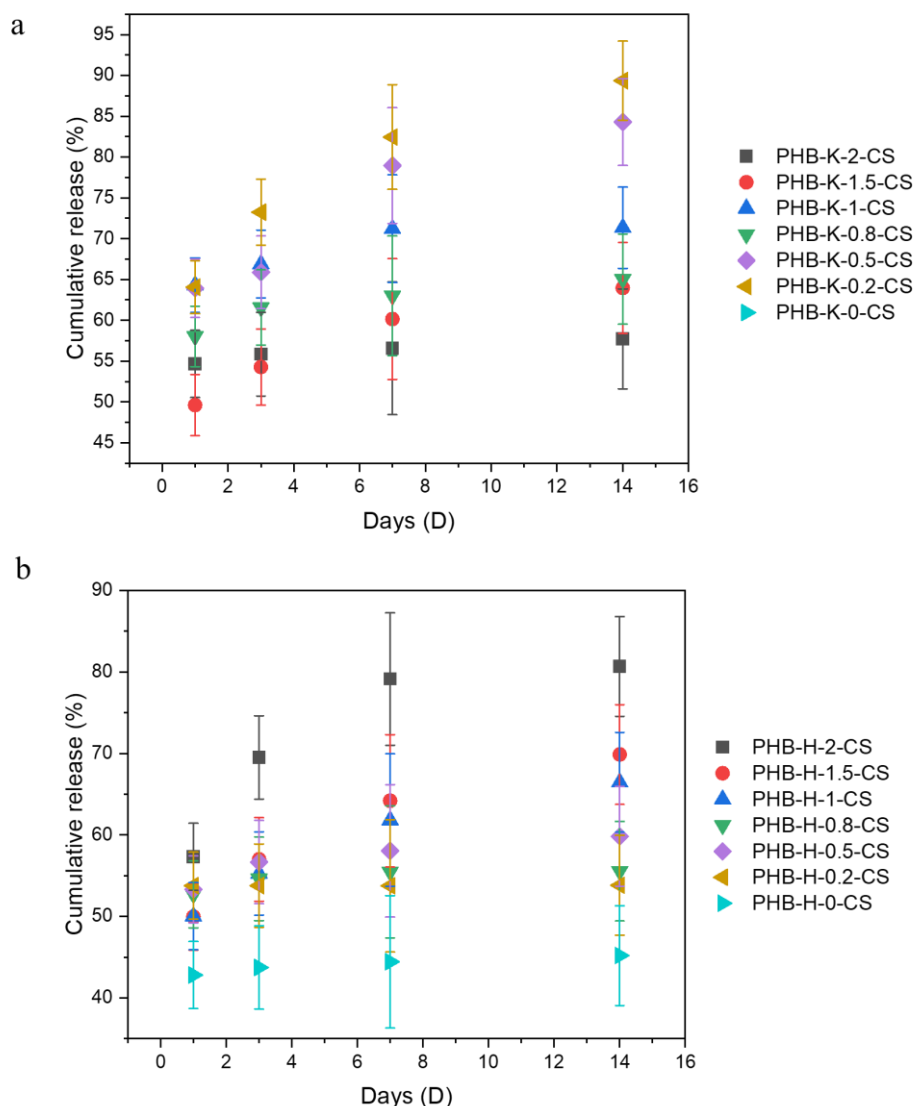


Figure 6.8: The UV-VIS of PHB electrospun fibres with (a) KOH and (b) H₂O₂ treated electrospun nanofibres with 2, 1.5, 1, 0.8, 0.5, 0.2, and 0 w/v% CS.

6.2.8 Mechanical Properties of KOH- and H₂O₂-Treated PHB Electrospun Nanofibres with Varying CS Concentrations: Tensile Strength, Toughness, Young's Modulus, and Elongation at Break

Table 14 and Table 15 showed details the mechanical properties, such as tensile strength, toughness, Young's modulus, and elongation at break, of both KOH- and H₂O₂-treated PHB electrospun nanofibres at varying CS concentrations (0, 0.2, 0.5, 0.8, 1, 1.5, and 2 w/v%). The application of CS coating on the PHB fibres led to a notable increase in their flexibility, as evidenced by the decrease in Young's modulus with the rise in CS content. This trend indicates that the fibres become less stiff as more CS is added.

Particularly, the PHB-DA-GA-CS fibres with a CS concentration of 2 w/v% showed the most significant drop in Young's modulus, suggesting they have the highest flexibility among the tested samples. Moreover, there was an inverse relationship observed between the CS content and the elongation at break of the fibres. As the CS concentration increased, the elongation values also rose, suggesting enhanced ductility and a better resistance to breakage. This improvement can be attributed to the successful coating of the PHB fibres with CS, which effectively reduces their natural brittleness.

Furthermore, when considering their thermal properties, as analyzed through TGA, it was found that CS-coated PHB fibres exhibited improved thermal stability compared to their uncoated counterparts. This increase in thermal stability is likely a contributing factor to the enhancements seen in the mechanical properties of the CS-coated fibres. The findings indicate that the addition of CS not only impacts the mechanical flexibility and ductility of the PHB fibres but also positively influences their thermal behavior.

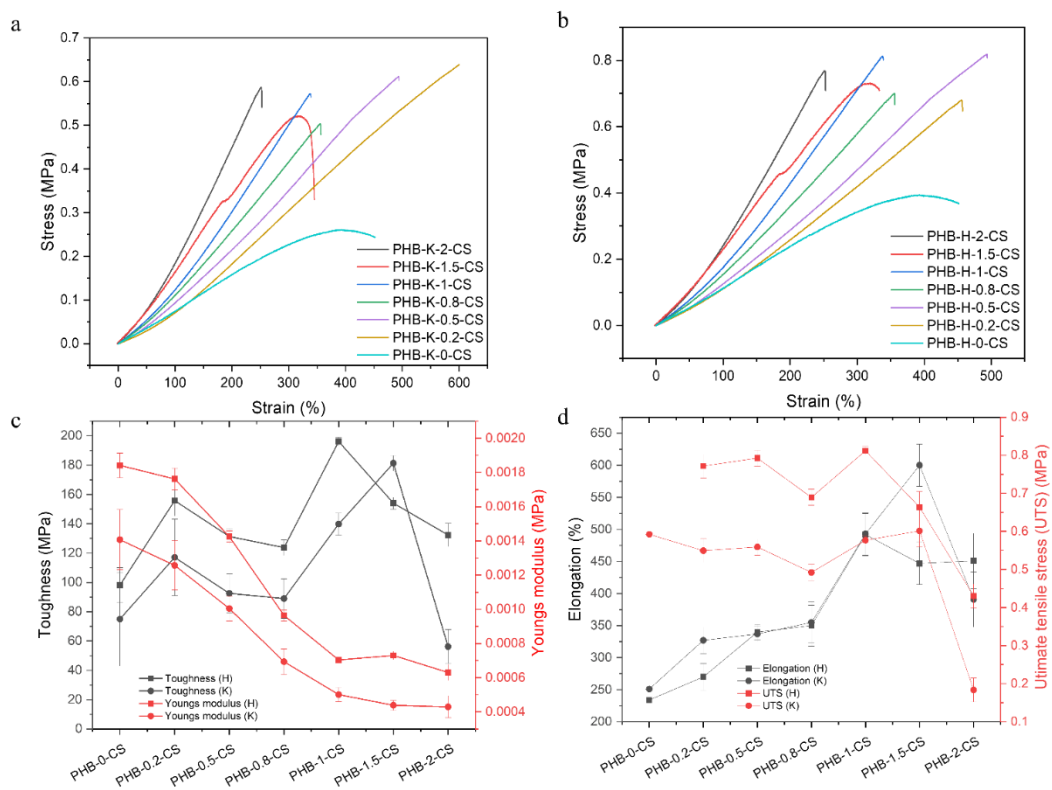


Figure 6.9: Mechanical properties of PHB electrospun fibres with CS concentrations of 2, 1.5, 1, 0.8, 0.5, 0.2, and 0 w/v%: (a) Tensile properties of KOH-treated samples, (b) tensile properties of H₂O₂-treated samples, (c) toughness and Young's modulus for both KOH and H₂O₂ treated samples, and (d) elongation and ultimate tensile strength (UTS) for both KOH and H₂O₂ treated samples.

Table 14: Mechanical properties of PHB-KOH treated electrospun nanofibres with 2, 1.5, 1, 0.8, 0.5, 0.2, and 0 w/v% CS.

Groups	Elongation at break (%)	Young's modulus (MPa)	Toughness (MPa)	UTS (MPa)
PHB-K-0-CS	390	0.00043	56	0.18
PHB-K-0.2-CS	600	0.00044	180	0.6
PHB-K-0.5-CS	490	0.0005	140	0.58
PHB-K-0.8-CS	360	0.00069	89	0.49
PHB-K-1-CS	340	0.001	93	0.56
PHB-K-1.5-CS	330	0.0013	120	0.55
PHB-K-2-CS	250	0.0014	75	0.59

Table 14 and Table 15 display the mechanical properties, including tensile strength, toughness, Young's modulus, and elongation at break, of PHB nanofibres treated with KOH and H₂O₂ at varying CS concentrations. The data reveals that the hydrolysis effect of KOH on PHB leads to lower UTS values for KOH-treated PHB fibres, ranging from 0.59 MPa to 0.18 MPa, compared to H₂O₂-treated fibres, which range from 0.77 MPa to 0.43 MPa, as the CS concentration increases from 0 to 2 w/v%. Notably, between 0 and 1.5 w/v% CS, the UTS values for both KOH and H₂O₂-treated fibres show minimal variations. When the CS content is increased from 1.5 w/v% to 2 w/v% for both treatments, there is no significant increase in UTS. This can be explained that saturated CS coated on PHB has little effect on the mechanical properties of PHB-CS, which could further be proven from SEM in Figure 6.1 and Figure 6.2.

The toughness of both KOH and H₂O₂-treated PHB membranes generally increases with CS concentrations up to 1.5 w/v%. However, upon adding 2 w/v% CS, a notable decrease in toughness is observed, particularly in the KOH-treated membranes. Additionally, as the concentration of CS increases, the elongation-at-break values for both KOH and H₂O₂-treated membranes show an overall upward trend. This improvement in toughness and elongation-at-break can be attributed to the crack-pinning mechanism of CS in the blended films, which enhances the overall resilience of the electrospun membranes.

The increased miscibility of KOH-treated PHB with high concentrations of CS, due to reduced crystallinity, may lead to CS becoming the mechanically dominant component in the blend. This shift could affect the overall mechanical

properties of the electrospun membranes, resulting in a significant reduction in toughness, especially at higher CS concentrations. The study's findings underscore the complex interactions between PHB, CS, and the chemical treatments, all of which play crucial roles in determining the final mechanical properties of the electrospun nanofibres.

Table 15: Mechanical properties of PHB- H₂O₂ treated electrospun nanofibres with 2, 1.5, 1, 0.8, 0.5, 0.2, and 0 w/v% CS.

Groups	Elongation at break (%)	Young's modulus (MPa)	Toughness (Nmm⁻³)	UTS (MPa)
PHB-H-0-CS	450	0.00063	130	0.43
PHB-H-0.2-CS	450	0.00073	150	0.66
PHB-H-0.5-CS	490	0.0007	200	0.81
PHB-H-0.8-CS	350	0.00096	120	0.69
PHB-H-1-CS	340	0.0014	130	0.79
PHB-H-1.5-CS	270	0.0018	160	0.77
PHB-H-2-CS	230	0.0018	98	0.77

6.3 Summary

In this study, the impact of KOH and H₂O₂ pre-treatments on PHB nanofibres was found to significantly differ, not only in altering the extent of CS binding to PHB fibres at low concentrations but also in modifying surface morphology, chemical composition, thermal and structural stability, and mechanical properties. The fibre morphology and porous structure exhibited noticeable changes post-treatment. Both KOH and H₂O₂ pre-treatments facilitated the formation of chemical linkages between CS and PHB, with KOH showing greater efficacy at low concentrations. However, both pre-treatments resulted in reduced thermal and structural stability, and mechanical properties, with KOH leading to more pronounced changes than H₂O₂. Additionally, KOH-treated samples demonstrated lower stability in CS binding compared to H₂O₂-treated samples, potentially due to the more extensive disruption of the PHB matrix. , Although the findings of this study are promising, they underscore the necessity for additional research, particularly concerning the cellular response to these enhanced nanofibres through both in vitro and in vivo trials. This further

investigation is crucial for confirming the modified nanofibres' appropriateness for use in regenerative medicine and other biomedical applications.

Chapter 7: Electrospinning of PHB/CS nanofibres for tuneable Forskolin

delivery

7.1 Overview

Electrospun nanofibres offer a promising platform for drug delivery due to their substantial specific surface area, which closely mimic the microstructures in the ECM. This chapter investigates the properties and drug release behaviour of PHB/CS co-electrospun fibres with PEO additive. Initially, we synthesized electrospun PHB samples with varying volume ratios of CF to DMF, ranging from 9:1 to 7:3, to explore changes in surface morphology. Then, we modified the PHB electrospun fibres by incorporating CS and combining them with PEO using single-jet electrospinning and co-electrospinning processes.

Our findings revealed that PHB/CS fibres with 8:2 and 9:1 CF/DMF volume ratios exhibited less variation in fibre diameters than other CF/DMF ratios. Additionally, incorporating both 5 and 10 w/v% PEO into the fibres resulted in larger fibre diameters, increased specific surface areas, and greater pore volumes, but with smaller pore sizes. The Forskolin release behaviour of the resulting nanofibres was characterized by a four-stage release profile, consisting of zero-order, first-order, Higuchi, and Korsmeyer-Peppas models. All samples closely correlated with these release profiles at different stages. Moreover, the release exponent from the Korsmeyer-Peppas equation indicated that, without the addition of PEO, Fickian diffusion predominates in the PHB/CS electrospun membranes across all CF/DMF ratios. In contrast, adding PEO shifted the PHB/CS to a skeleton diffusion mechanism. Co-electrospinning of PHB/CS fibres resulted in a faster release exponent than single-jet electrospinning, suggesting more pronounced skeleton dissolution in the former. Lastly, comparing single-jet and co-electrospun PHB/CS fibres, the degradation profile was influenced by their composition and processing methods, with single-jet nanofibres samples generally exhibiting more significant changes in degradation percentages over time compared to co-electrospinning samples, particularly in the 9:1 and 8:2 CF/DMF PHB/CS ratios.

7.2 Results and Discussion

7.2.1 SEM Analysis and Diameter Measurement of PHB/CS-based Electrospun Fibres

The preparation of PHB-2 w/v% CS electrospun fibres was previously described in the literature [31]. Figure 7.1 has shown that as the ratio changes between CF/DMF from 9:1 to 7:3, there is a notable increase in the mean diameter of the fibres from 1.056 μm in the 9:1 ratio to 1.784 μm in the 7:3 ratio. This pattern is consistent across measurements and strongly suggests that the composition ratio of PHB and CS exerts a significant influence on fibre diameter. Furthermore, an increase in standard deviation was observed alongside the increase in fibre diameter. For the 9:1 ratio, the observed standard deviation is 0.147 μm , which increases to 0.725 μm for the 7:3 ratio. The range of fibre diameters also exhibits significant expansion with the change in composition. In the 7:3 composition, the diameter range is remarkably broad, extending from 0.521 μm to 2.989 μm . This extensive range could be reflective of diverse dynamics in fibre formation, influenced by the changing composition. This can be explained by the fact that the DMF has relative high dielectric constant, which should be responsible for the decreasing fibre diameter, while it also slows down the rate of solvent volatilisation and causes the formation of more branching PHB fibres [26, 80, 101, 108]. Also, the reduction of CF will cause low solubility of PHB in the blended solvent and increase instability during fibre fabrication, which destroys the consistency of fibre formation [133]. Other research has further observed that the reduction of the total volume ratio of DMF can induce shrinkage of the fibre [121].

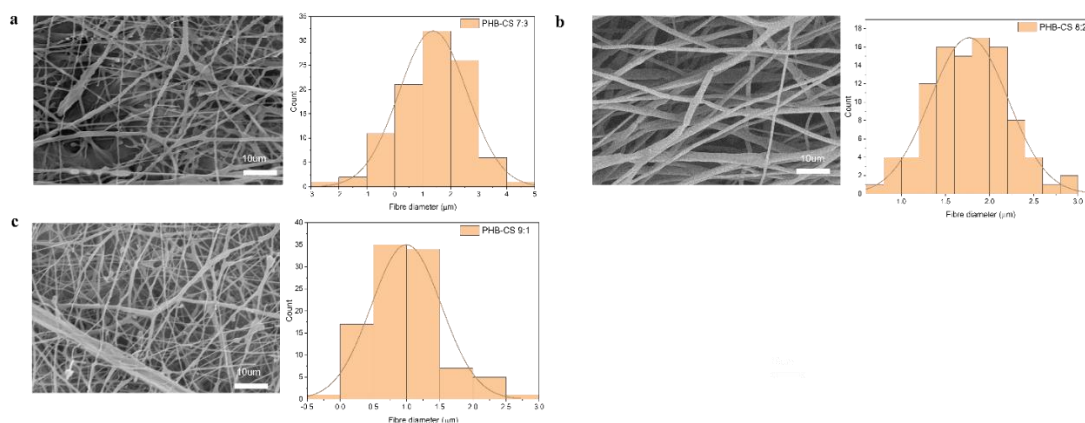


Figure 7.1: SEM graphs PHB/CS electrospun fibres with different CF/DMF ratio. (a) 7:3 CF/DMF (b) 8:2 CF/DMF (c) 9:1 CF/DMF

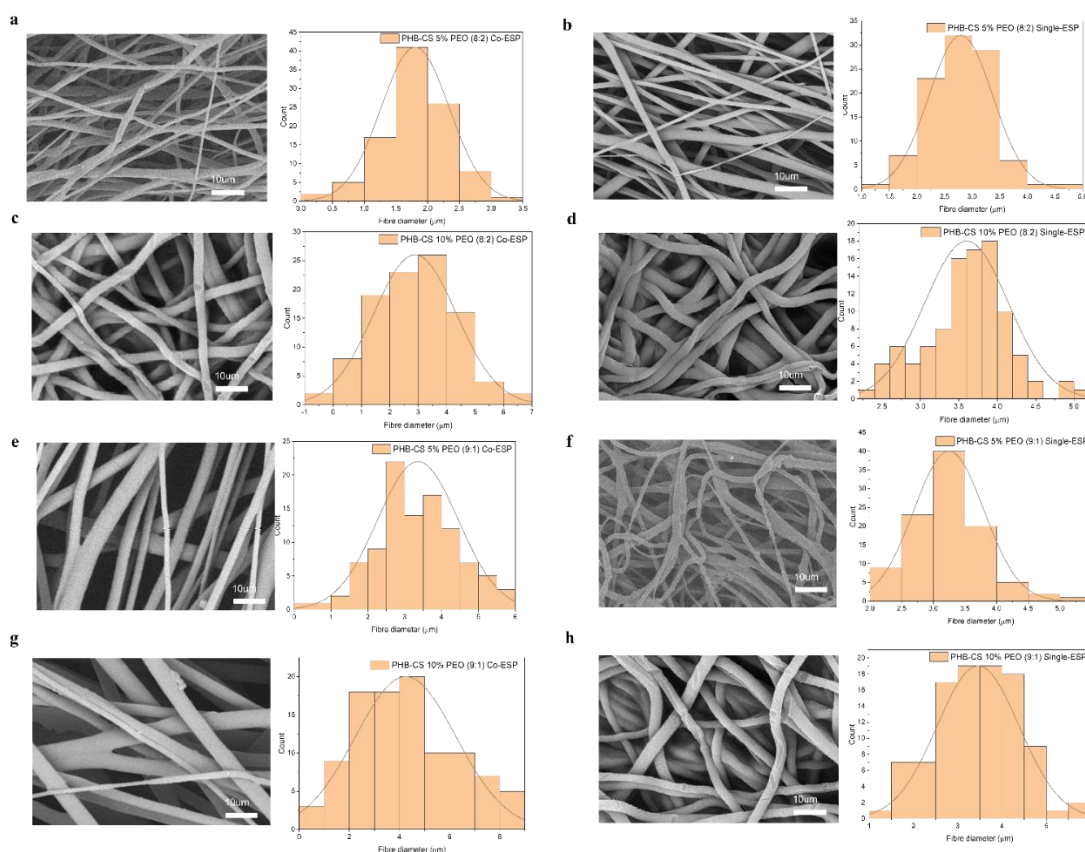


Figure 7.2: SEM graphs PHB/CS electrospun fibres with different concentration of PEO and fabrication techniques. (a) PHB-2wt CS-5 w/v% PEO (8:2) Co-ESP (b) PHB-2wt CS-5 w/v% PEO (8:2) Single-ESP (c) PHB-2wt CS-10 w/v% PEO (8:2) Co-ESP (d) PHB-2wt CS-10 w/v% PEO (8:2) Single-ESP (e) PHB-2wt CS-5 w/v% PEO (9:1) Co-ESP (f) PHB-2wt CS-10 w/v% PEO (9:1) Single-ESP (g) PHB-2wt CS-10 w/v% PEO (9:1) Co-ESP (h) PHB-2wt CS-5 w/v% PEO (9:1) Single-ESP

In Figure 7.2 and Table 16, the blend composition with PEO appeared to significantly influence the fibre diameters of PHB/CS. In the case of PHB-2 w/v% CS with 5 and 10 w/v% PEO (8:2) in Single-ESP, the average fibre diameter was measured at 2.80 and 3.54 μm , with a relatively low standard deviation of 0.54 μm . This can be explained that higher concentration PEO leads to the higher viscosity of PHB/CS solution, and causes thicker fibre. Also, it has proven that with addition of PEO, this polymer systems contributed to the formation of uniform, fine fibres form [43, 120, 121, 134]. Contrastingly, between the two different fabrication methods, the Co-ESP process using a PHB-2 w/v% CS-10 w/v% PEO (8:2) blend exhibited a decrease in average fibre diameter (3.10 μm) compared to its single-ESP counterpart. This reduction can be attributed to the synergistic effect of co-electrospinning, where the effective blending and binding of PHB, CS, and PEO in the solution lead to enhanced polymer entanglement. As a result, this leads to a more uniform solution and the formation of finer fibres. [41, 42].

Adjusting the ratio of PHB to CS to 9:1, the PHB with 2 w/v% CS and 10 v/v% PEO (9:1) in single electrospinning (Single-ESP) exhibited an average fibre diameter of 3.50 μm with a standard deviation of 0.89 μm . In contrast, PHB with 2 w/v% CS and 10 w/v% PEO (9:1) in co-electrospinning (Co-ESP) displayed a significantly larger average diameter of 4.00 μm , with a standard deviation of 2.11 μm . The Co-ESP process, in this case, appeared to result in a broader distribution of fibre diameters, possibly due to low solubility between CS and PEO and cause non-even fibre formation during the jetting. Besides, high concentration of PEO will increase the viscosity and cause larger fibre formation [18, 68, 69].

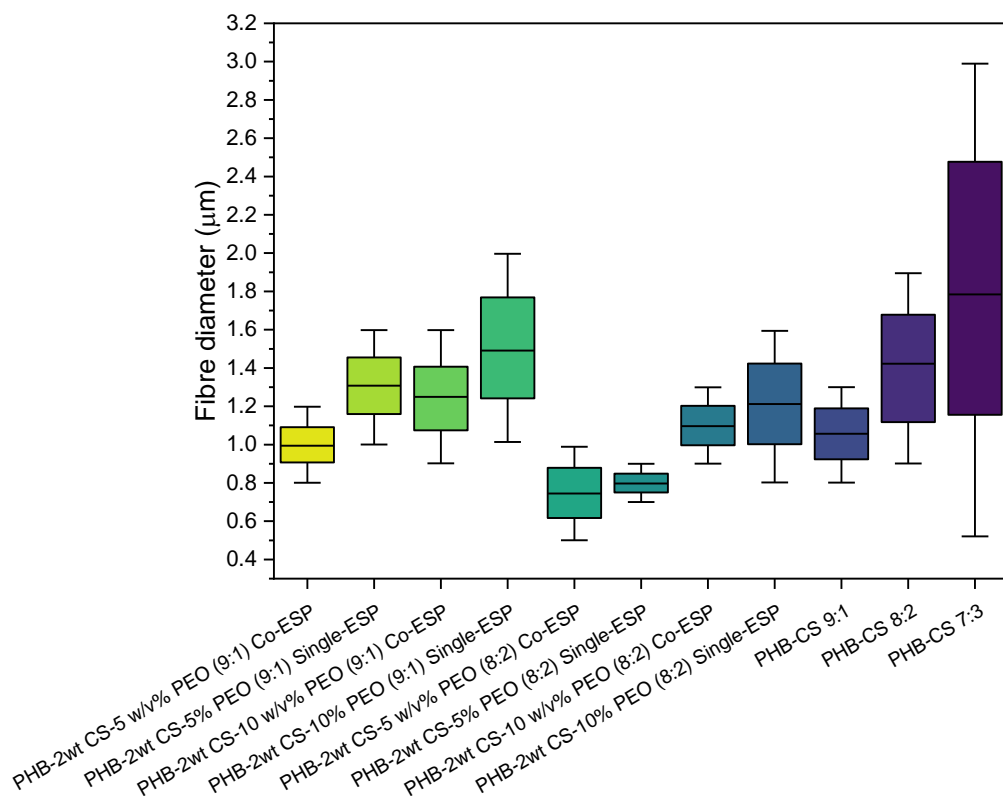


Figure 7.3: Fibre diameter variation across 11 groups influenced by PEO concentration, fabrication techniques, PHB-CS solution ratios, and nitrogen treatments.

Table 16: Fibre diameters of PHB/CS-based electrospun fibre

Experimental Group	Mean Fibre Diameter	Standard Deviation
PHB-CS 7:3	1.79	0.85
PHB-CS 8:2	1.42	0.22
PHB-CS 9:1	1.15	0.25
PHB-2wt CS-10% PEO (8:2) Single-ESP	3.54	0.54
PHB-2wt CS-10 w/v% PEO (8:2) Co-ESP	3.10	1.42
PHB-2wt CS-5% PEO (8:2) Single-ESP	2.80	0.59

PHB-2wt CS-5 w/v% PEO (8:2) Co-ESP	1.74	0.54
PHB-2wt CS-10% PEO (9:1) Single-ESP	3.50	0.89
PHB-2wt CS-10 w/v% PEO (9:1) Co-ESP	4.00	2.11
PHB-2wt CS-5% PEO (9:1) Single-ESP	3.31	0.57
PHB-2wt CS-5 w/v% PEO (9:1) Co-ESP	3.25	1.20

7.2.2 In vitro drug release of Forskolin

The release profiles were divided into three stages according to their slopes and were then fitted with a zeroth-order equation, a first-order equation, the Higuchi equation, and the Ritger–Peppas equation. Nonlinear curve fitting using Origin software was applied to all the release profiles. The cumulative release percentage at time t is defined as:

$$Q_t = \frac{M_t}{M_\infty} \times 100\% \quad (2)$$

where M_t is the cumulative amount of drug released at time t and M_∞ is the total amount released. The zeroth-order equation is

$$Q_t = Q_0 + k(t - t_0) \quad (3)$$

the first-order equation is

$$Q_t = Q_0 + (1 - e^{-k(t-t_0)}) \quad (4)$$

and the Higuchi equation is

$$Q_t = Q_0 + k(t - t_0)^{\frac{1}{2}} \quad (5)$$

where Q_0 and t_0 in each equation are fitting constants to adjust the starting point of the release mechanism in response to changes in membrane structure in the case where the initial fitting point is not the zero-time origin, such as the curves in stages II or III. The Ritger–Peppas equation is

$$Q_t = kt^n \quad (6)$$

where the parameter n characterizes the mechanism. In the cylindrical case, when $n < 0.45$, the drug release mechanism is Fickian diffusion; when $n > 0.89$, it is skeleton dissolution. When $0.45 < n < 0.89$, it is non-Fickian diffusion, involving the synergistic effect of drug diffusion and skeleton dissolution. This equation is used to fit the entire release profile in different stages.

The present study investigates the drug release behaviour of PHB/CS electrospun fibres by analysing the release profiles for each stage of the curve. The release behaviour was characterized by a three-stage release profile, which was identified based on a slope value of 0.06 (cumulative release percentage/h) in the release curve. Figure 7.4 and Table 17 showed that the first stage exhibited a short duration with a rapid drug release rate, while the second stage exhibited a longer duration but a slow-release rate. Most of the drug was released in the third stage with a large release rate. Most of the drug was released in the third stage with a large release rate. The fibre morphology at different stages was also investigated to reveal the underlying drug release pattern. Before incubation, the drug was uniformly distributed in the electrospun drug-loaded membrane, resulting in a smooth and regular fibre morphology with high porosity. As the incubation time increased, the fibres began to swell, resulting in an increase in fibre diameter. During stage II, fibres fused together, leading to a denser membrane with fewer drug release channels. Finally, depending on the properties of the polymer, the polymer degraded after a long time of incubation, resulting in the disappearance of fibre morphologies[41, 42, 84].

Table 17: Comparative Release Kinetics Analysis of PHB-CS Electrospun Samples with Varying CF/DMF Ratios and Single-jet and co-electrospinning. (R^2 represents the proportion of variance of regression line (ranges from 0 to 1)).

Samples	R^2 (Zero order)	R^2 (First order)	R^2 (Higuchi)	R^2 (Korsmeyer-Peppas)	Release exponent of Korsmeyer-Peppas equation
PHB-CS 9:1	0.95	0.96	0.90	0.95	0.30
PHB-CS 8:2	0.98	0.97	0.91	0.95	0.21
PHB-CS 7:3	0.99	0.94	0.94	0.97	0.31

PHB-2wt CS-5 w/v% PEO (9:1) Co-ESP	0.94	0.91	0.95	0.97	1.21
PHB-2wt CS-5% PEO (9:1) Single- ESP	0.94	0.96	0.92	0.97	0.95
PHB-2wt CS-5 w/v% PEO (8:2) Co-ESP	0.92	0.97	0.95	0.96	1.29
PHB-2wt CS-5% PEO (8:2) Single- ESP	0.96	0.96	0.94	0.97	1.02
PHB-2wt CS-10 w/v% PEO (9:1) Co-ESP	0.94	0.95	0.92	0.95	1.39
PHB-2wt CS-10% PEO (9:1) Single- ESP	0.98	0.94	0.90	0.94	1.10
"PHB-2wt CS-10 w/v% PEO (8:2) Co-ESP"	0.92	0.93	0.93	0.93	1.57
"PHB-2wt CS-10% PEO (8:2) Single- ESP"	0.95	0.96	0.93	0.93	1.18

To gain a better understanding of the release mechanism, four different kinetic equations were used to fit each stage of the release curve and the curve. The first-order equation was used to represent Fick's second law of diffusion associated with fibre swelling during stage I, while the zeroth-order equation was used for stage II, where the rate-determining step was the movement of drug molecules to the surface of the membrane. For stage III, the Higuchi equation was used to represent incorporated release kinetics, with a square-root time dependence. The whole-lifetime release profiles could not be fitted by any single type of kinetic equation since the release profile was a combination of different stages with several inflection points, with none of the stages being controlled by a single dominant process. The Ritger–Peppas equation was used to fit the whole-lifetime release data, covering all three stages, with a characteristic parameter value of indicating different dissolution mechanism. when $n < 0.45$, the drug release mechanism is Fickian diffusion; when $n > 0.89$,

it is skeleton dissolution. When $0.45 < n < 0.89$, it is non-Fickian diffusion, involving the synergistic effect of drug diffusion and skeleton dissolution[41, 42].

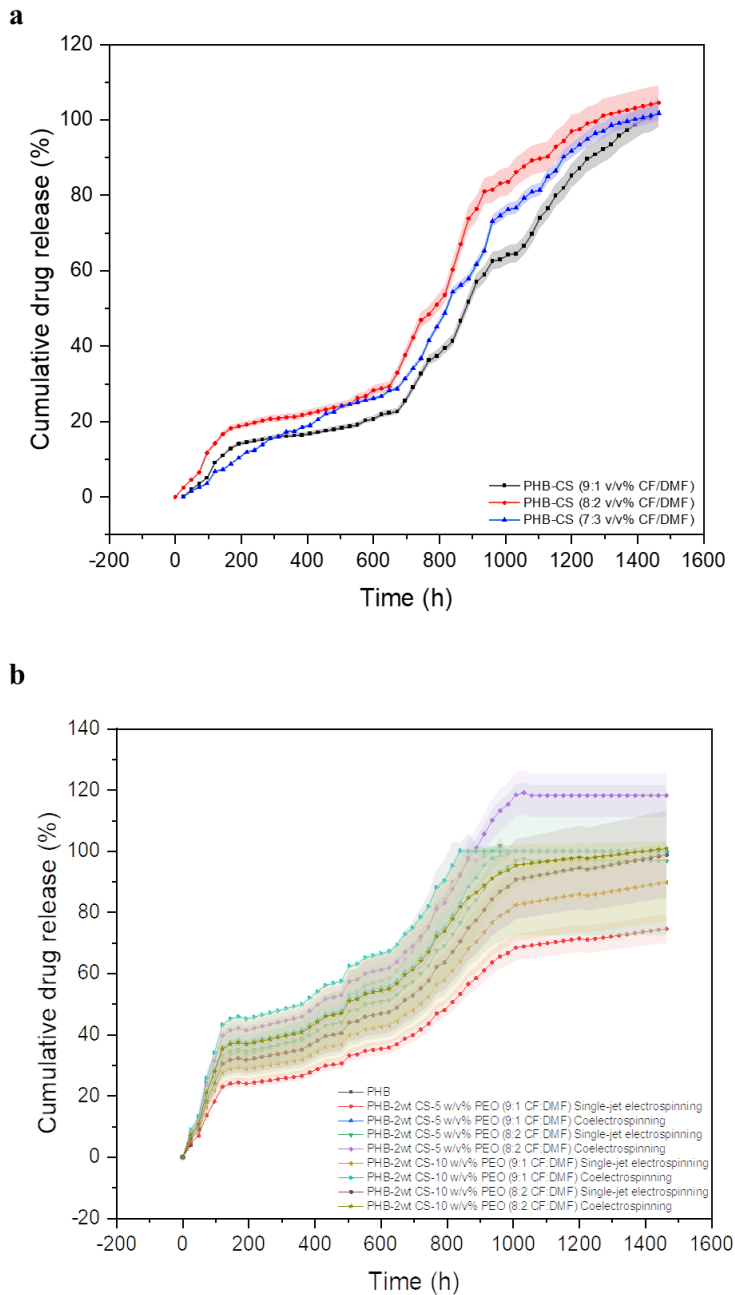


Figure 7.4: Cumulative drug release of Forskolol in PHB-CS based electrospun membranes with various modification. (a) PHB-CS with different CF/DMF ratio, (b) PHB and PHB-CS electrospun membrane with different CS concentration, and fabricated in Single-ESP or Co-ESP.

In the results and discussion of this analysis, the data provided represents various blends and treatments of PHB and CS polymers, and their release exponent values according to the Korsmeyer-Peppas equation. The table lists

the R² values for four different models (Zero order, First order, Higuchi, and Korsmeyer-Peppas) and the release exponent for each blend and treatment.

Figure 7.4 shows that all samples have high R² values (> 0.9) for all four models, which indicates that the models fit the data well. Figure 7.4a showed that the PHB/CS (7:3 v/v% CF/DMF) sample exhibits the highest R² value for the First order model (0.99) and Higuchi model (0.94), suggesting that these models might be more suitable for this blend. On the other hand, the PHB/CS (9:1 v/v% CF/DMF) For samples containing PEO, the R² values for the Korsmeyer-Peppas model are generally higher (0.93 to 0.97) than for the other models, suggesting that the Korsmeyer-Peppas model might be more suitable for describing the release behaviour of these samples. Figure 7.4b showed that the samples with the highest release exponent values are PHB/CS-10 w/v% PEO (8:2 v/v% CF/DMF) Co-electrospun (1.57) and PHB/CS-10 w/v% PEO (8:2 v/v% CF/DMF) Single-jet electrospun (1.68). These high values indicate a more rapid release profile compared to the other samples. de-Furthermore, when PEO was added to the composite system, the diffusion mechanism underwent a transition towards skeleton dissolution. This can be attributed to the degradation of PHB/CS under hydrolysis conditions. The hydrolytic degradation of the polymer matrix leads to the dissolution or erosion of the structural skeleton, contributing to the drug release mechanism. With the decrease of PEO concentration from 10 w/v% to 5 w/v% and the volume ratio between CF and DMF, the release exponent has decreased. The concentration of PEO in the composite system plays a crucial role in determining the release kinetics. As the PEO concentration decreases, the overall polymer content in the system decreases as well. Lower polymer concentrations can result in reduced polymer chain entanglements and increased mobility, leading to faster drug release rates. The volume ratio between CF and DMF affects the solubility and polymer chain organization within the electrospun fibres. Different volume ratios can result in variations in solvent evaporation rates, fibre morphology, and polymer crystallinity [88]. These factors influence the diffusion pathways and release mechanisms of the encapsulated drug. The specific changes in the release exponent due to different volume ratios may be attributed to alterations in the polymer-solvent interactions and subsequent drug diffusion rates [41].

The change in PEO concentration and solvent ratio can also affect the morphology of the electrospun fibres. Variations in fibre diameter, pore size, and surface area can influence the surface-to-volume ratio and the diffusion paths available for the drug molecules. A decrease in PEO concentration and changes in the solvent system can lead to modifications in fibre morphology, which, in turn, affect the drug release behaviour. These alterations in fibre morphology can contribute to the observed decrease in the release exponent. A comparison between the two different fabrication techniques, single-jet electrospun fibres and co-electrospinning, revealed differences in the release exponent values. single-jet electrospun fibres showed lower values of

exponents compared to co-electrospinning. This observation can be attributed to the core-shell structure of single-jet fibres, where the outer shell material (PHB/CS) acts as a sacrificial layer, slowly inducing the release of Forskolin encapsulated within the PEO core.

7.2.3 Mass remaining analysis of PHB/CS-based electrospun fibres

Figure 7.5a demonstrates that at the outset of the experiment (0 hours), all non-nitrogen-treated samples began with similar initial values, within the range of approximately 97.81% to 101.25%. Over the course of the experiment, the PHB-CS samples with varying ratios of CF/DMF displayed differential degradation patterns. Specifically, the PHB-CS (9:1 v/v% CF/DMF) samples exhibited a notable decrease in the remaining material over time. By the 144-hour mark, these samples retained around 78.52% of the original material. This observation indicates a significant reduction and suggests a relatively faster degradation rate within this particular formulation. The PHB-CS (8:2 v/v% CF/DMF) samples also showed a decline in the remaining material, with approximately 88.94% left after 144 hours. While this represents a slower degradation rate compared to the 9:1 ratio, it still reflects a considerable decrease over the specified duration. For the PHB-CS (7:3 v/v% CF/DMF) samples, the trend was consistent with the other ratios, where a decrease in the remaining material was observed over time. However, the exact remaining percentage was not specified in the provided text. The data underscores the influence of solvent ratios on the stability and degradation of PHB-CS samples, revealing that samples with a higher concentration of CF in the solvent mixture tend to degrade more slowly. This trend could be related to the effect of solvent on the microstructure of polymer and the interaction between PHB and CS in the fibre matrix. The varying rates of degradation highlight the importance of solvent composition in the design of electrospun scaffolds, particularly for applications where controlled degradation is essential [31, 80, 101, 135]. Further research is necessary to elucidate the mechanisms driving these differences and to optimize the degradation properties of PHB-CS scaffolds for their intended biomedical applications [31].

In Figure 7.5b, the PHB-CS (9:1) fibres with 5 w/v% PEO, when subjected to the Single-ESP process, demonstrate a more consistent and narrower degradation profile compared to the Co-ESP process. This suggests that the Single-ESP process may be more suitable for applications requiring a slow and predictable material degradation. Moreover, the PHB-CS (8:2) fibres with 5 w/v% PEO show a steeper degradation curve, indicating a faster breakdown of the material. These can be attributed to higher content of chitosan, which possesses inherently different degradation kinetics than PHB, likely contributes to the faster breakdown of the fibres [31, 50, 52, 136]. Due to the increased chitosan content would naturally attract more water, further promoting

hydrolysis [26, 27, 30, 137]. Additionally, the solvent system used during electrospinning can significantly impact fibre structure, and any changes in the evaporation dynamics could lead to fibres with a higher surface area exposed to degradative processes [51].

The increase in PEO concentration to 10 w/v% in both the 9:1 and 8:2 PHB-CS ratios appears to contribute to a faster degradation rate, which may be due to the higher solubility and mobility of PEO within the fibre matrix, leading to increased water uptake and accelerated breakdown. While this may limit the structural support over extended periods, it could be strategically employed in scenarios where such a characteristic is advantageous. The consistent decline in the performance of PHB-CS (9:1) fibres with 10 w/v% PEO across both Single-ESP and Co-ESP processes suggests a material property limitation. The interplay between the PHB-CS ratio, PEO concentration, and the choice of electrospinning process (Single-ESP vs. Co-ESP) emerges as a decisive factor influencing the long-term behaviour of the fibres. The accelerated degradation rate seen in PHB-CS fibres with an increased PEO concentration of 10 w/v% could be attributed to the inherent characteristics of PEO and its interaction with the PHB-CS matrix. PEO, known for its high solubility and mobility within polymer matrices, can introduce more hydrophilic domains into the fibres. This increased hydrophilicity likely facilitates water absorption, which can lead to an upsurge in the hydrolytic degradation rate of the fibres. As water molecules permeate the fibre matrix, they can break down the polymer chains, leading to a loss of structural integrity [16, 41]. Additionally, the mobility of PEO chains within the fibre matrix could lead to a less compact fibre structure, potentially creating larger pore sizes and more void spaces. This structural configuration can exacerbate the degradation process by allowing more water to penetrate and interact with the fibre components, further speeding up the breakdown of the material [42-44]. Furthermore, the consistent decline in performance of the fibres across both Single-ESP and Co-ESP processes, regardless of the PHB-CS ratio, points to a limitation inherent to the material properties of PEO when used at higher concentrations. While PEO enhances the processability of the electrospinning solution and can improve the initial fibre formation, its presence at higher concentrations seems to compromise the long-term stability of the fibres [27, 46, 48, 73, 134].

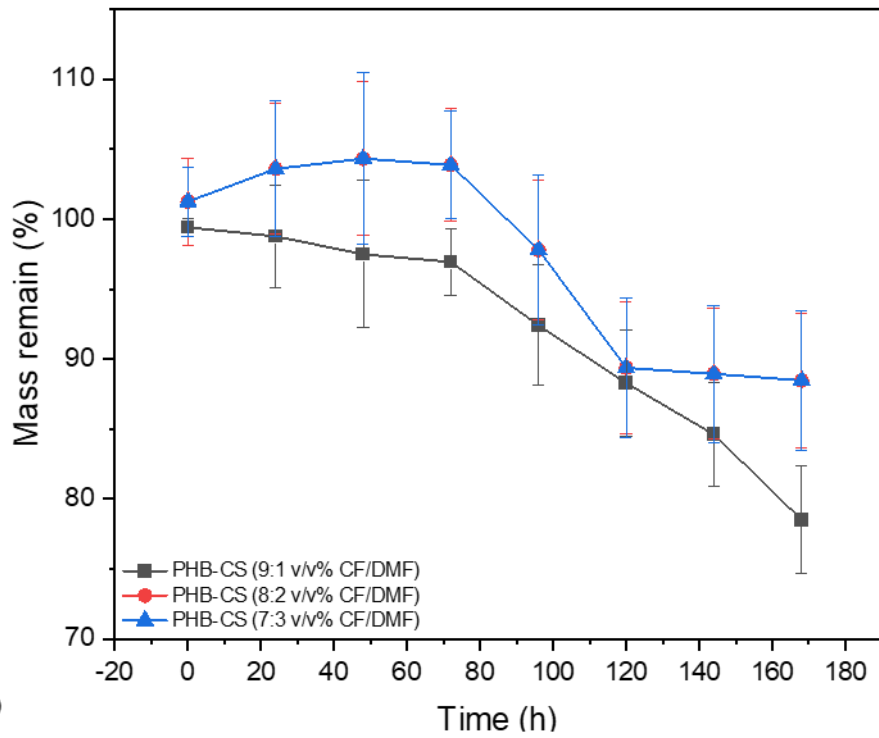
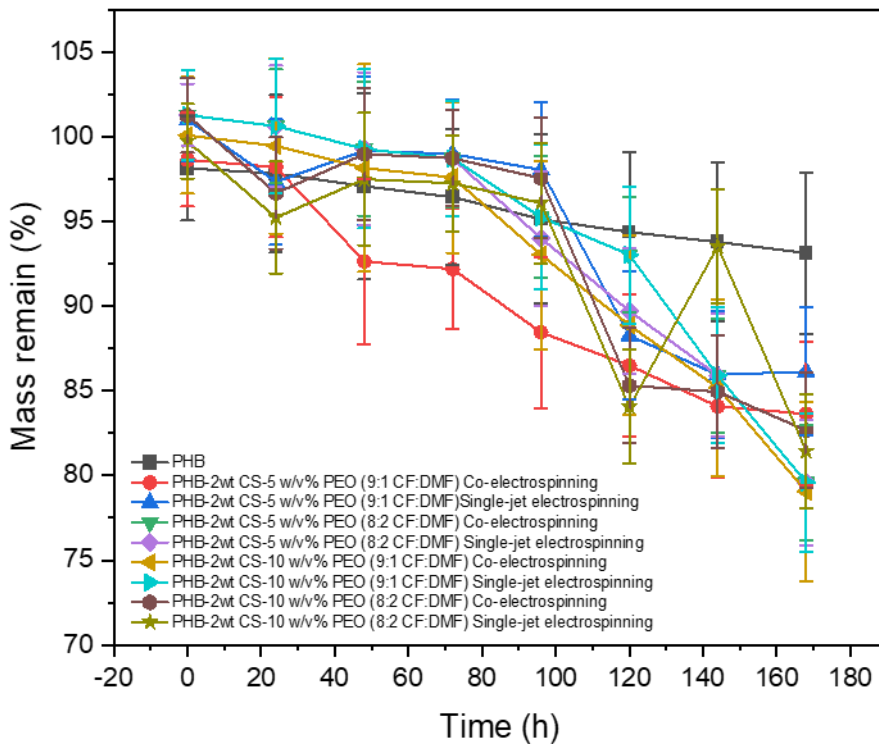
a**b**

Figure 7.5: Percentage mass remain of PHB-CS based electrospun membranes with various modification. (a) PHB-CS with different CF/DMF ratio, (b) PHB and PHB-CS electrospun membrane with different CS concentration, and fabricated in Single-ESP or Co-ESP

7.2.4 pH analysis of PHB-CS based electrospun fibres

The stable pH values exhibited by some samples indicate their ability to maintain pH stability over the 30-day period. This is a desirable trait for applications where pH-sensitive properties need to be maintained, such as in controlled drug release systems or biomedical devices. The stable pH values suggest that these materials are less prone to degradation or the release of acidic or alkaline components when exposed to the PBS solution.

The pH measurements for each sample at different time points are presented in Figure 7.6. The results indicate distinct pH trends among the samples, suggesting variations in stability and potential degradation. The pH values of the PHB-2wt CS-5 w/v% PEO (9:1) co-electrospun sample remained constant at 7.2 throughout the entire 30-day period. This stable pH indicates good material stability, with no significant release of acidic byproducts or degradation observed. In contrast, the PHB-2wt CS-5 w/v% PEO (9:1) single-jet electrospun sample exhibited a slight decrease in pH from 7.2 to 6.1 by day 7, indicating a mild acidity. However, the pH remained stable thereafter, ranging between 5.6 and 6.2. This suggests a stable composition with minor changes in pH over time. The PHB-2wt CS-10 w/v% PEO (9:1) co-electrospun sample maintained a constant pH of 7.2 throughout the 30-day period, like the PHB-2wt CS-5 w/v% PEO (9:1) co-electrospun sample. These results indicated the stability of these compositions and suggest minimal degradation or release of acidic byproducts. On the other hand, the PHB-2wt CS-10 w/v% PEO (9:1) single-jet electrospun sample showed a significant decrease in pH from 7.2 to 5.368 by day 7. The pH remained stable thereafter, ranging between 5.368 and 7.4. This substantial decrease in pH may be attributed to the release of acidic byproducts or degradation of the composite.

Similar pH trends were observed for samples prepared with PHB-2wt CS-5 w/v% PEO (8:2) co-electrospinning, PHB-2wt CS-5 w/v% PEO (8:2) single-jet electrospinning, PHB-2wt CS-10 w/v% PEO (8:2) co-electrospinning, and PHB-2wt CS-10 w/v% PEO (8:2) single-jet electrospinning. These samples exhibited a gradual decrease in pH over the 30-day period, indicating potential degradation or release of acidic components.

Samples involving PHB-CS (9:1 v/v% CF/DMF) and PHB-CS (8:2 v/v% CF/DMF), maintained a constant pH of 7.2 throughout the 30-day period. This pH stability suggests that the addition of CF/DMF did not significantly impact chemical properties of the composites or induce degradation. This could be explained by the neutralisation between the PHB and CS after degradation.

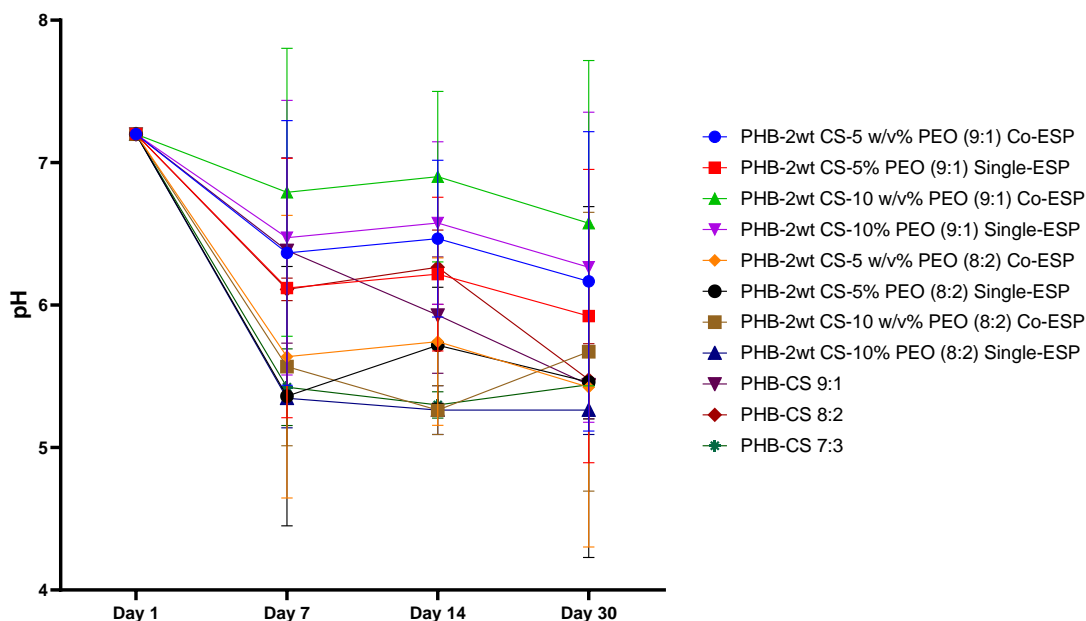


Figure 7.6: pH analysis of PHB-CS based electrospun membranes with various modification in PBS solution.

7.3 Summary

Our study has successfully demonstrated the potential of electrospun PHB/CS fibres in behaving a standard drug delivery system. By manipulating solvent composition and electrospinning techniques, we have tailored the microstructural properties of these fibres, notably pore size and specific surface area, thereby influencing the drug release behaviour of Forskolin. A key observation was the difference in drug release behaviour between single-jet and co-electrospun fibres. Co-electrospun fibres exhibited a more aggressive drug release profile, suggesting that the method of fibre fabrication plays a significant role in determining the release kinetics. This understanding is crucial for developing tailored drug delivery systems that can cater to specific therapeutic requirements. The findings revealed that varying the volume ratio of CF to DMF significantly impacted fibre diameter, with higher DMF ratios resulting in finer fibres. This alteration in fibre morphology was crucial in modulating the drug release profiles. Moreover, the incorporation of PEO into the PHB/CS fibres further refined the release mechanism. The presence of PEO was found to shift the release mechanism from predominantly Fickian diffusion to a more complex skeleton dissolution process, highlighting the role of polymer composition in drug release dynamics.

Chapter 8: Conclusion and Future works

8.1 Conclusion

In order to meet the urgent demand for bio-based natural materials, which could work as a supportive scaffold for treat PNI, PHB with CS electrospun membranes were successfully fabricated with proper process para and characterised according to their different uses. This thesis provides a platform for PHB/CS nanofibres, which showed its potential in using as scaffolds for nerve regeneration.

From Chapters 4 to 7, the thesis has investigated complex dynamics of PHB and CS solutions in electrospinning and their application in innovative biomedical engineering solutions has been significant. Chapter 4 established the fundamental understanding of how polymer concentration, solvent choice, and pH levels impact the conductivity and viscosity of PHB/CS solutions. This, in turn, influences their electro spinnability and effectiveness in creating scaffolds for nerve regeneration. This foundational knowledge was crucial for the development of novel nerve regeneration scaffolds discussed in Chapter 5, where the emphasis on biodegradable polymers highlighted their potential. The findings demonstrated that CS reduces the crystallinity of PHB, leading to decreased thermal stability of PHB/CS. Additionally, PHB/CS electrospun fibres exhibited faster degradation rates under both acidic and alkaline conditions, indicating their suitability for nerve repair applications, with a focus on the importance of material integrity and biodegradability after regeneration.

More advanced, in Chapter 6, exploring the improvement of biomaterials' biostability and biocompatibility through chemical treatments, specifically examining the effects of KOH and H₂O₂ pre-treatments on PHB membranes. The results suggested that both KOH and H₂O₂ enhance CS binding efficiency, with KOH-treated PHB showing less stability than H₂O₂-treated samples. Chapter 7 broadened the scope to froskolin delivery, demonstrating the versatility of PHB/CS nanofibers, augmented with polyethylene oxide, for controlled drug release. This was influenced by solvent ratios and electrospinning techniques.

The four experimental chapters detail the fabrication, biostability, biodegradability, and drug delivery capabilities of PHB/CS nanofibre membranes. This PhD project focuses on modifying the unique interconnected, naturally porous structure of PHB/CS to achieve specific functionalities, underscoring its potential as a composite material for nerve regeneration applications. However, to gauge the practicality of utilizing PHB/CS in clinical settings for realistic nerve regeneration, further experimental investigations, including in vitro cell biocompatibility tests and in vivo biocompatibility

assessments, are necessary. These additional studies will provide a clearer understanding of the material's efficacy and safety, which are critical for advancing towards clinical applications.

8.2 Future Works

Building on the substantial progress made in the study of PHB and CS-based biomaterials, future research endeavours are poised to address several critical areas, particularly in the context of biocompatibility and application diversification. The coronavirus pandemic has notably impacted collaborative lab access, leaving some essential tests, such as cytotoxicity, cell proliferation, and cell viability tests, incomplete. As medical products necessitate rigorous testing before being deemed safe for human application, the comprehensive biocompatibility testing of PHB and CS materials and their nanocomposites becomes a crucial focal point for future studies. To thoroughly assess the biocompatibility of these biomaterials, a series of *in vitro* tests should be prioritized. These tests would encompass cell attachment, viability, proliferation, and cytotoxicity assessments. The objective is to distinguish between non-dividing (quiescent or senescent) and actively dividing cells, thereby evaluating the materials' potential toxicity or irritancy. Successful completion of these *in vitro* assessments will lay the groundwork for subsequent *in vivo* tests. Such tests, possibly conducted on animal skin models, will offer complementary insights and more accurately mimic human exposure conditions. They will assess factors such as the toxicity of any chemical compounds involved and the behaviour of degradable materials in a living system. Furthermore, for the PHB and CS materials tailored for wound dressing applications, *in vivo* wound healing assays are imperative. These assays will provide valuable data on the effectiveness of these nature-based dressings compared to traditional, commercial, or antibiotic-based alternatives. Understanding their performance in actual wound healing scenarios is key to validating their efficacy and safety. In parallel, for applications like pH-sensitive materials derived from PHB and CS, optimization of mechanical strength and pH sensitivity is vital, especially in challenging environments like wound fluids rich in proteins. Long-term stability tests under varying pH conditions will be crucial in assessing their durability and consistent performance over time. Additionally, integrating these pH-sensitive materials into a comprehensive, wireless sensing system for use with antimicrobial wound dressings represents an exciting avenue for exploration. *In vitro* biocompatibility tests will be essential to ensure that these integrated systems are safe for human use, without causing allergic reactions or other adverse effects. In summary, as the demand for nature-based, environmentally friendly materials grows, especially in the context of global concerns over chemical contamination and potential side effects, the importance of this research cannot be overstated. By addressing these future research areas, the

potential for PHB and CS-based materials in medical applications can be fully realized, contributing significantly to a future where such innovative materials play a crucial role in enhancing health and well-being.

References

1. Liguori, G.A., *Complications of regional anesthesia: nerve injury and peripheral neural blockade*. Journal of neurosurgical anesthesiology, 2004. **16**(1): p. 84-86.
2. Prabhakaran, M.P., et al., *Electrospun biocomposite nanofibrous scaffolds for neural tissue engineering*. Tissue Engineering Part A, 2008. **14**(11): p. 1787-1797.
3. Yang, X., K. Zhao, and G.-Q. Chen, *Effect of surface treatment on the biocompatibility of microbial polyhydroxyalkanoates*. Biomaterials, 2002. **23**(5): p. 1391-1397.
4. Dickson, A.N., H.M. Abourayana, and D.P. Dowling, *3D printing of fibre-reinforced thermoplastic composites using fused filament fabrication—A review*. Polymers, 2020. **12**(10): p. 2188.
5. Sun, B., et al., *Advances in three-dimensional nanofibrous macrostructures via electrospinning*. Progress in Polymer Science, 2014. **39**(5): p. 862-890.
6. Yang, J., et al., *Electrospun Biodegradable Poly(L-lactic acid) Nanofiber Membranes as Highly Porous Oil Sorbent Nanomaterials*. Nanomaterials (Basel), 2022. **12**(15).
7. Abadi, B., et al., *Electrospun hybrid nanofibers: Fabrication, characterization, and biomedical applications*. Front Bioeng Biotechnol, 2022. **10**: p. 986975.
8. Righetti, M.C., et al., *Immiscible PHB/PBS and PHB/PBSA blends: Morphology, phase composition and modelling of elastic modulus*. Polymer International, 2022. **71**(1): p. 47-56.
9. Zou, Y., et al., *Recovery of polyhydroxyalkanoates (PHAs) polymers from a mixed microbial culture through combined ultrasonic disruption and alkaline digestion*. Journal of Environmental Management, 2023. **326**: p. 116786.
10. Kühn, S., et al., *The use of potassium hydroxide (KOH) solution as a suitable approach to isolate plastics ingested by marine organisms*. Marine Pollution Bulletin, 2017. **115**(1): p. 86-90.
11. Aibibu, D., et al., *Textile cell-free scaffolds for in situ tissue engineering applications*. Journal of Materials Science: Materials in Medicine, 2016. **27**(3): p. 63.
12. Arrieta, M.P., et al., *Development of flexible materials based on plasticized electrospun PLA–PHB blends: Structural, thermal, mechanical and disintegration properties*. European Polymer Journal, 2015. **73**: p. 433-446.
13. Barhoum, A., et al., *Nanofibers as new-generation materials: From spinning and nano-spinning fabrication techniques to emerging applications*. Applied Materials Today, 2019. **17**: p. 1-35.
14. Huang, Z.-M., et al., *A review on polymer nanofibers by electrospinning and their applications in nanocomposites*. Composites Science and Technology, 2003. **63**(15): p. 2223-2253.
15. Agarwal, S., J.H. Wendorff, and A. Greiner, *Use of electrospinning technique for biomedical applications*. Polymer, 2008. **49**(26): p. 5603-5621.
16. Xue, J., et al., *Electrospinning and Electrospun Nanofibers: Methods, Materials, and Applications*. Chem Rev, 2019. **119**(8): p. 5298-5415.
17. Sill, T.J. and H.A. von Recum, *Electrospinning: applications in drug delivery and tissue engineering*. Biomaterials, 2008. **29**(13): p. 1989-2006.

18. Bhardwaj, N. and S.C. Kundu, *Electrospinning: a fascinating fiber fabrication technique*. Biotechnol Adv, 2010. **28**(3): p. 325-47.
19. Zhang, Y., et al., *Electrospinning of gelatin fibers and gelatin/PCL composite fibrous scaffolds*. J Biomed Mater Res B Appl Biomater, 2005. **72**(1): p. 156-65.
20. Chen, C., M. Dirican, and X. Zhang, *Chapter 10 - Centrifugal Spinning—High Rate Production of Nanofibers*, in *Electrospinning: Nanofabrication and Applications*, B. Ding, X. Wang, and J. Yu, Editors. 2019, William Andrew Publishing. p. 321-338.
21. Aswathy, S.H., U. Narendrakumar, and I. Manjubala, *Commercial hydrogels for biomedical applications*. Heliyon, 2020. **6**(4): p. e03719.
22. Afinjuomo, F., et al., *Preparation and characterization of oxidized inulin hydrogel for controlled drug delivery*. Pharmaceutics, 2019. **11**(7): p. 356.
23. Larrañeta, E., et al., *Synthesis and characterization of hyaluronic acid hydrogels crosslinked using a solvent-free process for potential biomedical applications*. Carbohydr Polym, 2018. **181**: p. 1194-1205.
24. Rouxhet, L., et al., *Adsorption of albumin, collagen, and fibronectin on the surface of poly (hydroxybutyrate-hydroxyvalerate)(PHB/HV) and of poly (ϵ -caprolactone)(PCL) films modified by an alkaline hydrolysis and of poly (ethylene terephthalate)(PET) track-etched membranes*. Journal of Biomaterials Science, Polymer Edition, 1998. **9**(12): p. 1279-1304.
25. Gnani, S., et al., *The effect of electrospun gelatin fibers alignment on schwann cell and axon behavior and organization in the perspective of artificial nerve design*. International Journal of Molecular Sciences, 2015. **16**(6): p. 12925-12942.
26. Kang, J. and S.I. Yun, *Chitosan-reinforced PHB hydrogel and aerogel monoliths fabricated by phase separation with the solvent-exchange method*. Carbohydrate Polymers, 2022. **284**: p. 119184.
27. Zhou, Y., et al., *A Comparison of Chitosan Adhesion to KOH and H₂O₂ Pre-Treated Electrospun Poly(3-Hydroxybutyrate) Nanofibers*. Fibers, 2023. **11**(11): p. 91.
28. Ikejima, T. and Y. Inoue, *Crystallization behavior and environmental biodegradability of the blend films of poly(3-hydroxybutyric acid) with chitin and chitosan*. Carbohydrate Polymers, 2000. **41**(4): p. 351-356.
29. Karbasi, S. and Z.M. Alizadeh, *Effects of multi-wall carbon nanotubes on structural and mechanical properties of poly(3-hydroxybutyrate)/chitosan electrospun scaffolds for cartilage tissue engineering*. Bulletin of Materials Science, 2017. **40**(6): p. 1247-1253.
30. Seddighian, A., et al., *Electrospun PCL scaffold modified with chitosan nanoparticles for enhanced bone regeneration*. Prog Biomater, 2021. **10**(1): p. 65-76.
31. Zhou, Y., et al., *Electrospun PHB/Chitosan Composite Fibrous Membrane and Its Degradation Behaviours in Different pH Conditions*. Journal of Functional Biomaterials, 2022. **13**(2): p. 58.
32. Megelski, S., et al., *Micro-and nanostructured surface morphology on electrospun polymer fibers*. Macromolecules, 2002. **35**(22): p. 8456-8466.
33. Saremi, J., et al., *Tissue - engineered nerve graft using silk - fibroin/polycaprolactone fibrous mats decorated with bioactive cerium oxide nanoparticles*. Journal of Biomedical Materials Research Part A, 2021. **109**(9): p. 1588-1599.
34. Vert, M., J. Mauduit, and S. Li, *Biodegradation of PLA/GA polymers: increasing*

- complexity*. *Biomaterials*, 1994. **15**(15): p. 1209-1213.
35. Kim, J., et al., *Bone regeneration using hyaluronic acid-based hydrogel with bone morphogenic protein-2 and human mesenchymal stem cells*. *Biomaterials*, 2007. **28**(10): p. 1830-7.
 36. Zhou, L., et al., *Combining PLGA Scaffold and MSCs for Brain Tissue Engineering: A Potential Tool for Treatment of Brain Injury*. *Stem Cells Int*, 2018. **2018**: p. 5024175.
 37. Reddy, M.S.B., et al., *A Comparative Review of Natural and Synthetic Biopolymer Composite Scaffolds*. *Polymers (Basel)*, 2021. **13**(7).
 38. Mohanna, P.-N., G. Terenghi, and M. Wiberg, *Composite PHB-GGF conduit for long nerve gap repair: A long-term evaluation*. *Scandinavian Journal of Plastic and Reconstructive Surgery and Hand Surgery*, 2005. **39**(3): p. 129-137.
 39. Krucińska, I., et al., *Fabrication of PLGA/HAP and PLGA/PHB/HAP fibrous nanocomposite materials for osseous tissue regeneration*. *Autex Research Journal*, 2014. **14**(2): p. 95-110.
 40. Haider, A., K.C. Gupta, and I.-K. Kang, *PLGA/nHA hybrid nanofiber scaffold as a nanocargo carrier of insulin for accelerating bone tissue regeneration*. *Nanoscale research letters*, 2014. **9**(1): p. 1-12.
 41. Fernandes, J., et al., *PHB-PEO electrospun fiber membranes containing chlorhexidine for drug delivery applications*. *Polymer Testing*, 2014. **34**: p. 64-71.
 42. Ergul Yilmaz, Z., et al., *Protein encapsulation and release from PEO-b-polyphosphoester templated calcium carbonate particles*. *Int J Pharm*, 2016. **513**(1-2): p. 130-137.
 43. Li, J., et al., *Self-assembled supramolecular hydrogels formed by biodegradable PEO–PHB–PEO triblock copolymers and α -cyclodextrin for controlled drug delivery*. *Biomaterials*, 2006. **27**(22): p. 4132-4140.
 44. Zhang, P.X., et al., *Tissue engineering for the repair of peripheral nerve injury*. *Neural Regen Res*, 2019. **14**(1): p. 51-58.
 45. Redenti, S., et al., *Engineering retinal progenitor cell and scrollable poly(glycerol-sebacate) composites for expansion and subretinal transplantation*. *Biomaterials*, 2009. **30**(20): p. 3405-14.
 46. Taylor, C.S., et al., *Aligned Polyhydroxyalkanoate Blend Electrospun Fibers as Intraluminal Guidance Scaffolds for Peripheral Nerve Repair*. *ACS Biomater Sci Eng*, 2023. **9**(3): p. 1472-1485.
 47. Pant, H.R., et al., *Fabrication of highly porous poly (ϵ -caprolactone) fibers for novel tissue scaffold via water-bath electrospinning*. *Colloids and Surfaces B: Biointerfaces*, 2011. **88**(2): p. 587-592.
 48. Puhl, D.L., et al., *Aligned fingolimod-releasing electrospun fibers increase dorsal root ganglia neurite extension and decrease Schwann cell expression of promyelinating factors*. *Frontiers in bioengineering and biotechnology*, 2020. **8**: p. 937.
 49. Mohanna, P.N., G. Terenghi, and M. Wiberg, *Composite PHB-GGF conduit for long nerve gap repair: a long-term evaluation*. *Scand J Plast Reconstr Surg Hand Surg*, 2005. **39**(3): p. 129-37.
 50. Gu, B.K., et al., *Fabrication of sonicated chitosan nanofiber mat with enlarged porosity for use as hemostatic materials*. *Carbohydrate Polymers*, 2013. **97**(1): p. 65-73.

51. Kumar, S. and J. Koh, *Physiochemical, Optical and Biological Activity of Chitosan-Chromone Derivative for Biomedical Applications*. International Journal of Molecular Sciences, 2012. **13**(5): p. 6102-6116.
52. Foroughi, M.R., et al., *Polyhydroxybutyrate/chitosan/bioglass nanocomposite as a novel electrospun scaffold: fabrication and characterization*. Journal of Porous Materials, 2017. **24**(6): p. 1447-1460.
53. Yellanki, S.K., B. Anna, and M.R. Kishan, *Preparation and in vivo evaluation of sodium alginate-poly (vinyl alcohol) electrospun nanofibers of forskolin for glaucoma treatment*. Pakistan Journal of Pharmaceutical Sciences, 2019. **32**(2).
54. Yang, Y., et al., *Fabrication and properties of a porous chitin/chitosan conduit for nerve regeneration*. Biotechnology letters, 2004. **26**(23): p. 1793-1797.
55. Ljungberg, C., et al., *Neuronal survival using a resorbable synthetic conduit as an alternative to primary nerve repair*. Microsurgery: Official Journal of the International Microsurgical Society and the European Federation of Societies for Microsurgery, 1999. **19**(6): p. 259-264.
56. Tan, G.-Y.A., et al., *Start a Research on Biopolymer Polyhydroxyalkanoate (PHA): A Review*. Polymers, 2014. **6**(3): p. 706-754.
57. Wei, G. and P. Ma, *Polymeric biomaterials for tissue engineering*, in *Tissue engineering using ceramics and polymers*. 2014, Elsevier. p. 35-66.
58. Reneker, D.H. and H. Fong, *Polymeric nanofibers: introduction*. 2006, ACS Publications.
59. Radulescu, D., et al., *Tissue engineering scaffolds for nerve regeneration manufactured by ink-jet technology*. Materials Science and Engineering: C, 2007. **27**(3): p. 534-539.
60. Milosevic, M., et al., *Preparation and modeling of three - layered PCL/PLGA/PCL fibrous scaffolds for prolonged drug release*. Scientific reports, 2020. **10**(1): p. 1-12.
61. Charpentier, P.A., A. Maguire, and W.-k. Wan, *Surface modification of polyester to produce a bacterial cellulose-based vascular prosthetic device*. Applied Surface Science, 2006. **252**(18): p. 6360-6367.
62. Liu, M., et al., *Recent advances in electrospun for drug delivery purpose*. Journal of Drug Targeting, 2019. **27**(3): p. 270-282.
63. Angamma, C.J. and S.H. Jayaram, *Analysis of the effects of solution conductivity on electrospinning process and fiber morphology*. IEEE Transactions on industry applications, 2011. **47**(3): p. 1109-1117.
64. Mendelovits, A., et al., *Improved colorimetric determination of chitosan concentrations by dye binding*. Applied Spectroscopy, 2012. **66**(8): p. 979-982.
65. Lim, S.K., et al., *Photocatalytic deposition of silver nanoparticles onto organic/inorganic composite nanofibers*. Macromolecular Materials and Engineering, 2006. **291**(10): p. 1265-1270.
66. Peng, Y., et al., *Preparation of polysulfone membranes via vapor-induced phase separation and simulation of direct-contact membrane distillation by measuring hydrophobic layer thickness*. Desalination, 2013. **316**: p. 53-66.
67. Yongquan, D., et al., *Preparation, characterization of P(VDF-HFP)/[bmim]BF₄ ionic liquids hybrid membranes and their pervaporation performance for ethyl acetate*

- recovery from water. *Desalination*, 2012. **295**: p. 53-60.
68. Filimon, A., et al., *Design of Biologically Active Surfaces Based on Functionalized Polysulfones by Electrospinning*. *Proceedings*, 2019. **41**(1): p. 35.
 69. Haider, A., S. Haider, and I.-K. Kang, *A comprehensive review summarizing the effect of electrospinning parameters and potential applications of nanofibers in biomedical and biotechnology*. *Arabian Journal of Chemistry*, 2018. **11**(8): p. 1165-1188.
 70. Matabola, K. and R. Moutloali, *The influence of electrospinning parameters on the morphology and diameter of poly (vinylidene fluoride) nanofibers-effect of sodium chloride*. *Journal of Materials Science*, 2013. **48**(16): p. 5475-5482.
 71. Deitzel, J.M., et al., *The effect of processing variables on the morphology of electrospun nanofibers and textiles*. *Polymer*, 2001. **42**(1): p. 261-272.
 72. Baumgarten, P.K., *Electrostatic spinning of acrylic microfibers*. *Journal of colloid and interface science*, 1971. **36**(1): p. 71-79.
 73. Behtaj, S., J.A.K. Ekberg, and J.A. St John, *Advances in Electrospun Nerve Guidance Conduits for Engineering Neural Regeneration*. *Pharmaceutics*, 2022. **14**(2).
 74. Belkas, J.S., et al., *Long-term in vivo biomechanical properties and biocompatibility of poly(2-hydroxyethyl methacrylate-co-methyl methacrylate) nerve conduits*. *Biomaterials*, 2005. **26**(14): p. 1741-9.
 75. Dalton, P.D., L. Flynn, and M.S. Shoichet, *Manufacture of poly (2-hydroxyethyl methacrylate-co-methyl methacrylate) hydrogel tubes for use as nerve guidance channels*. *Biomaterials*, 2002. **23**(18): p. 3843-3851.
 76. Fairbairn, N.G., et al., *Augmenting peripheral nerve regeneration using stem cells: A review of current opinion*. *World J Stem Cells*, 2015. **7**(1): p. 11-26.
 77. Fornasari, B.E., et al., *Natural-Based Biomaterials for Peripheral Nerve Injury Repair*. *Front Bioeng Biotechnol*, 2020. **8**: p. 554257.
 78. Hazari, A., et al., *A new resorbable wrap-around implant as an alternative nerve repair technique*. *J Hand Surg Br*, 1999. **24**(3): p. 291-5.
 79. Houshyar, S., A. Bhattacharyya, and R. Shanks, *Peripheral Nerve Conduit: Materials and Structures*. *ACS Chemical Neuroscience*, 2019. **10**(8): p. 3349-3365.
 80. Khorasani, M., S. Mirmohammadi, and S. Irani, *Polyhydroxybutyrate (PHB) scaffolds as a model for nerve tissue engineering application: fabrication and in vitro assay*. *International Journal of Polymeric Materials*, 2011. **60**(8): p. 562-575.
 81. Lezcano, M.F., et al., *Polyhydroxybutyrate (PHB) Scaffolds for Peripheral Nerve Regeneration: A Systematic Review of Animal Models*. *Biology*, 2022. **11**(5): p. 706.
 82. Ljungberg, C., et al., *Neuronal survival using a resorbable synthetic conduit as an alternative to primary nerve repair*. *Microsurgery*, 1999. **19**(6): p. 259-64.
 83. Tiwari, A.P., et al., *A Review on the Technological Advances and Future Perspectives of Axon Guidance and Regeneration in Peripheral Nerve Repair*. *Bioengineering*, 2022. **9**(10): p. 562.
 84. Chou, S.-F., D. Carson, and K.A. Woodrow, *Current strategies for sustaining drug release from electrospun nanofibers*. *Journal of Controlled Release*, 2015. **220**: p. 584-591.
 85. Dai, Z.X., et al., *Cyclosporine A-loaded drug delivery systems inhibit scar formation after glaucoma surgery in rabbits*. *Chin Med J (Engl)*, 2019. **132**(11): p. 1381-1384.

86. Kawaguchi, T., et al., *Control of drug release with a combination of prodrug and polymer matrix: Antitumor activity and release profiles of 2', 3' - diacyl - 5 - fluoro - 2' - deoxyuridine from poly (3 - hydroxybutyrate) microspheres*. Journal of pharmaceutical sciences, 1992. **81**(6): p. 508-512.
87. Li, J., Y. Liu, and H.E. Abdelhakim, *Drug Delivery Applications of Coaxial Electrospun Nanofibres in Cancer Therapy*. Molecules, 2022. **27**(6): p. 1803.
88. Lezcano, M.F., et al., *Polyhydroxybutyrate (PHB) Scaffolds for Peripheral Nerve Regeneration: A Systematic Review of Animal Models*. Biology (Basel), 2022. **11**(5).
89. Lin, Y.-D., et al., *Instructive nanofiber scaffolds with VEGF create a microenvironment for arteriogenesis and cardiac repair*. Science translational medicine, 2012. **4**(146): p. 146ra109.
90. Desai, K.G.H. and H.J. Park, *Preparation and characterization of drug-loaded chitosan-tripolyphosphate microspheres by spray drying*. Drug Development Research, 2005. **64**(2): p. 114-128.
91. Zhang, C., F. Feng, and H. Zhang, *Emulsion electrospinning: Fundamentals, food applications and prospects*. Trends in Food Science & Technology, 2018. **80**: p. 175-186.
92. Mikula, K., et al., *From hazardous waste to fertilizer: Recovery of high-value metals from smelter slags*. Chemosphere, 2022. **297**: p. 134226.
93. Singhi, B., E.N. Ford, and M.W. King, *The effect of wet spinning conditions on the structure and properties of poly-4-hydroxybutyrate fibers*. J Biomed Mater Res B Appl Biomater, 2021. **109**(7): p. 982-989.
94. Guo, W., et al., *Polyhydroxyalkanoates in tissue repair and regeneration*. Engineered Regeneration, 2022.
95. Finch, C.A., *Encyclopedia of polymer science and engineering, volume 6: Editor-in-Chief Jacqueline I. Kroschwitz, John Wiley & Sons, New York and Chichester, 1986. pp. xxiv + 839, price £145.00. ISBN 0-471-80050-3*. British Polymer Journal, 1987. **19**: p. 483-483.
96. Imura, Y., R.M.C. Hogan, and M. Jaffe, *10 - Dry spinning of synthetic polymer fibers*, in *Advances in Filament Yarn Spinning of Textiles and Polymers*, D. Zhang, Editor. 2014, Woodhead Publishing. p. 187-202.
97. Abdal-hay, A., F.A. Sheikh, and J.K. Lim, *Air jet spinning of hydroxyapatite/poly(lactic acid) hybrid nanocomposite membrane mats for bone tissue engineering*. Colloids and Surfaces B: Biointerfaces, 2013. **102**: p. 635-643.
98. DeFrates, K.G., et al., *Protein-Based Fiber Materials in Medicine: A Review*. Nanomaterials, 2018. **8**(7): p. 457.
99. Puhl, D.L., et al., *Electrospun Fiber Scaffolds for Engineering Glial Cell Behavior to Promote Neural Regeneration*. Bioengineering (Basel), 2020. **8**(1).
100. Nagam Hanumantharao, S. and S. Rao, *Multi-Functional Electrospun Nanofibers from Polymer Blends for Scaffold Tissue Engineering*. Fibers, 2019. **7**(7): p. 66.
101. Khorasani, M.T., S.A. Mirmohammadi, and S. Irani, *Polyhydroxybutyrate (PHB) Scaffolds as a Model for Nerve Tissue Engineering Application: Fabrication and In Vitro Assay*. International Journal of Polymeric Materials and Polymeric Biomaterials, 2011. **60**(8): p. 562-575.

102. Murase, Y. and A. Nagai, *11 - Emulsion spinning*, in *Advanced Fiber Spinning Technology*, T. Nakajima, K. Kajiwara, and J.E. McIntyre, Editors. 1994, Woodhead Publishing. p. 25-64.
103. Simitzis, J.C. and P.C. Georgiou, *Functional group changes of polyacrylonitrile fibres during their oxidative, carbonization and electrochemical treatment*. *Journal of Materials Science*, 2015. **50**: p. 4547-4564.
104. Kalousková, R., et al., *A new strategy for plasticizing and stabilization of PVC mixtures*. *Journal of Applied Polymer Science*, 2014. **131**(22).
105. Kim, S.Y., P. Purnama, and S.H. Kim, *Fabrication of poly(l-lactide) fibers/sheets using supercritical fluid through flash-spinning process*. *Macromolecular Research*, 2010. **18**(12): p. 1233-1236.
106. Zhou, C., et al., *Electrospun Bio-Nanocomposite Scaffolds for Bone Tissue Engineering by Cellulose Nanocrystals Reinforcing Maleic Anhydride Grafted PLA*. *ACS applied materials & interfaces*, 2013. **5**.
107. Yao, J., C.W.M. Bastiaansen, and T. Peijs, *High Strength and High Modulus Electrospun Nanofibers*. *Fibers*, 2014. **2**(2): p. 158-186.
108. El-hadi, A.M. and F.Y. Al-Jabri, *Influence of Electrospinning Parameters on Fiber Diameter and Mechanical Properties of Poly(3-Hydroxybutyrate) (PHB) and Polyanilines (PANI) Blends*. *Polymers*, 2016. **8**(3): p. 97.
109. Hashizume, R., et al., *Morphological and mechanical characteristics of the reconstructed rat abdominal wall following use of a wet electrospun biodegradable polyurethane elastomer scaffold*. *Biomaterials*, 2010. **31**(12): p. 3253-3265.
110. Wu, J., et al., *Mechanism of a long-term controlled drug release system based on simple blended electrospun fibers*. *Journal of Controlled Release*, 2020. **320**: p. 337-346.
111. Ke, Y., et al., *Surface modification of polyhydroxyalkanoates toward enhancing cell compatibility and antibacterial activity*. *Macromolecular Materials and Engineering*, 2017. **302**(11): p. 1700258.
112. Li, X., et al., *Improving hydrophilicity, mechanical properties and biocompatibility of poly [(R)-3-hydroxybutyrate-co-(R)-3-hydroxyvalerate] through blending with poly [(R)-3-hydroxybutyrate]-alt-poly (ethylene oxide)*. *Acta biomaterialia*, 2009. **5**(6): p. 2002-2012.
113. Tohill, M., et al., *Rat bone marrow mesenchymal stem cells express glial markers and stimulate nerve regeneration*. *Neuroscience Letters*, 2004. **362**(3): p. 200-203.
114. Schaub, N.J., et al., *The Effect of Surface Modification of Aligned Poly-L-Lactic Acid Electrospun Fibers on Fiber Degradation and Neurite Extension*. *PLoS One*, 2015. **10**(9): p. e0136780.
115. Kumar, R., R. Singh, and I. Farina, *On the 3D printing of recycled ABS, PLA and HIPS thermoplastics for structural applications*. *PSU Research Review*, 2018. **2**(2): p. 115-137.
116. Demcisakova, Z., et al., *Evaluation of Angiogenesis in an Acellular Porous Biomaterial Based on Polyhydroxybutyrate and Chitosan Using the Chicken Ex Ovo Chorioallantoic Membrane Model*. *Cancers*, 2022. **14**(17): p. 4194.
117. Mohammadalipour, M., et al., *Effect of cellulose nanofibers on polyhydroxybutyrate electrospun scaffold for bone tissue engineering applications*. *International Journal of*

- Biological Macromolecules, 2022.
118. Jiang, Y., et al., *Feasibility study of an alkaline-based chemical treatment for the purification of polyhydroxybutyrate produced by a mixed enriched culture*. *Amb Express*, 2015. **5**(1): p. 1-13.
 119. Kann, Y., M. Shurgalin, and R.K. Krishnaswamy, *FTIR spectroscopy for analysis of crystallinity of poly(3-hydroxybutyrate-co-4-hydroxybutyrate) polymers and its utilization in evaluation of aging, orientation and composition*. *Polymer Testing*, 2014. **40**: p. 218-224.
 120. Yeo, J.C.C., et al., *Insights into the nucleation and crystallization analysis of PHB-rubber toughened PLA biocomposites*. *Composites Communications*, 2021. **27**: p. 100894.
 121. McAdam, B., et al., *Production of Polyhydroxybutyrate (PHB) and Factors Impacting Its Chemical and Mechanical Characteristics*. *Polymers (Basel)*, 2020. **12**(12).
 122. Ikejima, T. and Y. Inoue, *Crystallization behavior and environmental biodegradability of the blend films of poly (3-hydroxybutyric acid) with chitin and chitosan*. *Carbohydrate polymers*, 2000. **41**(4): p. 351-356.
 123. Sudesh, K., H. Abe, and Y. Doi, *Synthesis, structure and properties of polyhydroxyalkanoates: biological polyesters*. *Progress in polymer science*, 2000. **25**(10): p. 1503-1555.
 124. Yu, J., D. Plackett, and L.X.L. Chen, *Kinetics and mechanism of the monomeric products from abiotic hydrolysis of poly[(R)-3-hydroxybutyrate] under acidic and alkaline conditions*. *Polymer Degradation and Stability*, 2005. **89**(2): p. 289-299.
 125. Pires, C.T.G.V.M.T., J.A.P. Vilela, and C. Airoidi, *The Effect of Chitin Alkaline Deacetylation at Different Condition on Particle Properties*. *Procedia Chemistry*, 2014. **9**: p. 220-225.
 126. Park, J.S., et al., *Surface hydrolysis of fibrous poly (ϵ -caprolactone) scaffolds for enhanced osteoblast adhesion and proliferation*. *Macromolecular research*, 2007. **15**(5): p. 424-429.
 127. Choong, C., et al., *Optimization of poly (ϵ - caprolactone) surface properties for apatite formation and improved osteogenic stimulation*. *Journal of Biomedical Materials Research Part A*, 2012. **100**(2): p. 353-361.
 128. Chong, M.S.K., et al., *Beyond cell capture: antibody conjugation improves hemocompatibility for vascular tissue engineering applications*. *Tissue Engineering Part A*, 2010. **16**(8): p. 2485-2495.
 129. Saratale, G.D. and M.-K. Oh, *Characterization of poly-3-hydroxybutyrate (PHB) produced from *Ralstonia eutropha* using an alkali-pretreated biomass feedstock*. *International journal of biological macromolecules*, 2015. **80**: p. 627-635.
 130. Rajan, R., et al., *Thermal and mechanical properties of chitosan reinforced polyhydroxybutyrate composites*. *Journal of applied polymer science*, 2012. **124**(4): p. 3357-3362.
 131. Young, R., G. Terenghi, and M. Wiberg, *Poly-3-hydroxybutyrate (PHB): a resorbable conduit for long-gap repair in peripheral nerves*. *British journal of plastic surgery*, 2002. **55**(3): p. 235-240.
 132. Mothes, G., C. Schnorpfeil, and J.U. Ackermann, *Production of PHB from crude*

- glycerol*. *Engineering in Life Sciences*, 2007. **7**(5): p. 475-479.
133. Smith, M.K.M., et al., *Sustainable composites from poly(3-hydroxybutyrate) (PHB) bioplastic and agave natural fibre*. *Green Chemistry*, 2020. **22**(12): p. 3906-3916.
134. Pryadko, A.S., et al., *Comprehensive Study on the Reinforcement of Electrospun PHB Scaffolds with Composite Magnetic Fe₃O₄-rGO Fillers: Structure, Physico-Mechanical Properties, and Piezoelectric Response*. *ACS Omega*, 2022. **7**(45): p. 41392-41411.
135. Kim, M., S. Jeon, and H. Kim, *Physical properties and degradability of PHB/chitosan blend films*. *International Journal of Consumer Studies*, 2003. **27**(3): p. 250-250.
136. Liu, Z., et al., *Electrostimulation of fibroblast proliferation by an electrospun poly (lactide-co-glycolide)/polydopamine/chitosan membrane in a humid environment*. *Colloids and Surfaces B: Biointerfaces*, 2022. **220**: p. 112902.
137. Yang, L., D. Park, and Z. Qin, *Material Function of Mycelium-Based Bio-Composite: A Review*. *Frontiers in Materials*, 2021. **8**.